

Abstract

Today, sand has been used effectively and popularly in many countries for many types of structures against rockfall hazards. To design a protective structure with the ideal of performance-based design, it is necessary to evaluate the limitation capacity of structure as well as get insight into structural response. Experimental approach in cooperation with numerical simulation has been assumed the most economic and promising method. According to these points of view, this research performs three sub-studies concerning structural response of rockfall structures and sand cushioning layer.

The first sub-study, as shown in Chapter 3, successfully uses FE code of LS-DYNA to reproduce impacts on sand tank and sand cell and investigate the effects of material parameters and boundary conditions on dynamic behaviors. The results of parametric study using this numerical model indicate that geometrical parameters of sand such as the shear modulus G , bulk modulus K , angle of internal friction φ , and relationship of pressure versus volumetric strain are very important for numerical model of sand. Boundary conditions surrounding sand–cell strongly affect impact characteristics, e.g. impact force, transmitted force, weight displacement, and impulse by impact.

With the aims of testing the reactions of sand cushioning layer on steel rockfall galleries, the second sub-research of Chapter 4 concerns series of impact experiment on sand tank over steel H-beams. The results demonstrate that the energy absorbing effective of gravel cushion is higher than that of sand cushion. On the other hand, the transmitted force (P_t) at the bottom of sand tank and two equivalent forces (P_s , P_d) are evidently affected by the length of beam span L . Typically, this research presents the relationships between the dynamic multiplication factor (D_{MF}) and energy transfer rate (ETR) and ratio of T_d/T according to exponential functions. These relationships were expressed through two equations by using nonlinear regression analysis.

Chapter 5 in this study shows the content of the third sub-research, dealing with simulation of the dynamic reaction of flexible rockfall fence with and without covered sand–packs by using FE approach. The validated models of the fences, then, are gone through many applicable investigations. The results of numerical study on fence with and without sand–packs clearly show the effects of sand–packs on structural impact response, e.g. displacements, impact forces, impulses by impact, reaction forces, cable

stresses, and deflections of the posts. The achieved results reveal that the sand-packs may not reduce much the impact forces, but evidently redistribute impact force on cable net and reduce tensile stresses of net cables. In other words, the role of sand-packs in this study is also the same as cushioning layer of rockfall walls and galleries rather than braking devices of the normal flexible fence. Arrangement of sand-packs and diagonal cables under the net are also affected to structure response, especially impact forces, impulses by impact and displacements of the weight and fence.

The research does not deal with limited capacities of structure and mass, dimensions, and shape as well as effect of impact position of the weight on fence. Range size of sand particle also one of among limitations of research. In the future, the author will solve above-mentioned limitations as well as propose some applicants of practical equations concerning D_{FM} and ETR and numerical models of sand cell with walls, galleries and fences. In the overall, although some limitations are remained, this research have completed well with many noticeable scientific and technical achievements.

Contents

Abstract	i
Chapter 1	Introduction.....1
1.1	Rockfall and objectives to be impacted1
1.2	Introduction of mitigation countermeasures2
1.3	The purpose and content of research3
References	4
Chapter 2	State of the art concerning rockfall protection measures.....6
2.1	Galleries6
2.2	Embankment for rockfall9
2.3	Flexible fences11
2.4	Conclusion13
References	14
Chapter 3	Numerical modeling of impact on sand tank and sand cell17
3.1	Introduction.....17
3.2	Prior experimental studies of impacts on sand20
3.2.1	Sand tank experiment.....20
3.2.2	Sand-filled geocell experiment22
3.3	Modeling by finite element method.....23
3.3.1	Finite element model.....23
3.3.2	Constitutive model used in the simulations24
3.4	Model calibration through a parametric study of the sand characteristics.....26
3.4.1	Effect of the elastic constants27
3.4.2	Effect of the Mohr–Coulomb constants31
3.4.3	Effect of the pressure versus volumetric strain relationship31

3.4.4	Conclusion	31
3.5	Model validation	32
3.5.1	Impact in the sand tank	32
3.5.2	Impact on the sand cell	34
3.6	Effect of drop height on the impact response of a sand cell	36
3.7	Conclusion	38
	References	39
Chapter 4	Impact experiment on sand tank over steel H-beams	42
4.1	Introduction.....	42
4.2	Outline of experiment	44
4.2.1	Method of experiment.....	44
4.2.2	Measurement Items and Measurement Method.....	45
4.3	Results of experiment	47
4.3.1	Dynamic behavior of impact experiment.....	47
4.3.2	Maximum impact force.....	52
4.3.3	Impulse by impact force.....	52
4.3.4	Dynamic multiplication and energy transfer.....	54
4.4	CONCLUSION.....	56
	References	57
Chapter 5	Numerical simulation of impact on rockfall protection fence	59
5.1	Introduction.....	59
5.2	Outline of preceding experiments	61
5.2.1	Setup of the fence excluding sand-pack (FES)	61
5.2.2	Set-up of the fence including sand-pack (FIS).....	64
5.2.3	Experiment implementation.....	65
5.3	Numerical model approach.....	67
5.3.1	Setup of fence configurations and weight in numerical analysis.....	67
5.3.2	Finite element model.....	68

5.3.3	Constitutive law of material and contact types	69
5.3.4	Numerical analysis	71
5.4	Numerical model validation.....	71
5.4.1	Displacement of the fence and weight	72
5.4.2	Impact force and impulse by impact	74
5.4.3	Deflection of the top of the post	74
5.4.4	Reaction forces.....	75
5.4.5	Other parameters	76
5.4.6	Conclusion for validation step	77
5.5	Investigation into the effects of sand–packs according to the increase of drop height 78	
5.5.1	General impact phenomenon	78
5.5.2	Energy dissipation and transmission.....	79
5.5.3	Cable stress distribution.....	80
5.6	Application.....	82
5.6.1	Effects of collision point on sand–pack.....	82
5.6.2	Effect of diagonal cables.....	83
5.6.3	Effect of impact direction	85
5.7	Discussion and conclusion.....	87
References	88	
Chapter 6	Conclusion	90

List of Figures

Figure 1.1 Rockfall event at Nui Cam Mountain, An Giang province, Vietnam on June, 6th 2012.....	1
Figure 2.1 Concrete rockfall gallery.....	6
Figure 2.2 Steel rockfall gallery	7
Figure 2.3 Rockfall protection galleries: a) Concrete slab type and b) shell type (Vogel et al., 2009).....	7
Figure 2.4 Different types of cushion element; a) direct using sand; b) TLAS (Ikeda et al., 1999); c) fence box structure (Schellenberg et al., 2008); and multi-layer sandwich structure (Lorent et al., 2008).....	8
Figure 2.5 Different types of rockfall protection walls: a) geo-rock wall with sand cushion (Yoshida et al., 2002); b) geo-grid wall (Peila et al., 2002); and c) concrete wall (Lambert et al., 2011).....	10
Figure 3.1 Rockfall protection wall with a sand cushion	17
Figure 3.2 Apparatus for the sand tank impact experiment.....	19
Figure 3.3 Particle size accumulation curve of sand	20
Figure 3.4 Experimental strain versus pressure.....	20
Figure 3.5 Schematic view of the sand cell experiment: (a) free deformation (FD) condition, (b) material confinement (MC) condition. Units: m	21
Figure 3.6 FEM model of the sand tank	23
Figure 3.7 FEM model of the geocell: (a) free deformation (FD) condition, (b) material confinement (MC) condition	23
Figure 3.8 Volumetric strain versus pressure curve of soil and crushable foam.....	25
Figure 3.9 Study strain versus pressure relationship	26
Figure 3.10 Impact responses as functions of the elastic parameters (Series E): a) impact force; b) transmitted force; c) penetration depth	28
Figure 3.11 Impact responses as functions of the Mohr–Coulomb parameters (Series A): a) impact force; b) transmitted force; c) penetration depth	29

Figure 3.12 Impact responses as functions of the volumetric strain versus pressure relationship (Series V): a) impact force; b) transmitted force; c) penetration depth.....	30
Figure 3.13 Experimental and analytical impact response results: a) impact force; b) transmitted force; c) penetration depth.....	33
Figure 3.14 Time histories of the impact force	34
Figure 3.15 Time histories of the transmitted force	34
Figure 3.16 Relationship between the impact force and penetration depth.....	35
Figure 3.17 Time histories of the impact force for various drop heights	36
Figure 3.18 Time histories of the transmitted force for various drop heights.....	36
Figure 3.19 Relationships between the drop height, maximum impact force, and maximum transmitted.....	37
Figure 3.20 Relationship between the drop height and maximum penetration depth....	37
Figure 3.21 Relationships between the drop height and the impulse from the impact force and the transmitted force	37
Figure 4.1 Steel rockshed	42
Figure 4.2 An impact experiment using 1.8 m span length.....	43
Figure 4.3 Particle size accumulation curve.....	44
Figure 4.4 Measure devices and dimensions	46
Figure 4.5 Measurement system.....	46
Figure 4.6 Time histories of measured data (Sand, 1.8 m in span length, 2.0 m in falling height): a) acceleration; b) transmitted force; c) strain; d) deflection	48
Figure 4.7 Bending moment diagram M and displacement curve D of the simple beam resulted from equivalent static forces P_d and P_s ; a and b are distances from support to load cell and between two load cells respectively.....	49
Figure 4.8 Impact force, transmitted force and equivalent forces by strain and deflection: a) Sand ($L = 1.8$ m, $H = 2.0$ m); b) Sand ($L = 3.8$ m, $H = 2.0$ m); c) Gravel ($L = 1.8$ m, $H = 2.0$ m); d) Gravel ($L = 3.8$ m, $H = 2.0$ m)	50
Figure 4.9 Relationship between falling height and various maximum forces for sand: a) Falling height and impact force P_a ; b) Falling height and transmitted force P_t ; c) Falling height and equivalent force P_s	51
Figure 4.10 Relationship between falling height and various maximum forces for gravel: a) impact force P_a ; b) transmitted force P_t ; c) equivalent force P_s	53

Figure 4.11 Relationship between falling height and impulse by impact force	53
Figure 4.12 Falling height and dynamic multiplication factor (D_{MF}): a) sand cushion; b) gravel cushion.....	54
Figure 4.13 Relationship between T_d/T and dynamic multiplication factor D_{MF} (T_d : duration of impact force, T : the first natural period of beam) and its corresponding practical equation.....	55
Figure 4.14 Relationship between T_d/T and of energy transfer rate (ETR) and its corresponding practical equation.....	56
Figure 5.1 Rockfall protection fence	60
Figure 5.2 Drawing of the fence excluding sand-packs (FES).....	62
Figure 5.3 Cross-section of steel post.....	63
Figure 5.4 Full-scale fence installation: a) view of experiment; b) weight; and c) cable net	63
Figure 5.5 Drawing of the fence including sand-packs (FIS).....	65
Figure 5.6 Design drawing of bending test for post (unit: millimeter)	65
Figure 5.7 Bending test result of post and its cross section.....	66
Figure 5.8 Tensional test results on cables	66
Figure 5.9 Tensional test results on geotextile	67
Figure 5.10 Finite element models: a) fence excluding sand-packs (FES_10); b) fence including sand-packs (FIS_7)	69
Figure 5.11 Stress versus strain relationship of sand and the test schematic	69
Figure 5.12 Displacement of FES_10 model from experiment and simulation corresponding to three different timepoints during collision	72
Figure 5.13 Displacement of FIS_7 model from experiment and simulation corresponding to three different timepoints during collision	72
Figure 5.14 Experimental and numerical weight displacement from FES_10 model....	73
Figure 5.15 Experimental and numerical weight displacement from FIS_7 model.....	73
Figure 5.16 Impact force and impulse by impact time-histories from the experimental and numerical result of FES_10 model	73
Figure 5.17 Impact force and impulse by impact time-histories from the experimental and numerical result of FIS_7 model	73
Figure 5.18 Relationship of impact force and weight displacement of FES_10 model .	74

Figure 5.19 Relationship of impact force and weight displacement of FIS_7 model	74
Figure 5.20 Deflection of the top of the post No. 2 and No. 3 of FES_10 model.....	75
Figure 5.21 Deflection of the top of the post No. 2 and No. 3 of FIS_7 model.....	75
Figure 5.22 Reaction force histories of FES_10 model.....	76
Figure 5.23 Reaction force histories of FIS_7 model.....	76
Figure 5.24 The relationship between drop height and maximum impact force of FES and FIS models	79
Figure 5.25 The relationship between drop height and impulse by impact of FES and FIS models.....	79
Figure 5.26 The relationship between drop height and maximum reaction force of FES and FIS models at upward load cells	79
Figure 5.27 The relationship between drop height and maximum reaction force of FES and FIS models at downward load cells	79
Figure 5.28 Proportion of the maximum total energy transferring through sand-packs of FIS model, fence of FIS model and fence of FES models with respect to drop height..	80
Figure 5.29 Variation of energy transferring through sand-packs of FIS_14 model, fence of FIS_14 model and fence of FES models with 14 m of drop height.....	80
Figure 5.30 The relationship between maximum tensile stress of cable and drop height from FES model	81
Figure 5.31 The relationship between maximum tensile stress of cable and drop height from FIS model.....	81
Figure 5.32 FEM model of impact at center of sand-pack (FIS_7_C)	81
Figure 5.33 Histories of impact force and impulse of FIS_7 and FIS_7_C models.....	82
Figure 5.34 Histories of penetration depth of the weight of FIS_7 and FIS_7_C models	82
Figure 5.35 The relationship between impact force and penetration depth of the weight of FIS_7 and FIS_7_C models	82
Figure 5.36 Histories of reaction force of FIS_7 and FIS_7_C models	83
Figure 5.37 Histories of impact force and impulse by impact of FIS_7_D and FIS_7 models.....	83
Figure 5.38 Histories of penetration depth of the weight of FIS_7_D and FIS_7 models	84

Figure 5.39 The relationship between impact force and penetration depth of the weight of FIS_7_D and FIS_7 models	84
Figure 5.40 Histories of reaction force of FIS_7_D and FIS_7 models.....	85
Figure 5.41 Histories of tensile stresses in net cable of FIS_7_D and FIS_7 models....	85
Figure 5.42 Impact and impulse by impact force histories obtained from FES_10 and FES_10_H	86
Figure 5.43 The relationship of impact force and displacement from FES_10 and FES_10_H	86

List of Tables

Table 3.1 Mechanical properties of sand for the sand tank analysis	24
Table 3.2 Mechanical properties of sand for the geocell analysis.....	31
Table 3.3 Geocell experimental and analytical results	32
Table 4.1 Properties of used cushions	44
Table 4.2 List of impact experiments	45
Table 5.1 Material characteristic of steel tubes	65
Table 5.2 Geometrical dimension of kits of fence.....	68
Table 5.3 Main material parameters used for numerical analysis	70
Table 5.4 A comparison between numerical and experimental models based on concrete parameters.....	77

Chapter 1 Introduction

1.1 Rockfall and objectives to be impacted

Rockfall is a technical term, used to describe a rock fragments falling from its position on mountainous slope or cliff. Occurred rockfall generally continues movement in its propagation by falling, jumping and rolling on the slope until it is prevented by topography or artificial structures. The definition of rockfall first presented by Ladd (1935): *“Rockfalls are precipitated loosened rock groups, or individual boulders, initially from faces of cuts, or from nearly or remove cliffs and rock outcrops, which present vertical or steeply sloped face. They are distinguished from landslides by being distinctly extreme surface-phenomenon; solid rock; usually very small in volume; and consisting, generally, of individual rather than massed units. The repeated fall of rock fragments and shale particles (dribble) from cliffs or approximately vertical faces must be included in this class of superficial earth-movement. Such material, accumulated, forms what is known as talus”*.



Figure 1.1 Rockfall event at Nui Cam Mountain, An Giang province, Vietnam on June, 6th 2012.

Taken from Nguyen Thoai Trung

The causes inducing rockfalls are separated into two groups as internal and external influences. The internal influences indicate insight properties of rock and ground such as rock strength, discontinuities and ground water (TRB, 2012). The external influences are conditions that change the forces acting on a rock (Pantelidis, 2009) such as the influences of rainfall, snowmelt, seepage, channeled, water runoff, weathering, erosion, freeze-thaw and heating-cooling cycles, free roots, wind, disturbance by animals, and earthquakes (TRB, 2012). The human activities could be included as the external influences, for example: construction practices, blasting, vibration from equipment and trains, and stress relief due to excavation (Hoek, 2007). Now days, the climate changes caused by global warming and the frequent appearance of unusual earthquakes may increase the potential external influences for rockfall events.

The ricks, damages or accidents actively or passively caused by rockfalls could be considered as rockfall hazards. The fallen rock fragments or boulders during their runoffs accumulate the energy by increasing their velocities. Significant damages could be induced directly when the rocks with high velocities hit the objects, e.g. transportation and mining facilities, buildings, electric lines. Instead of posing such the damages, the fragments of the fallen rocks may cause accidents and crashes of vehicles and trains, traffic interruption and restoration expense. Populated areas, transportation infrastructures, and mining and power facilities are possible objectives to be subjected to rockfalls. Among these target objectives, transportation routes such as high ways and railways are especially vulnerable to rockfall, because they spread within long line and normally accompany with mountainous areas, where are sources of rockfall. For example, on May 5, 2012 a rockfall hazard that occurred in Cam Mountain, An Giang province of Vietnam, killing six people in a car and destroying it as shown in Figure 1 (Tienphong online, 2012). The traffic connecting to tourism area on the mountain was stopped for many days to cut and remove the large mass of rocks.

1.2 Introduction of mitigation countermeasures

As presented by Volkwein, A. and et. al. (2011), rockfall is a natural hazard that – compared to other hazards – usually impacts only small areas. However, the damage to the infrastructure or persons directly affected may be high with serious consequences. It is experienced as harmful event. To mitigate the effects of rockfall hazards, it is general-

ly needed to prepare a good understanding and managing about risks as well as provide suitable active and passive protection solutions. Therefore, over decades, many researches dealing with knowledge of rockfall causes as well as rockfall risks analysis, assessment, and management have been done by many researchers in various countries. Along with the improvement of rockfall hazard knowledge, monitoring technology and related instrumentation have been advanced. Description of the movement of a falling rock along a slope, namely trajectory of a rockfall, is important. This allows the description of existing hazard susceptibility or hazard assessment for a certain area, also providing information (velocities, impact height and affected area) for protection countermeasures (Volkwein, A. 2011). Therefore, many rockfall modeling methods have been developed dealing with spatial dimensions, reactions between rocks and the ground, terrains, and barrier effects of trees. For the protection area, single or a compound protective countermeasure should be considered to apply. Such countermeasures are separated into active and passive groups. The approaches of active solutions are reinforcement the rock ground and cliffs (i.e. by anchoring, covering, grouting, drainage, and excavating and reshaping talus) or removal the potential rockfalls. Accepting occurrences of rockfalls, passive protection structures such as catchment areas, barriers, drapery systems, and rock sheds could be selected basing on site conditions, rockfall energy magnitudes, and economy conditions. Such structures are designed with the principles of arresting rock by containing space (ditch), firm barriers (walls), or flexible configuration (fences) and deviating the rock (rock sheds). Among the countermeasures, this research mostly focused on passive structures using sand as cushioning material, namely galleries, walls, and fences.

1.3 The purpose and content of research

The effectiveness of rockfall protection structure, beside the stiffness of its configuration, the energy absorbing element cannot be ignored. Sand is assumed as one of the most effective, economical and applicable materials for various kinds of structure. Gallery, embankment and wall are the most traditional rockfall protection structures using sand cushion layer. In recently years, several ideals have been proposed to apply sand for flexible rockfall protection fence. Nishita (2011) has conducted several experimental studies following this approach. The early results of these studies are worth to

consider. However, discrete characteristics of sand, contrasting to the continuous characteristic of steel and concrete material of gallery, wall or fence is though as the most challenge for research dealing with sand cushion. Experimental approach is expected to provide reliable and persuasive results, but it is impossible to reach insight into structural response. By using finite element method (FEM), the aims of this research are to improve the knowledge about impact behaviors of such rockfall protection structures using sand cushioning layer.

In Chapter 2, recent researches and achievements concerning rockfall protection countermeasures, namely galleries, embankments as well as flexible fences are reviewed.

Based on above knowledge, some applications of sand cushion are proposed and discussed. To obtain the above-mentioned targets, this study conducted three sub-studies involving numerical modeling and experiment, namely (1) numerical modeling of impact on sand tank and sand-cell (Chapter 3); (2) impact experiment on sand tank over steel H-beams (Chapter 4); and (3) numerical modeling of impact on flexible fence with sand-packs cushion (Chapter 5).

Finally, achievements, limitations and relevant future works of the research are concluded in Chapter 6.

References

- Hoek, E. 2007. Practical Rock Engineering. Rocscience Inc., Toronto, Ontario, Canada.
http://www.rocscience.com/education/hoek_corner.
- Ladd, G. E. 1935. Landslides, Subsidence and Rockfall as Problems for the Railroad Engineer. In Proc., 36th Annual Convention of the American Railway Engineering Association, Vol. 36, pp. 1091-1162.
- Nishita, Y., Inoue, S., Masuya, H., Experimental Study on the Performance of Impact Absorption of Sand Cushion on Wire Net, Proceedings of the 9th International Conference on Shock & Impact Loads on Structures, pp.527-532, Nov. 2011.
- Pantelidis, L., Rock Slope Stability Assessment Through Rock mass Classification Systems. International Journal of Rock Mechanics and Mining Sciences, Vol. 46, pp. 315-325, 2009.
- Tienphong online, <http://www.tienphong.vn>, 2012

TRB - Rockfall Characterization and Control, Transportation Research Board of the National Academies, United States of America, 2012, <http://www.TRB.org>.

Volkwein, A. and et. al., Rockfall characterization and structural protection – a review, Nat. Hazards Earth Syst. Sci., 11, pp. 2617-2651, 2011.

Chapter 2 State of the art concerning rockfall protection measures

2.1 Galleries



Figure 2.1 Concrete rockfall gallery

Rockfall protection gallery (also called rock shed) is mostly used for high steep slope and short and well defined hazard zone. It is assumed as the most reliable structure, properly based on its following advantages. (1) Gallery provides a high impact energy range, for instance it is estimated up to about 5,000 kJ with added energy dissipating supports (Vogel et al., 2009). (2) This type of rockfall protection structure enables to decrease risks from uncertainty in predicting rockfall trajectories. (3) It is generally estimated low frequent maintenance cost after impact by small or low energy rock. (4) It can provide multi-objective protection task from other natural hazards: snow avalanches, landslides, or debris (TRB, 2012). Although rockfall protection gallery has

shown much positive characteristics comparing with other rockfall protection measures, it is no doubt that this type of protective structure just has been used moderately in some developed countries such as Japan and Switzerland. High initial construction costs are the most reason limiting the uses of gallery popularly over the World. However, life cycle cost of a gallery is considered relative low for the long life range as like general bridges.



Figure 2.2 Steel rockfall gallery

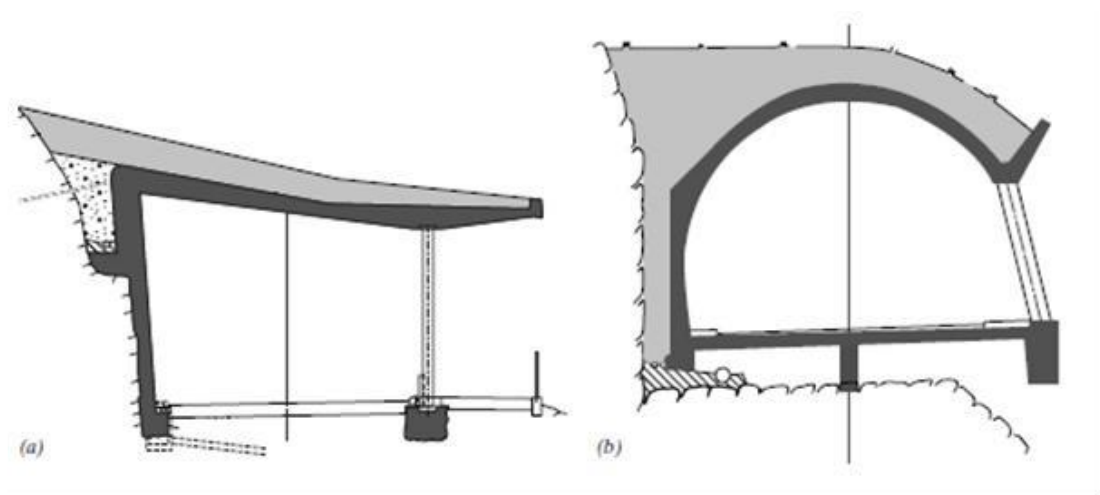


Figure 2.3 Rockfall protection galleries: a) Concrete slab type and b) shell type (Vogel et al., 2009)

Rockfall protection gallery configuration involves protective proof with cushioning layer and firm supporting structures. Concerning the material used, it could be classified into concrete (Figure 2.1), steel (Figure 2.2), or concrete-steel composite galleries. The most common type of gallery for large energy range is reinforced concrete structure. The stiffness of main members of concrete gallery is large, especially pre-stressed concrete structure, therefore, an effective cushioning layer is necessary for rockfall actions. By contrast, steel gallery, which has large flexibility, requires small cushioning layer. Accordingly, steel gallery is generally designed for multi-purpose in small impact energy range such as snow avalanche, small land-slide and small rockfall event. Concrete-steel composite gallery has the potential to mobilize the advantages of two above types of gallery, however it is still expensive recently. With regards to geometry, rockfall protection gallery can be categorized as a slab supported by columns or walls (Figure 2.3 a) or a shell (Figure 2.3 b) (Schellenberg et al., 2009). The shell structure generally has larger bearing capacity than the flat slab, because a portion of impact load is transmitted by compression in the arch (TRB, 2012). However, the complications of structure design and difficulties in construction may limit the application of this gallery type. By contrast, slab roof gallery is assumed the most common type because of its wide range of capacity, ease in design and suitability for various types of protective site.

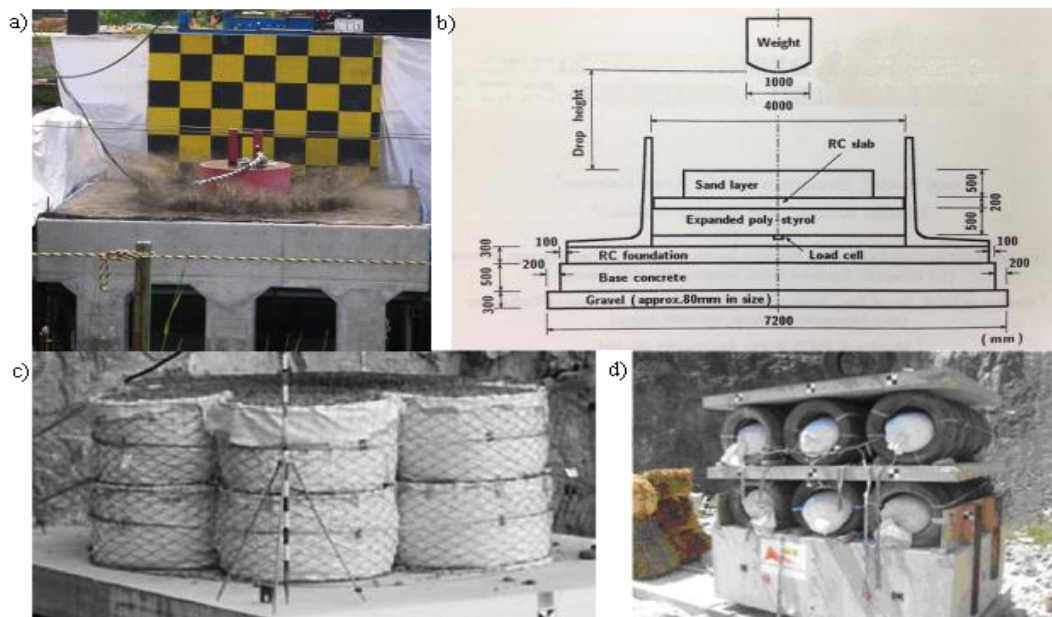


Figure 2.4 Different types of cushion element; a) direct using sand; b) TLAS (Ikeda et al., 1999); c) fence box structure (Schellenberg et al., 2008); and multi-layer sandwich structure (Lorent et al., 2008)

There are many types of cushion layers, which have been proposed for rockfall protection galleries, such as direct using sand (Figure 2.4 a), three layered absorbing system (Figure 2.4b, Nakano et al., 1995 and Ikeda et al., 1999), fence box structure with cellular glass material (Figure 2.4 c) (Schellenberg et al., 2008), and multi-layer sandwich structure (Figure 2.4 d) (Lorent et al., 2008). The absorbing effectiveness of cushion is concretely shown in three types of cushion except the type using only sand. However, the type of cushion using only sand has been applied widely, because of economical reasons and ease of supply at construction site. For example, in Japan, the thickness 0.9 m of sand cushion layer has been adopted as a standard value.

For the sake of improving understanding about impact behaviors of rockfall protection gallery and providing the tool for performance-based design approach, recently many researches concerning experiment and simulation on galleries subjected to rockfall impact load have been conducted and presented. Many researches have focused on providing the method to evaluation impact load (both value and loading area) (Ishikawa et al., 1999 and Sonoda et al., 1999). Based on experiment results or assumption of material behavior or contact type, many empirical or analytical equations were proposed to evaluate impact force and transmitted force (Ishikawa et al., 1999; Sonoda et al., 1999; and Schellenberg et al., 2009). Two recent decades, Switzerland and Japan have published and updated several guidelines related to designing rock fall galleries (Japan Road Association, 2000; ASTRA, 2008; SES 15, 2004; and SES 22, 2013). Now days, as results of rapid development of numerical approach, LS-DYNA, ADINA and ABAQUS dynamic FEM codes have been used to simulate full-scale or small-scale models of impact on galleries with or without sand cushions (Kishi et al., 2009; and Shikhow et al., 2012). The most advantages of these numerical approaches are to reproduce the dynamic behavior for various conditions, enable to obtain not only impact and transmitted forces but also internal stress-strain distributions of the structures. The dynamic information given by numerical approach is necessary for the performance-base design of rockfall protection structures.

2.2 Embankment for rockfall

Embankment (also called wall) has been known as relatively high capacity ability with moderate construction cost. Materials used for embankments are various, for

example reinforced concrete, stone, soil or soil with geo-grid. Therefore, local materials can be utilized to avoid environmental effects and reduce construction costs. However, the cross sections of embankments are large, then they are thought suitable for the construction site with large area in front of the protective objects (Volkwein et al., 2011).

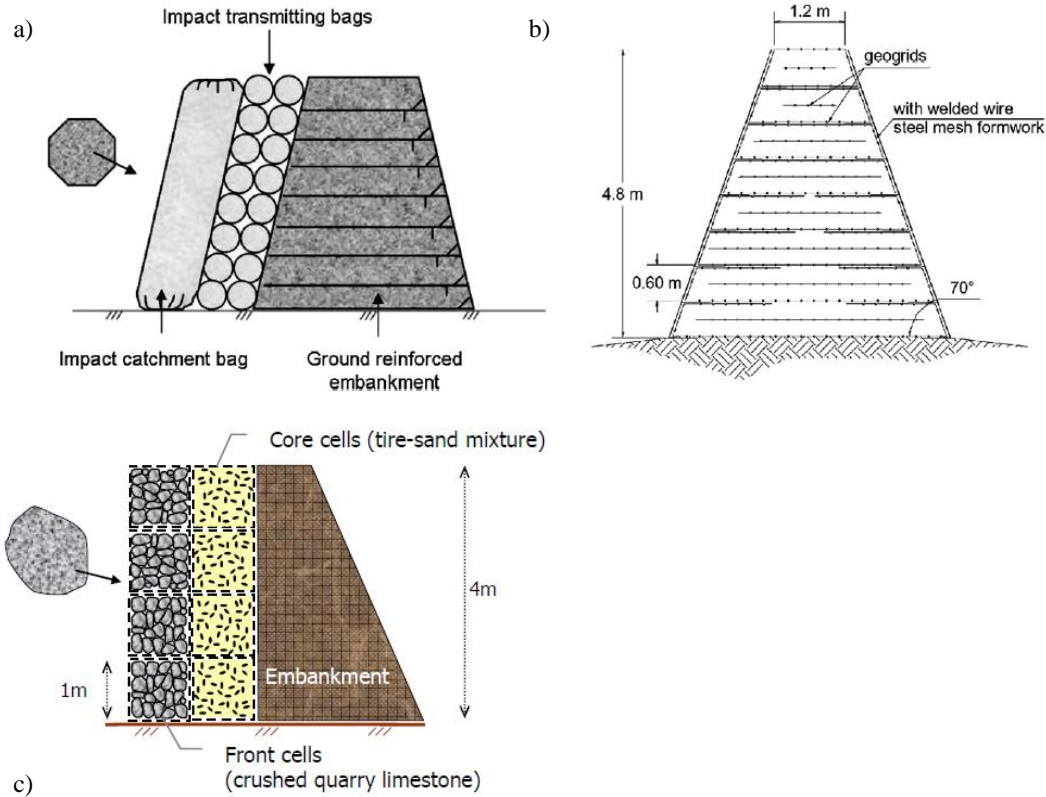


Figure 2.5 Different types of rockfall protection walls: a) geo-rock wall with sand cushion (Yoshida et al., 2002); b) geo-grid wall (Peila et al., 2002); and c) concrete wall (Lambert et al., 2011)

Generally, one or several granular materials e.g. sand, gravel or stone are used to protect the mountainous sides of embankments (Figure 2.5). These materials are normally contained by geo-textile bags or steel cases, this solution is not only to form the shapes, but also to enhance the stability of structures.

It is clear that the combination of main supporting structures and cushioning materials may result in many types of rockfall protection embankments. Therefore, as mentioned by Volkwein et al. (2011), there are many questions remaining about structural responses of embankments in the relationship with impact energy, dynamic characteristics of materials and others. Nevertheless, some researches have been conducted for the individual types of embankment using both experimental and numerical

approaches. For example, various kinds of experiment and numerical analysis by distinct element method had been done for concrete walls considering the effect of stone and sand materials contained in steel cases (Francois N. et al., 2007, Pichler et al., 2005). Numerical and experimental studies on earth embankment with and without damping layers have been performed by Yoshida et al. (2002), Peila et al. (2002), Ronco et al. (2009), and Lambert et al. (2011). These researches have obtained some advances, especially in experiments and numerical modeling for geo-wall without cushioning layers. However, accurate numerical analysis methods dealing with geo-walls and concrete walls with damping layers of discrete materials are still not established.

2.3 Flexible fences

Flexible fence systems normally consist from some components, namely interceptive net, supporters (posts and wire ropes), connectors (bolts and additional ropes), and energy absorbing devices. All such components of the fences are made from steel and other metal materials, which are required to have high durability and capacity. Combining these components could induce many types of fence with wide range of energy retention capacity, e.g. arch fence, wire netting fence, wire ring net fence and pocket fence. Each type of fences is generally corresponding to one energy level of rockfall and suitable for the type of topography of protected site.

Concerning initial construction cost, it is generally considered that rockfall protection fences are more economical than other countermeasures in the same working range, e.g. rockfall galleries and concrete walls. It is thought that they give relative low effect to landscapes and environment. Generally, they can be quickly installed requiring little equipment even at the difficult topography (Volkwein et al., 2011). Due to above-mentioned advantages of flexible fences, it is no doubt that these protective systems have been applied more commonly against rockfall hazards now days.

The flexible fences have also shown several limitations. Short working life is one of the most disadvantages; it is estimated about 25 years (EOTA, 2008), depending on environmental conditions and maintenance conditions. Typically, the running state of the fences is strongly affected by various natural factors. For example, the bearing capacity of the fence may not reach to the design level after a small impact of a rockfall

or even a tree fall or being covered by snow avalanches, debris flows or landslides (Volkwein et al., 2011). Therefore, it is required a high annual maintenance fee to monitor, replace the components to be impacted, and remove the covered landslide or debris. The principle of flexible fences to stop and catch the rock is based on the large plastic deformations of energy absorbing systems or friction connectors. Accordingly, it is noticed to keep a safe distance from downstream face of the fence to the objective to be protected.

Over past decades, flexible fences against rockfall hazard have gained remarkable attention from researchers and manufacturers. Actual designs of them have also changed dramatically because of increased testing, innovation, and market demand. At the beginning, the fence was simple and applied mostly for snow avalanches, rockfall protection tasks were exposed after that, during its working life for snow avalanche protection purpose (TRB, 2012). With the time, fence configurations have been developed, thus many types of fences have been proposed, tested and applied, gaining large step of capacity increasing.

The experimental studies were achieved very small capacity (about 50 kJ) according to the idea of how to stop falling rocks efficiently in the early 1990s (Duffy et al., 1992). Recently, the retention capacities of the flexible fences could reach to around 5000 kJ. In the development process, the testing method and design of the fences have been also changed and improved significantly due to the advances of measuring method and technology. For example, recently field experiments can obtain very detail results such as the histories impact force, transmitted forces at the supporting points, reaction of each cable rope or supplement devices as well as translation and rotation acceleration and displacement of the weight. The testing fence kits are also installed consistently with various experiment site and equipment condition, e.g. vertical fences subjected to horizontal impact (Nishita et al., 2011), inclined fences subjected to impact of the weight guided by cable rope, slope or coulisse (Peila et al., 1998, Tran et al., 2012, Dhakal et al., 2011) and horizontal fences subjected to vertical drop weight (Nishita et al., 2011, Gottardi et al., 2010). With the aim of testing the application of sand cushion for flexible fence, Nishita et al. (2011) presented his research through series of impact experiment on fence covered by many sand-packs on the surface.

At the beginning, analytical and numerical modeling researches concerned and obtained remarkable results later than experimental researches did. A corresponding numerical simulation enables a more efficient development or optimization of new types due to a reduced number of expensive prototype field tests. In addition, the use of software allows the simulation of designed barriers by considering special load cases that cannot be reproduced in field tests (high-speed rockfall, post/rope strikes, etc.), as well as special geometrical boundary conditions for individual topographical situations or the influence of structural changes on barrier performance (Volkwein et al., 2011). Numerical tools have been either self-developed code (Sonoda et al., 2011) or commercial program (Dhakal et al., 2011) basing on discrete element (Bertrand et al., 2012) or finite element method (Cazzani et al., 2002). Researches by numerical approach have achieved a significant step for modeling many types of flexible fence. However, researches concerning the fences with sand-pack cushion or fence covered by landslide mass subjected to impact by rockfall have never conducted so far.

2.4 Conclusion

Achievements from researches on rockfall protection structures have contributed effectively to develop and enhance their retention capacities and to improve the understanding structural response characteristics. However, some limitations of numerical studies on sand as well as other discrete materials acting as cushioning layer in rockfall protection structures can be seen clearly.

Sand used directly for cushioning layers in full-scale galleries has been somehow successfully reproduced in several researches. However, sand filled in containers such as cases, bag considering together with the response of galleries or wall has been insufficient. Now days, these types of sand cushion (sand-cell) have been used widely based on the aims of improving the absorbing abilities or enhancing the stabilities. Moreover, impact response characteristics of steel structures with sand cushioning layers have not been attended sufficiently.

Approaches for simulating rockfall protection fence have been verified and obtained remarkable achievements. With the limitations of simulating sand cushion as discussed above, simulation of fence with sand cushion could be a challenge and should be studied much more.

Finally, according the content of performance-based design, a numerical tool enable to simulate rockfall protection countermeasures such as galleries, walls, and fences will be very useful and serviceable for engineers and researchers.

References

- ASTRA: Einwirkungen infolge Steinschlags auf Schutzgalerien, Richtlinie, Bundesamt für Strassen, Baudirektion SBB, Eidgenössische Drucksachen- und Materialzentrale, Bern, 2008.
- D. Peila, S. Pelizza, F. Sassudelli, Evaluation of behavior of rockfall restraining nets by full scale tests, *Rock Mechanics and Rock Engineering*, Vol. 31, pp. 1-24, 1998.
- EOTA: ETAG 027 – guideline for the European technical approval of falling rock protection kits, Tech. rep., European Organization for Technical Approvals, Brussels, 2008.
- Francois Nicot, Philippe Gooteland, David Bertrand, and Stephane Lambert, Multiscale approach to geo-composite cellular structures subjected to rock impacts, *International Journal for Numerical and Analytical methods in Geomechanics*, Vol. 31, pp. 1477-1515, 2007.
- Guido Gottardi, Laura Govoni, Full-scale modeling of falling rock protection barriers, *Rock Mechanics and Rock Engineering*, Vol. 43, pp.261-274, 2010.
- Ishikawa, N., Recent progress on rock-shed studies in Japan, in: *Joint Japan-Swiss Scientific Seminar on Impact Load by Rock Falls and Design of Protection Structures*, 1-6, Kanazawa, Japan, 1999.
- Japan Road Association, *Manual for anti-impact structures against falling rock*, Tokyo, Japan, 2000.
- Kishi, N., S. Okada, and N. Konno, Numerical impact response analysis of rockfall protection galleries, *Structural Engineering International*, Vol. 19, pp. 313-320, 2009.
- Kritsada SRIKHOW, Hiroshi MASUYA, Akira SATO and Sachio NAKAMURA, Fundamental study on evaluation of deflection of H-beam under impact load aimed for the performance based design, *Journal of Structural Engineering* Vol.58A, JSCE, March 2012, pp. 991-999.

- Lambert, S., Heymann, A., Gotteland, P., 2011. Real-scale experimental assessment of cellular rockfall protection structures. Proceedings of Interdisciplinary Workshop on Rockfall Protection — Rocexs 2011, Innsbruck, Austria, pp. 36–37.
- Lorentz, J., Perrotin, P., and Donz´e, F.: A new sandwich design structure for protection against rockfalls, in: Interdisciplinary workshop on rockfall protection, edited by Volkwein, A., Labiouse, V., and Schellenberg, K., Swiss Fed. Research Inst. WSL, Morschach, Switzerland, 2008
- Nakano, O., Sato, M., Kishi, N., Matsuoka, K., and Nomachi, S.: Full scale impact tests of PC multi-girder with three-layered absorbing system, in: 13th International Conference on SMiRT, IV, 201–206, 1995.
- Nishita, Y., Inoue, S., Masuya, H., Experimental Study on the Performance of Impact Absorption of Sand Cushion on Wire Net, Proceedings of the 9th International Conference on Shock & Impact Loads on Structures, pp.527-532, Nov. 2011.
- Pichler, B., Hellmich, C., and Mang, H., Impact of rocks onto gravel – Design and evaluation experiments, *int. J. Impact Eng.*, Vol. 31, pp. 559-578, 2005.
- Peila, D., Oggeri, C., Castiglia, C., Recalcati, P., Rimoldi, P., 2002. Testing and modeling geogrid reinforced soil embankments to high energy rock impacts. Proceedings of the 7th International Conference on Geosynthetics, Nice, France, pp. 133–136.
- Peila, D., Oggeri, C., Castiglia, C., 2007. Ground reinforced embankments for rockfall protection: design and evaluation of full scale tests. *Landslides* 4 (3), 255–265.
- Phuc Van Tran, Koji Maegawa, Experiments and numerical modeling of a rockfall protective fence, *International Journal of GEOMAT*, Vol. 2, No. 2, Serial 4, pp. 219-226, 2012.
- Ronco, C., Oggeri, C., Peila, D., 2009. Design of reinforced ground embankments used for rockfall protection. *Natural Hazards and Earth System Sciences* 9, 1189–1199.
- S. Dhakal, N. P. Bhandary, R. Yatabe, N. Kinoshita, Experimental, numerical and analytical modeling of a newly developed rockfall protective cable-net structure, *Natural Hazard and Earth Science Systems*, Vol. 11, pp. 3197-3212, 2011.
- SES 15 - Structural Engineering Series 15: Practical Methods for Impact Test and Analysis, Edited by Norimitsu Kishi, Japanese Society of Civil Engineers, Tokyo, Japan, 2004.

- SES 22 - Structural Engineering Series 22: Performance based design guideline for civil engineering protective structures subjected to impact loading, Edited by Yoshimi Sonoda, Japanese Society of Civil Engineers, Tokyo, Japan, 2013.
- Sonoda, Y., A study on the simple estimation method of impact load by the one dimensional stress wave analysis, in: Joint Japan-Swiss Scientific Seminar on Impact Load by Rock Falls and Design of Protection Structures, 43-50, Kanazawa, Japan, 1999.
- Schellenberg, K., Volkwein, A., Denk, M., and Vogel, T.: Falling weight tests on rock fall protection galleries with cushion layers, in: Interdisciplinary Workshop on Rockfall Protection, edited by: Volkwein, A., Labiouse, V., and Schellenberg, K., Swiss Fed. Research Inst. WSL, Morschach, Switzerland, 2008
- Schellenberg, K., and Vogel, T., A Dynamic Design Method for Rockfall Protection Galleries, *Struct. Eng. Int.*, 19(3), 321-326, 2009.
- TRB - Rockfall Characterization and Control, Transportation Research Board of the National Academies, United States of America, 2012, <http://www.TRB.org>.
- Vogel, T., V. Labiouse, and H. Masuya. Rockfall protection as an Integral Task. *Structural Engineering International*. pp. 304-312. 2009.
- Yoshida, H., 1999. Recent experimental studies on rockfall control in Japan. *Proceedings of the Joint Japan-Swiss Scientific Seminar on Impact Load by Rock Fall and Design of Protection Structures*, Kanazawa, Japan, pp. 69-78.
- Yoshimi Sonoda, Yoshihiro Hata, Kazuki Fukunaga, Analytical study on impact response characteristic of wire ring net system by using the concept of particle method, *Proceedings of the 9th International Conference on Shock & Impact Loads on Structures*, pp.605-613, Nov. 2011.

Chapter 3 Numerical modeling of impact on sand tank and sand cell

3.1 Introduction

Rockfall is a natural disaster that frequently occurs in mountainous areas. Roads, railways, electricity lines, power stations, other infrastructure, and especially human lives are often subjected to hazards due to rockfall (Vogel et al., 2009). Many counter-measures have been proposed and applied to mitigate the risk of rockfall disasters, such as walls (Figure 3.1), embankments, and galleries (Matsuo et al., 1999; 2002). These protection structures, which include a cushioning layer, are well-known positive measures, providing solutions for high-energy impact from rockfall. Recently, various new technologies concerning rockfall hazards have been studied and advanced world-wide.



Figure 3.1 Rockfall protection wall with a sand cushion

Sand is a natural discrete material that is used as a cushioning layer for many types of rockfall hazard protection structures, especially embankments, concrete walls, and galleries. Sand can be installed in close contact with structures directly, or through containers like geotextile bags or cages, known as sand cells. Many studies have recently examined the effect of a sand cushion versus the shock impact of a rockfall. Satisfactory results have been achieved through small-scale and full-scale models using experiments and numerical simulations. A small-scale experimental study of an impact in a sand tank was performed by Masuya et al. (2009) to develop a performance-based design. A sand layer has also been used as an absorption component on the top of a gallery in full-scale experiments (Yoshida et al., 1998; Konno et al., 2009; and Bhatti et al., 2011). Fundamental static compression experiments have been performed to investigate the mechanical behavior and strength of geocells filled with sand and other types of material (Wesseloo et al., 2009 and Lambert et al., 2011a). A series of dynamic impact tests for a low-impact energy range were conducted by Lambert et al. (2009) on geocells filled with crushed quarry limestone, sand, and a mixture of sand and scrapped tires using three different boundary conditions. To further study the performance of cellular material, experiments using a rockfall structure with a geocell cushion were also conducted and assessed at various scales by Nicot et al. (2007) and Lambert et al. (2011b). But although experimental approaches have achieved many positive results, these studies have been costly, time-consuming, and inflexible.

A dependable numerical approach for dynamic analyses of protective structures with sand cushions is being advanced by many researchers. Sonoda et al. (1999) proposed a simplified finite element method (FEM) based on an assumption of one-dimensional stress wave propagation to estimate the stress distribution. The discrete element method (DEM) is another promising approach to investigate the impact response of discontinuous structures, such as sand or sand-cell cushions. Several studies using DEM have evaluated the impact phenomenon of sand or other granular soils acting as a cushioning layer in a gallery or embankment (Masuya et al., 2002; Calvetti et al., 2005; and Bourrier et al., 2011). The approach of modeling one geocell by a sphere was presented by Bertrand et al. (2006). Dynamic behavior analysis using FEM is one of the most effective methods to simulate continuous structures, whereas DEM seems to be suitable for sand used as granular material.

It is difficult to determine the dynamic behavior of structures with sand cushions using FEM because of the complex characteristics of the sand, which acts as a discrete material. Even if a combined FEM and DEM analysis is conducted (Breugnot et al., 2010), reproduction of the complex behavior is not straightforward because of the interactions between the structure and the sand cushion (Masuya et al., 2002) as well as the large number of particles. However, a geocell filled with sand is often used instead of sand because of its high ability to absorb impact energy and its ease of handling on a construction site. In the future, it is expected that sand cells will be utilized more for various protection measures. Thus, the FEM code LS-DYNA, which has a reasonable material model for sand, could be expected to overcome the modeling obstacles. A successful analysis of protection systems, including cushioning materials, by FEM will contribute to the development of new protection measures.

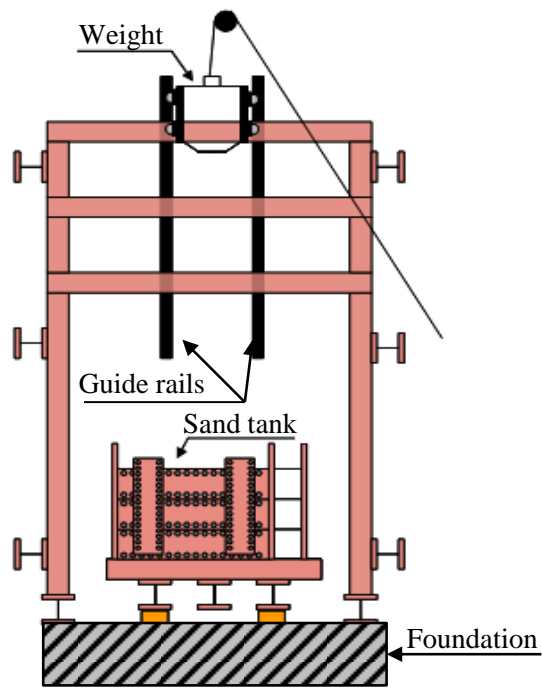


Figure 3.2 Apparatus for the sand tank impact experiment

The objectives of this study were to use FEM to reproduce the main phenomena of the impact behavior of sand cushions subjected to rockfall and to analyze the effects of the important parameters. The approach described in this study is expected to be suitable for general protective structures that make use of a sand cushion. To achieve these aims, the investigation examined impacts in a sand tank and on a sand cell. The sand tank tests consisted of direct collisions of a weight on a sand layer acting as cushioning element for galleries designed to protect from rockfall. The sand cell tests consisted of impact experiments on sand-filled containers generally used in walls or embankments. These tests are described in detail in the next section. A range of sand material characteristics were taken into account in the investigation to evaluate the most suitable sand parameters, which are not available from experiments. The numerical model was then

validated by comparing its results to experimental data. Finally, the validated numerical model was utilized for a parametric study.

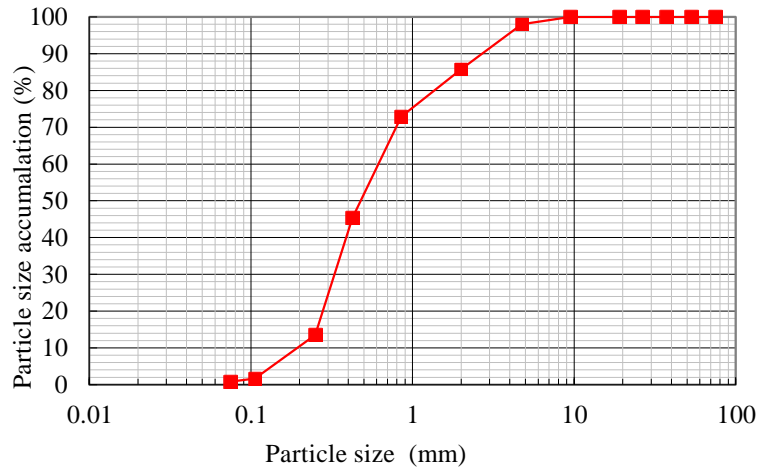


Figure 3.3 Particle size accumulation curve of sand

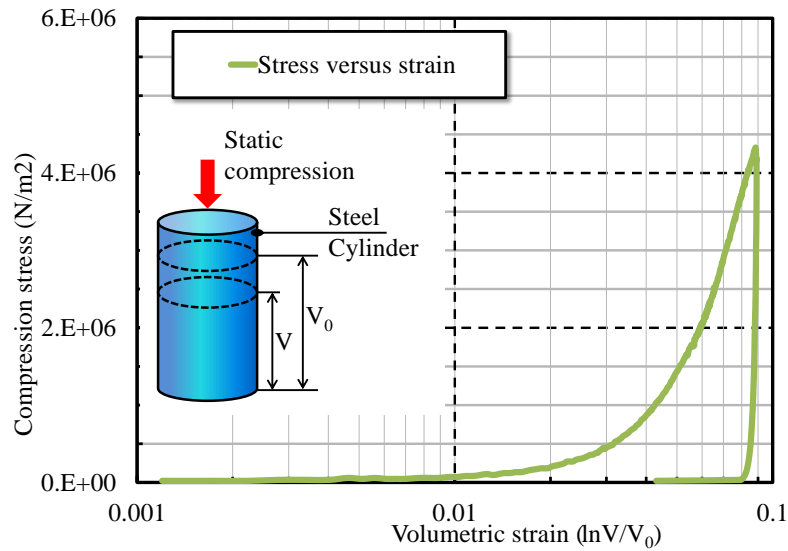


Figure 3.4 Experimental strain versus pressure

3.2 Prior experimental studies of impacts on sand

3.2.1 Sand tank experiment

The apparatus for the sand tank impact experiment (Masuya et al., 2009) consisted of a falling weight, a sand tank, a steel frame, and guide rails, as shown in Figure 3.2. The weight was a 204-kg, 0.5-m-diameter cylinder consisting of a steel shell filled with concrete. To induce a collision with the sand, this weight was freely dropped from 1.5 m

above the sand. The tank was made from steel and had inside dimensions of 1.1×1.1 m. The sand was loose, with a cumulative particle-size distribution as given in Figure 3.3. The sand density was $16,020 \text{ kg/m}^3$, and the angle of internal friction was 32.5° . The depth of the sand in the tank was 50 cm. A firm frame structure was erected above the tank to hang the guide rails. The frame and rails were used to locate the position of impact and control the vertical falling direction of the weight. The impact force was calculated by multiplying the measured acceleration by the mass of the weight. The pressure measured by 36 load cells was used to calculate the transmitted force; these load cells were installed in the bottom quarter of the tank.

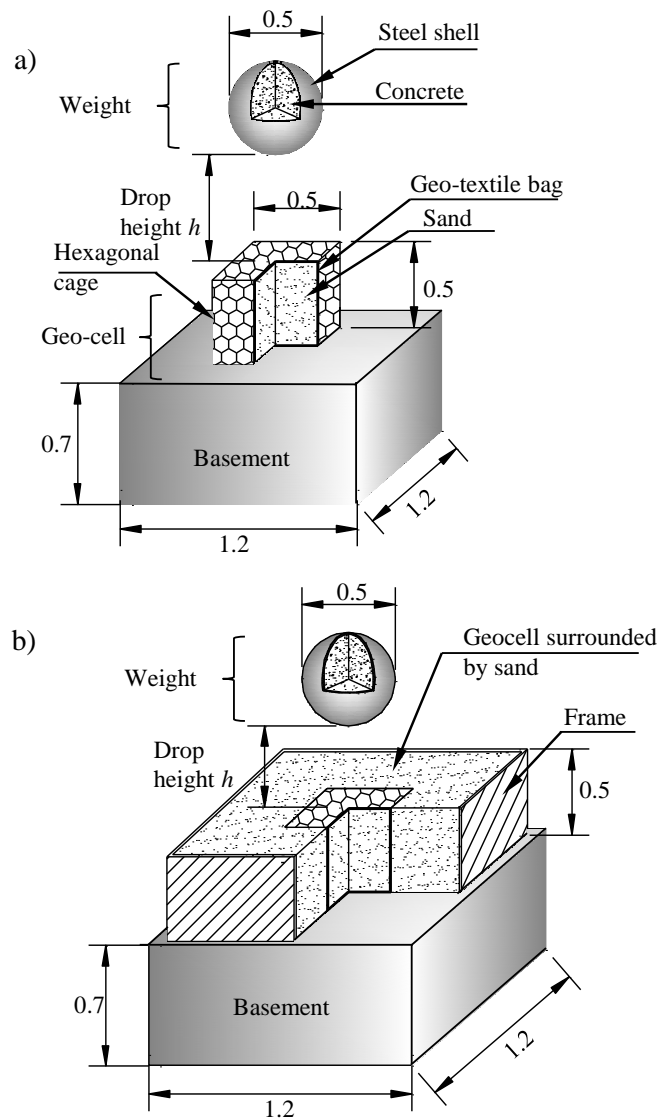


Figure 3.5 Schematic view of the sand cell experiment: (a) free deformation (FD) condition, (b) material confinement (MC) condition. Units: m

To provide supplementary information for the numerical study, a single-element stress–strain test was conducted using sand. The results of this test are shown in Figure 3.4. The experimental curve was obtained from an odometer test using a rigid cylinder 20 cm in height and 10 cm in diameter. This volumetric strain was expressed in terms of the natural logarithm of the relative volume, V/V_0 , where V is the volume and V_0 is the initial volume.

3.2.2 Sand-filled geocell experiment

Figure 3.5 shows a schematic diagram of the impact experiment using a geocell filled with sand, referred to as a sand cell (Lambert et al., 2009). The experimental apparatus included a falling weight, a sand cell, and a concrete block (basement). The weight was a 260-kg sphere, 54 cm in diameter, made from a steel shell filled with concrete. The impact was produced by dropping a free weight from a height (h) of 5.3 m, measured from the bottom of the weight to the surface of the sand cell before impact. The sand cell was $0.5 \times 0.5 \times 0.5$ m, including the sand fill, bag, and cage. Hostun sand was used, with a size distribution ranging from 0.08 to 1 mm. The density of sand was 16.8 t/m³, and the internal friction angle was 32.5°. The cage consisted of a steel hexagonal mesh, 80 mm in height and 100 mm in width, associated with a geotextile bag that was used as an envelope (container). The sand cell was placed on the concrete block basement. The dimensions of the basement were $1.2 \times 1.2 \times 0.7$ m. The acceleration of the weight was measured using an accelerometer installed at the center of the sphere, and the transmitted forces were measured by three load cells under the basement. The impact force was calculated by multiplying the measured acceleration by the mass of the sphere. Two numerical models were considered to examine the effect of boundary conditions on the behavior of the sand cell: (1) a sand cell with four lateral faces free to deform, referred to as the free deformation (FD) condition (Figure 3.5 a) and (2) a sand cell surrounded by sand, referred to as the material confinement (MC) condition (Figure 3.5 b). An impact on the sand cell modeled with the MC condition was assumed to reproduce the behavior of a sand cell surrounded by other sand cells.

3.3 Modeling by finite element method

3.3.1 Finite element model

The sand tank in Figure 3.2 was simulated by FEM as shown in Figure 3.6, including the cylindrical weight, sand fill, and tank. The weight and sand were discretized by eight-node solid elements, and the tank was discretized by four-node shell elements. The inside dimensions of the tank were 1.1×1.1 m, and the thickness of the tank walls were 0.05 m. In total, 1,525 solid elements and 473 shell elements were used.

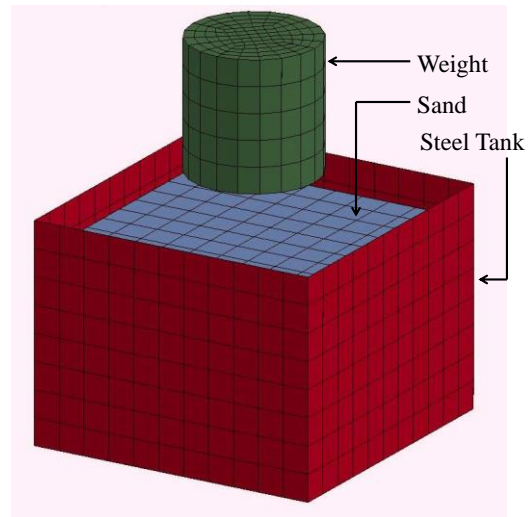


Figure 3.6 FEM model of the sand tank

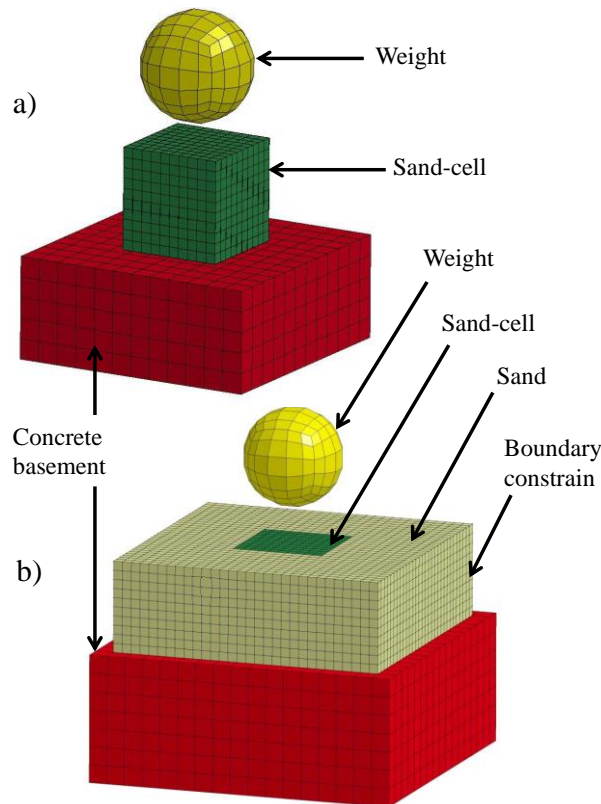


Figure 3.7 FEM model of the geocell: (a) free deformation (FD) condition, (b) material confinement (MC) condition

Figure 3.7 illustrates the numerical sand cell model, which included the falling weight, sand, textile bag, and basement. The effect of the steel net cage on the impact

behavior was assumed to be small, and therefore this element was neglected to simplify the model. Only the geotextile bag was kept to act as an envelope for the sand cell. The weight, sand block, and concrete basement were simulated by eight-node elements, while the textile bag was simulated by four-node shell elements. The dimensions of all parts of the numerical model were the same as those of the experimental model. The numerical simulation of the impact on the sand cell required one of two lateral boundary conditions: FD or MC, as shown in Figure 3.7 a and b. Sand cells under the FD and MC conditions were modeled by 2,595 solid elements and 600 shell elements and by 14,250 solid elements and 600 shell elements, respectively.

Table 3.1 Mechanical properties of sand for the sand tank analysis

Cases	Density ρ [kg/m ³]	Poisson ratio ν	Shear modulus G [kN/m ²]	Bulk modulus K [kN/m ²]	Angle of internal friction φ [degree]	Cohe- sion C [kN/m ²]	Scale factor of stress- volumetric strain a (refer to fig. 3.9)
Elastic parametric study							
E1			2.56×10^3	5.05×10^4			
E2			1.28×10^4	2.53×10^4			
E3	1602	0.47	2.56×10^4	5.05×10^5	32.50	1	1
E4			1.28×10^5	2.53×10^6			
E5			2.56×10^5	5.05×10^6			
Mohr–Coulomb parametric study							
A1					26.00		
A2					29.26		
A3	1602	0.47	2.56×10^4	5.05×10^5	32.50	1	1
A4					35.75		
A5					42.25		
Volumetric strain versus stress study							
V1							0.2
V2							0.5
V3	1602	0.47	2.56×10^4	5.05×10^5	32.50	1	1
V4							2
V5							5

Bold characters in the table indicate the selected parameters

3.3.2 Constitutive model used in the simulations

LS-DYNA offers various constitutive models for a wide range of material behaviors (LST, 2011). The sand was the most important part of our models. Therefore, the “Soil and Crushable Foam with Failure” material model was used, which was expected to reproduce the impact behavior of sand. Wang et al. (2006, 2009) also used this model to simulate the attenuation effect of expanded polystyrene (EPS) geo-foam for various material parameters. This model was first presented by Krieg (1972) based on the Drucker–Prager yield criterion. The Drucker–Prager yield criterion has the form

$$\alpha I_1 + \sqrt{J_2} = k \quad 3.1$$

where I_1 is the first invariant of the Cauchy stress tensor, and J_2 is the second invariant of the deviatoric part of the Cauchy stress tensor. The constants α and k are determined by experiments. In LS-DYNA, $I_1 = 3p$, where p is the pressure p . J_2 is expressed as follows:

$$\begin{aligned} J_2 &= (-\alpha I_1 + k)^2 = (-3\alpha p + k)^2 \\ &= 9\alpha^2 p^2 - 6\alpha k p + k^2. \end{aligned} \quad 3.2$$

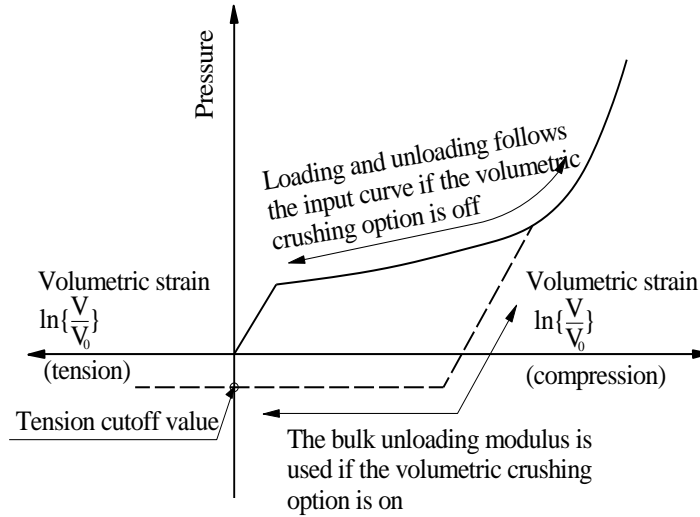


Figure 3.8 Volumetric strain versus pressure curve of soil and crushable foam

Because the Drucker–Prager yield surface is a smooth version of the Mohr–Coulomb yield surface, it can be expressed in terms of the cohesion (C) and the angle of internal friction (φ) that are used to describe the Mohr–Coulomb yield surface. If we assume that the Drucker–Prager yield surface circumscribes the Mohr–Coulomb yield surface, then the expressions for α and k are:

$$\alpha = \frac{2 \sin \varphi}{\sqrt{3}(3 - \sin \varphi)} ; \quad k = \frac{6C \cos \varphi}{\sqrt{3}(3 - \sin \varphi)}. \quad 3.3$$

Hence, the following equations give the necessary parameters for the LS-DYNA FEM code:

$$a_0 = k^2 ; \quad a_1 = -6\alpha k ; \quad a_2 = 9\alpha^2. \quad 3.4$$

In these equations, a_0 , a_1 , and a_2 are user-defined material constants.

Figure 3.8 presents the constitutive law of LS-DYNA’s “MAT_SOIL_AND_FOAM” model and two options for loading and unloading the volumetric strain relationships (LST, 2011).

The required input characteristics of sand for the numerical model include the density ρ , Poisson ratio μ , shear modulus G , bulk modulus K , friction parameters φ and C , and stress–volumetric strain relationships. The density ρ was measured directly. The Poisson ratio μ and cohesion C were assumed based on known characteristics of sand, and the other characteristics were evaluated through the parametric study described in Section 3.4.

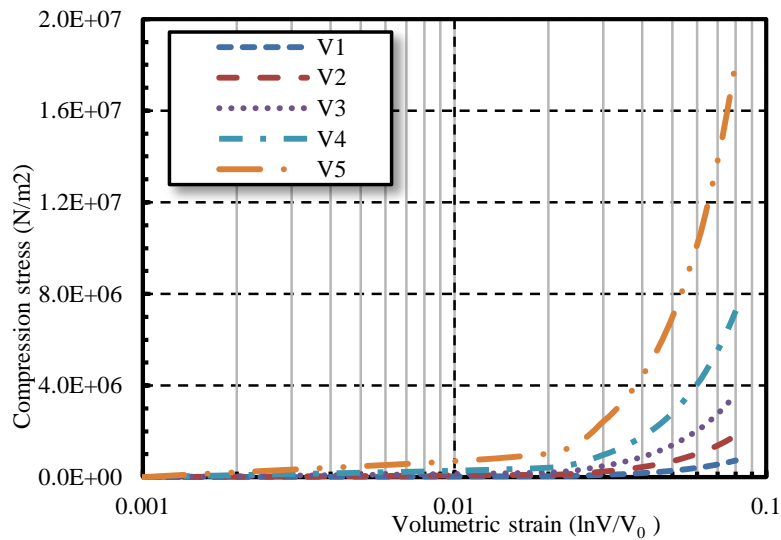


Figure 3.9 Study strain versus pressure relationship

An elastic linear material model was adopted to model the material behavior of the tank, basement, and weight. The fabric material model, which is a variation of Layered Orthotropic Composite materials (LST, 2011) and is valid for three- and four-node membrane elements, was employed to describe the mechanical properties of the textile bag.

3.4 Model calibration through a parametric study of the sand characteristics

The input data for the sand material model required various parameters. However, these parameters were either unavailable or not easy to obtain from existing laboratory conditions. Therefore, it was necessary to evaluate our assumed sand parameters

through a numerical parametric study in which various sand parameters were varied, namely the elastic constants (shear modulus G and bulk modulus K), angles of internal friction φ , and stress–strain relationship.

Three series of calculations were performed, based on the data shown in Table 3.1. Five sets of elastic constants (shear modulus G and bulk modulus K) and Mohr–Coulomb constants (angle of internal friction φ) were chosen within the range of real sand characteristics. The shear modulus G and bulk modulus K were varied, but the Poisson ratio ν was always kept constant. The curves for cases V_1 to V_5 of the stress–strain relationship (Figure 3.9) were obtained by multiplying the experimental pressure (Figure 3.4) by the factor a shown in Table 3.1. The parameters were investigated separately; when one of the parameters was varied, the others were kept constant and equal to their mean values.

3.4.1 Effect of the elastic constants

Figure 3.10 shows the time histories of the impact force, transmitted force, and penetration depth into the sand for five sets of shear modulus G and bulk modulus K values. The impact forces rapidly increased at the instant of the collision and, after the first peak, exhibited a quasi-plateau at low values for all cases. With increasing elastic constants (shear modulus G and bulk modulus K), the first peak values of the impact forces increased from 204 to 266 kN, and the impact durations decreased by 33% from 0.015 to 0.010 s. The transmitted forces appeared with time lags of 0.002 to 0.004 s after the impact forces, and their maximum values decreased monotonously. The maximum values of the transmitted forces increased from 156 to 244 kN. In contrast, the durations of the transmitted forces decreased from 0.011 to 0.0075 s with increasing shear modulus G and bulk modulus K . The final penetration depth for case E_1 was 40 to 50% larger than the values obtained for the other cases; the penetration depth decreased steadily with increasing elastic constants. It is thought that the increase in the bulk modulus K also increased the wave propagation velocity, which shortened the time lags of the transmitted forces, as shown in Figure 3.10 b.

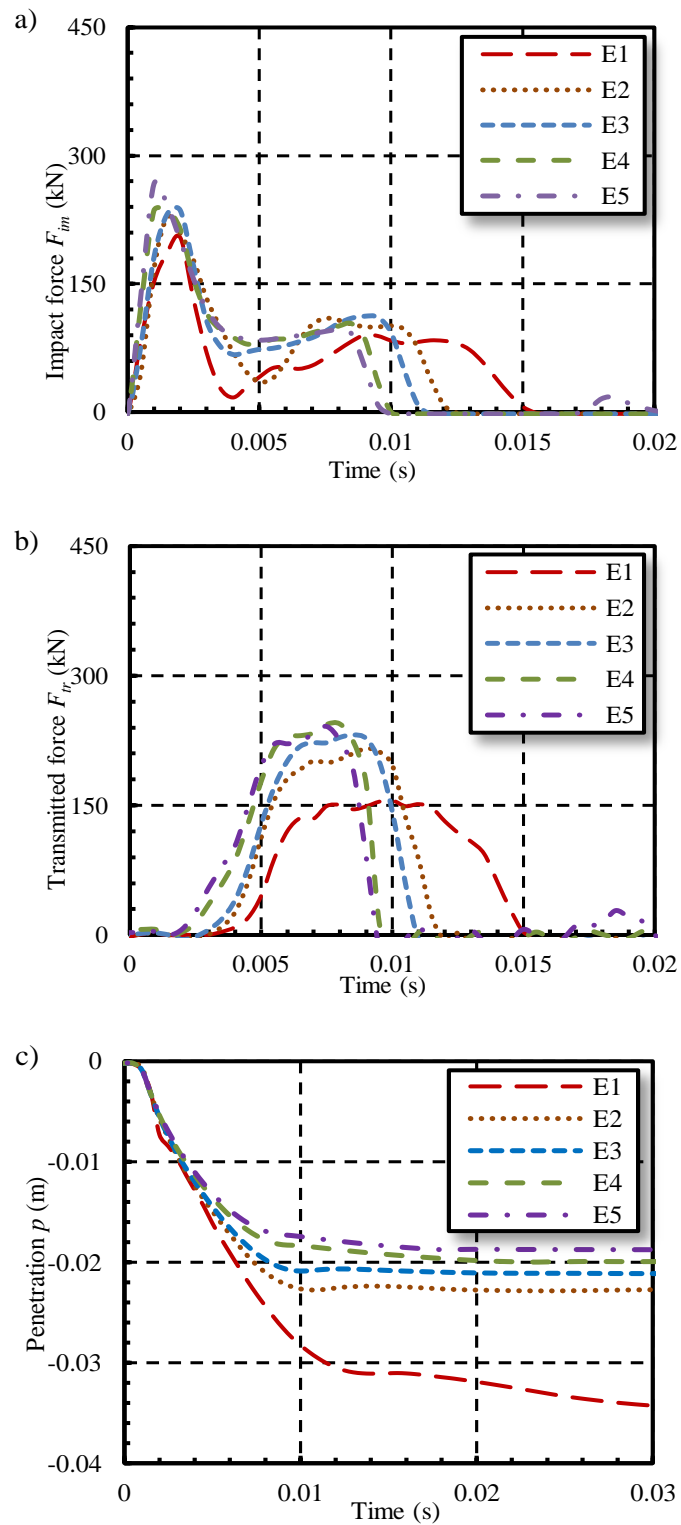


Figure 3.10 Impact responses as functions of the elastic parameters (Series E): a) impact force; b) transmitted force; c) penetration depth

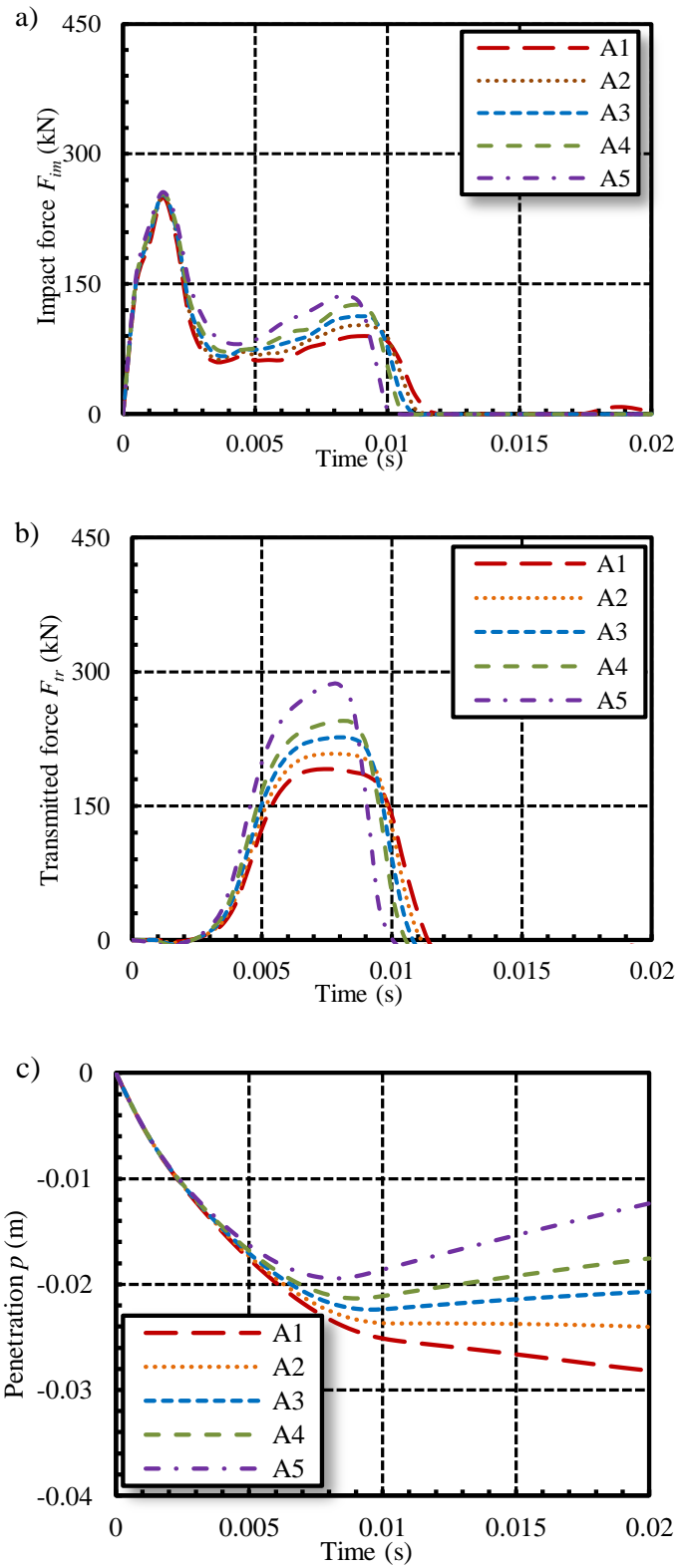
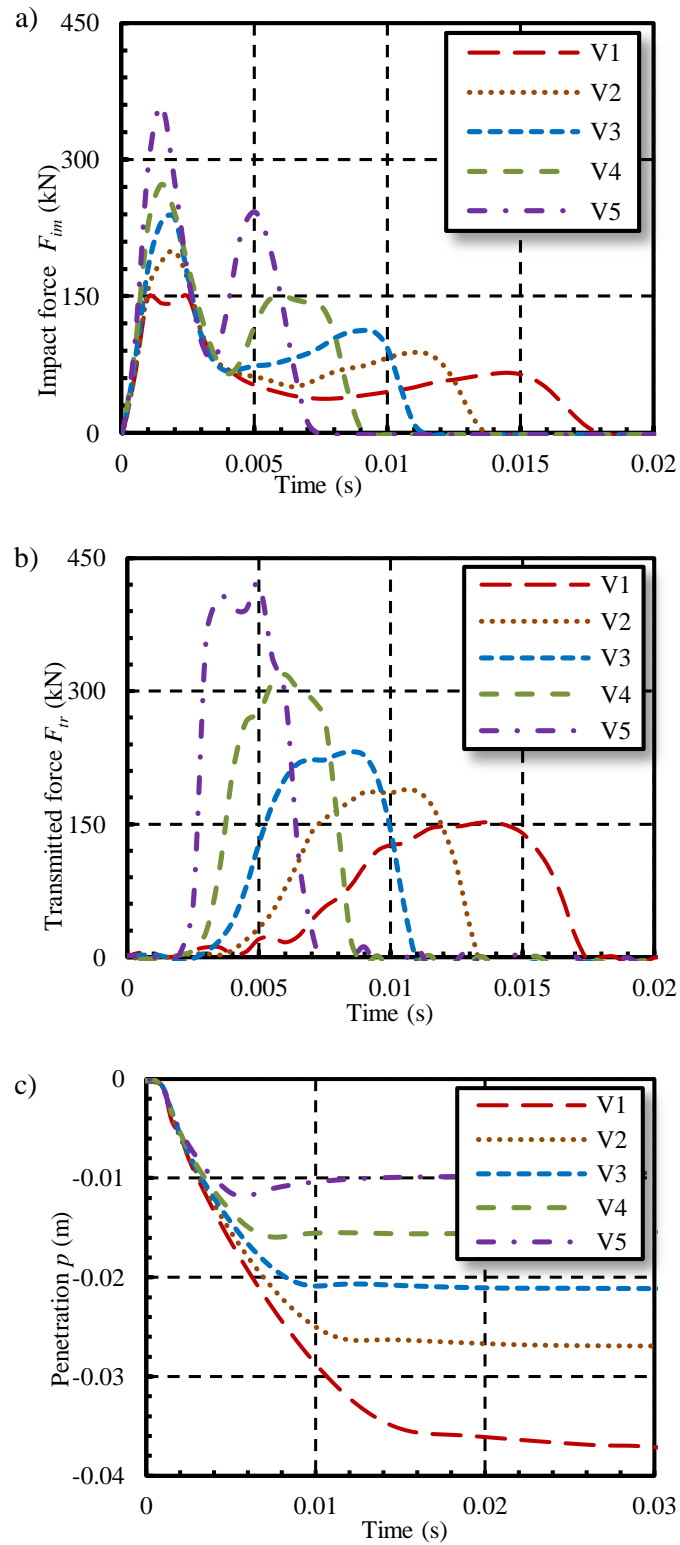


Figure 3.11 Impact responses as functions of the Mohr–Coulomb parameters (Series A): a) impact force; b) transmitted force; c) penetration depth



**Figure 3.12 Impact responses as functions of the volumetric strain versus pressure relationship
(Series V): a) impact force; b) transmitted force; c) penetration depth**

3.4.2 Effect of the Mohr–Coulomb constants

Figure 3.11 shows the time histories of the impact force, transmitted force, and penetration depth into the sand for five different angles of internal friction φ . With increasing φ , the durations of the impact and transmitted forces were reduced by 0.002 s. There was no change in the maximum values of the impact forces. In contrast, the maximum values of the transmitted forces and the values of the second peaks of the impact forces increased by 50%. In particular, φ had a significant effect on the penetration depth and the rebound of the weight after impact, as shown in Figure 3.11 c; the higher the angle of internal friction φ was, the smaller the penetration depth and the larger the rebound became. This study also investigated the effects of the cohesion C on the impact behavior. However, in the range of cohesion C found for our sand material properties, these effects were insignificant, and thus are not presented here.

3.4.3 Effect of the pressure versus volumetric strain relationship

Figure 3.12 illustrates the effects of the pressure versus volumetric strain relationship on the time histories of the impact force, transmitted force, and penetration depth. When the scale factor a was increased from 0.2 to 5, the histories of the impact forces, transmitted forces, and penetration depths tended to change rapidly by 150 to 180%. The durations of the impact and transmitted forces were reduced from 0.018 to 0.007 s and from 0.015 to 0.005 s, respectively. Furthermore, the final penetration depth dropped by 73%, from 0.031 m for case V_1 to only 0.010 m for case V_5 . Thus, material stress–strain relationship is very important in our FEM material model for sand.

Table 3.2 Mechanical properties of sand for the geocell analysis

Density ρ [kg/m ³]	Poisson ratio ν	Shear modulus G [kN/m ²]	Bulk modulus K [kN/m ²]	Angle of internal friction φ [degree]	Cohesion C [kN/m ²]	Scale factor of stress– volumetric strain a (refer to Fig. 3.9)
1680	0.35	2.08×10^4	6.27×10^5	32.50	1	1

3.4.4 Conclusion

After considering the effects of the sand parameters on the numerical results and comparing them with experimental data (presented in Section 3.5), the mechanical parameters of sand shown in bold in Table 3.1 were selected for the sand in the tank.

For the sand in the sand cell, the density was calculated from the size of the cell and its mass (supplied by the author), and the elastic constants (shear modulus G and bulk modulus K) were assumed based on the reference values of the sand in the tank. The Mohr–Coulomb constants (φ , C) and the stress–volumetric strain relationship were also based on the properties of the sand in the tank. The parameters of the sand in the cell are listed in Table 3.2.

Table 3.3 Geocell experimental and analytical results

Experiment cases	F_{im}^{\max} kN	F_{tr}^{\max} kN	T_{im} ms	p_{\max} cm	I_{im} kN·s	I_{tr} kN·s
FD5.3m_Exp.	90.0	128.0	52	28	2.99	3.52
FD5.3m_FEM	88.7	140.2	58	31	3.09	4.37
FEM/Exp.	0.99	1.10	1.12	1.11	1.03	1.24
MC5.3m_Exp.	130.0	226.0	30	16	2.64	3.49
MC5.3m_FEM	101.9	251.1	36	19	2.73	3.86
FEM/Exp.	0.78	1.11	1.20	1.19	1.03	1.11

3.5 Model validation

3.5.1 Impact in the sand tank

Figure 3.13 compares the numerical and experimental time histories of the impact force, transmitted force, and penetration depth. The input data for the simulation were the selected parameters indicated in Table 3.1. Although the impact force history from the simulation tended to increase and decrease more quickly than that from the experiment, the shapes of the two impact force history curves were similar. The transmitted force histories had simple shapes. The maximum value of the impact force from the simulation was about 20% lower than that from the experiment. The final penetration depth of the weight into the sand from the simulation was 21 mm, compared with 31 mm from the experiment. Although there was a gap between the experimental and numerical results, the final results of the sand tank impact behavior were in reasonable agreement.

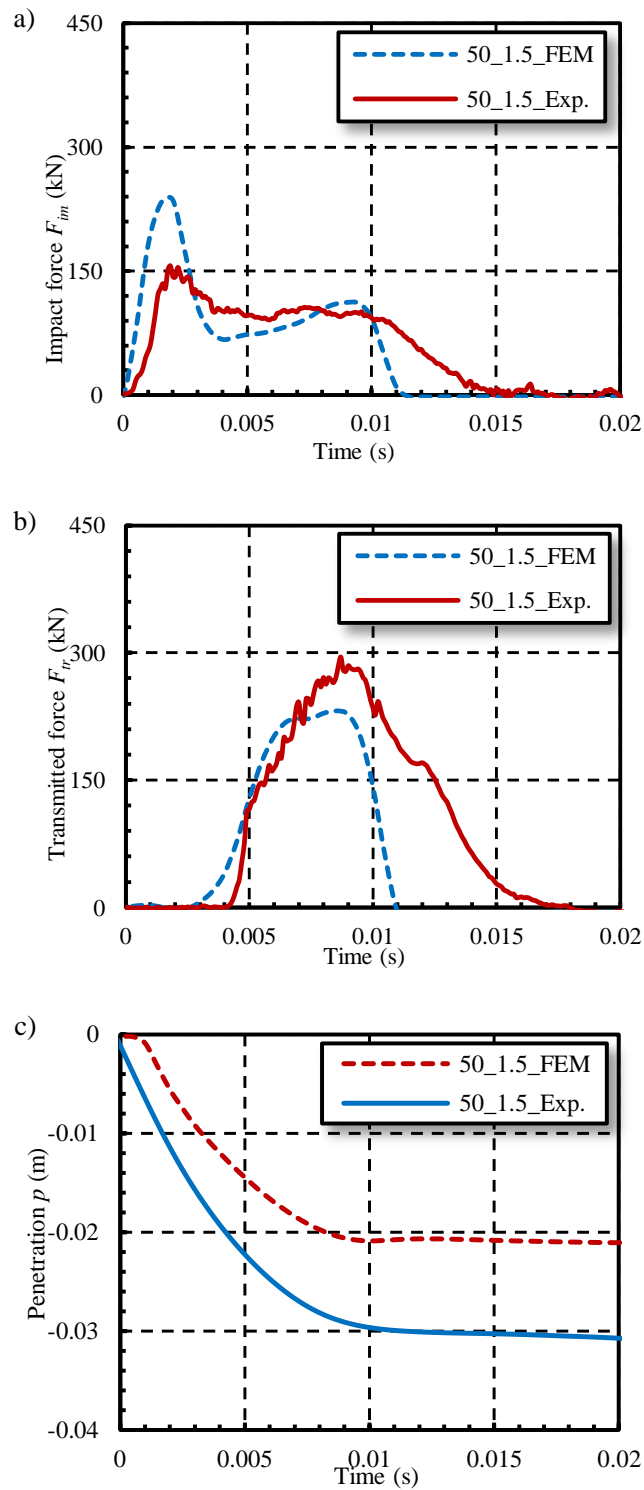


Figure 3.13 Experimental and analytical impact response results: a) impact force; b) transmitted force; c) penetration depth

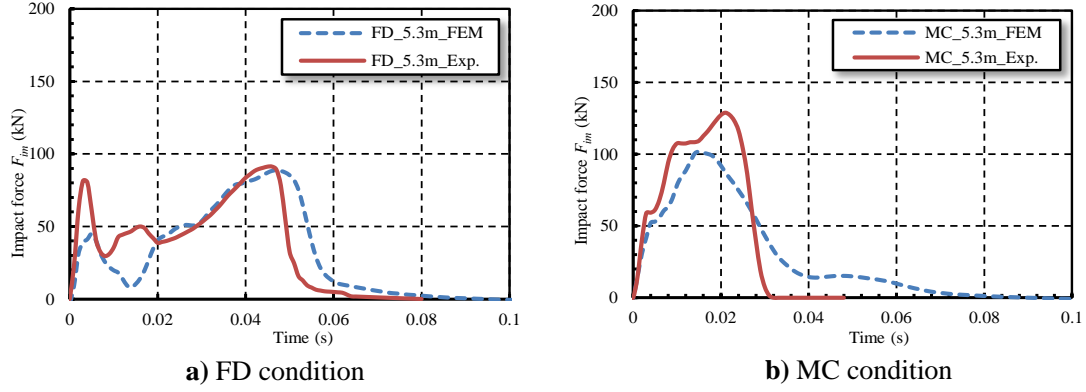


Figure 3.14 Time histories of the impact force

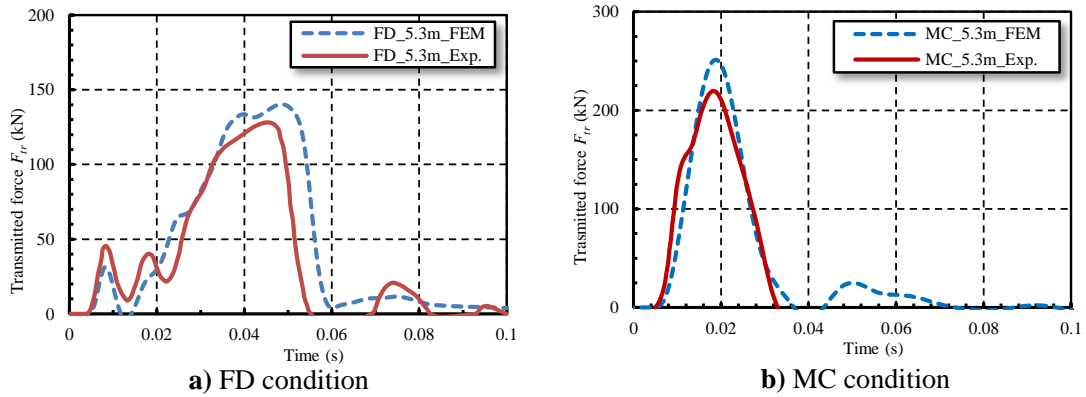


Figure 3.15 Time histories of the transmitted force

3.5.2 Impact on the sand cell

Figures 3.14 to 16 compare the numerical and experimental (Lambert et al., 2009) results of the impact on the sand cell. These results are expressed in terms of the histories of the impact force, transmitted force, and penetration depth for the FD (free deformation) condition and MC (material confinement) condition. The simulated and experimental data were in good general agreement, as summarized in Table 3.3. A detailed comparison follows.

Table 3.3 gives the primary results for the experiments and simulations with the two types of boundary conditions. There was good agreement between the maximum values of the impact forces F_{im}^{\max} , transmitted forces F_{tr}^{\max} , impact durations T_{im} , penetration depth p_{\max} , impulse from the impact force $I_{im} = \int F_{im} dt$, and transmitted force $I_{tr} = \int F_{tr} dt$ between the simulations and experiments. The ratio of the simulated to experimental (FEM/Exp.) values varied from 0.78 to 1.24.

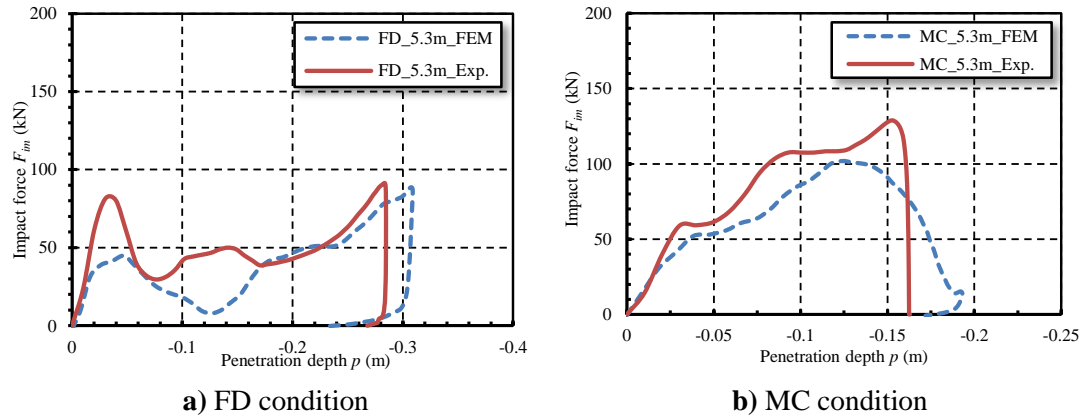


Figure 3.16 Relationship between the impact force and penetration depth

The maximum values of the impact forces from both the experiment and simulation for the FD condition were similar, as shown in Figure 3.14 a. The maximum impact force value from the simulation was 90 kN, which is slightly less than that from the experiment. The experimental force rapidly decreased to zero after its peak value, whereas the simulated force decreased more slowly. The shapes of the experimental and numerical impact forces for the MC condition were somewhat different in terms of the maximum values and duration, as presented in Figure 3.14 b.

A good match existed between the experimental and simulated transmitted force histories, as shown in Figure 3.15. The maximum values of the simulated transmitted forces for both the FD and MC conditions were only 10 and 30 kN greater than the values from the experiments, respectively. For the FD condition, the duration of the transmitted force from the experiment was 5 ms longer than that from the simulation, whereas the values were almost equal for the MC condition.

Figure 3.16 shows the relationship between the impact force and penetration depth into the sand cell for the simulations and experiments. The curves are similar in shape. Except for the impact force characteristics described above, the final penetration depths from the numerical analysis for the FD and MC conditions were 3 cm larger than the values obtained from the experiments.

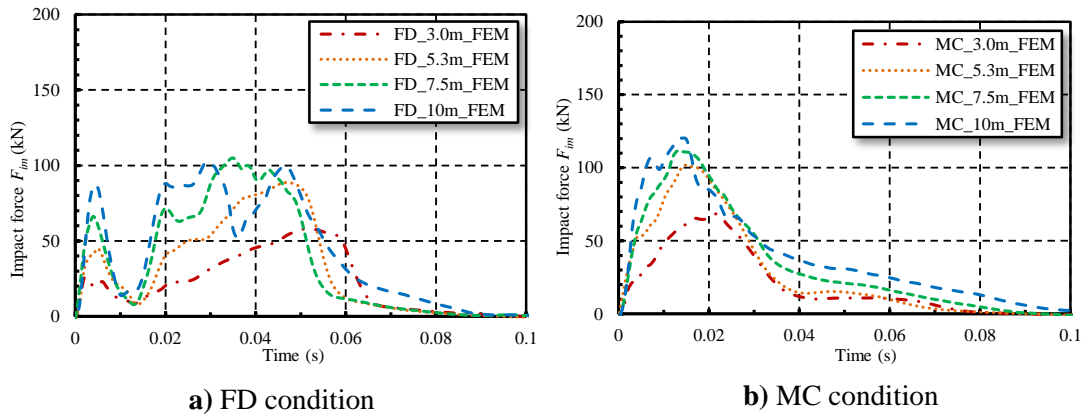


Figure 3.17 Time histories of the impact force for various drop heights

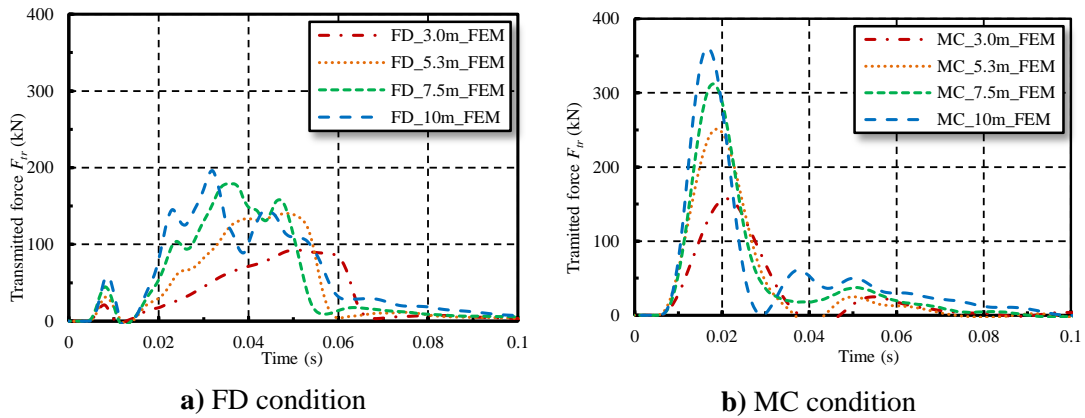


Figure 3.18 Time histories of the transmitted force for various drop heights

3.6 Effect of drop height on the impact response of a sand cell

The validation of the sand cell numerical model indicated good performance. Therefore, the model was applied further to investigate the impacts from four different drop heights to evaluate the impact phenomenon for different magnitudes of energy. The drop heights H were 3.0, 5.3, 7.5, and 10.0 m. The impact forces, transmitted forces, penetration depths, and impulses are shown in Figures 3.17 to 20.

Figure 3.17 a) shows the histories of the impact forces for different drop heights for the FD condition. The histories have two clear peaks. With increasing drop height, the first peak values increased regularly; the second peak values also increased but tended to level off around 100 kN for drop heights of 7.5 and 10 m.

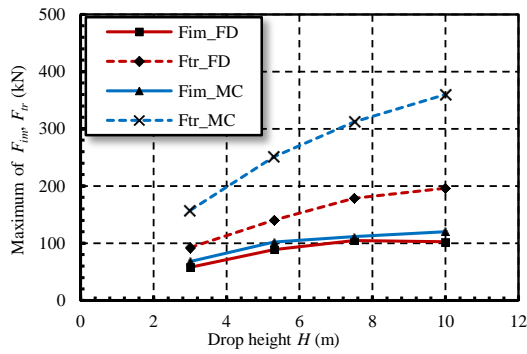


Figure 3.19 Relationships between the drop height, maximum impact force, and maximum transmitted

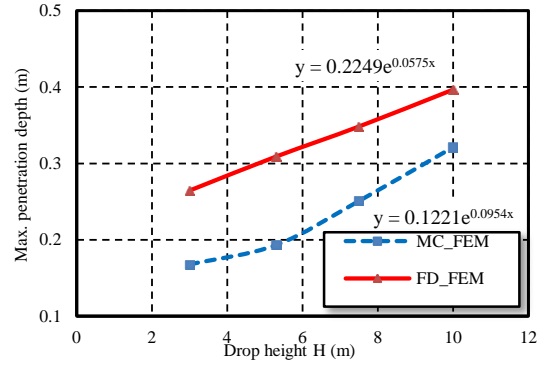


Figure 3.20 Relationship between the drop height and maximum penetration depth

Figure 3.17 b gives the impact force curves for the MC condition. The peak values changed significantly from 68 to 102 kN for heights of 3 and 5.3 m, respectively. The maximum values increased more slowly for the other drop heights.

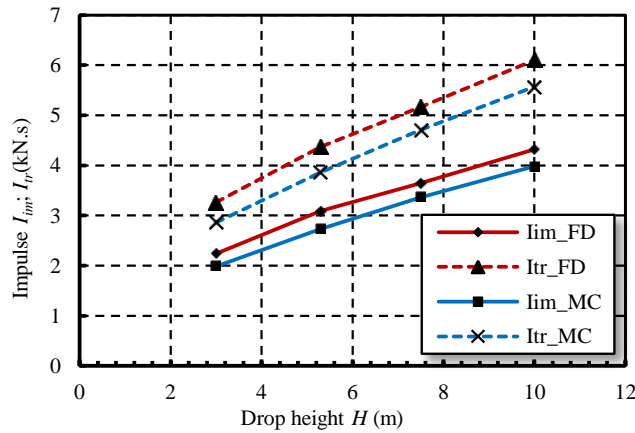


Figure 3.21 Relationships between the drop height and the impulse from the impact force and the transmitted force

The time histories of the transmitted force for the FD and MC conditions are shown in Figure 3.18. They were similar in shape to the corresponding impact force histories shown in Figure 3.17. However, with increasing drop height, the maximum values clearly increased from 93 to 193 kN and from 157 to 360 kN for the FD and MC conditions, respectively. The time lag of the transmitted forces for the FD condition was less than that for the MC condition (5.0 and 7.5 ms, respectively). In contrast, the

duration of the transmitted force for the FD condition was twice as long as that for the MC condition.

Figure 3.19 shows the relationships between the maximum impact force, maximum transmitted force, and drop height. The transmitted forces were always higher than the impact forces. The impact force values for the MC condition were 3 to 5% greater than those for the FD condition, whereas the transmitted force values were 70 to 80% higher than those for the FD condition. In particular, each curve in this figure tended to approach a limiting value.

Figure 3.20 shows the relationship between the drop height and the maximum penetration depth for the two boundary conditions. The penetration depth increased with the drop height and was much greater for the FD condition than for the MC condition. As the drop height increased from 3 to 10 m, the maximum penetration depths for the FD and MC conditions also increase, from 26 to 40 cm and from 17 to 32 cm, respectively.

The relationships between the drop height and the impulse from the impact force and transmitted force for both the FD and MC conditions are shown in Figure 3.21. The impulse increased almost linearly with the drop height. The impulses were slightly larger than the initial momentums of the weight for both the FD and MC conditions. The rebound of the weight caused these differences. Observation of animations of the simulated results and analysis of the velocity, penetration depth, and contact force histories of the weight also confirmed this assessment. Impulses from the transmitted force were larger than those from the impact force for both the FD and MC conditions. Also, the impulses for the FD condition were slightly greater than those for the MC condition. This indicates that the rebound of the weight for the FD condition was larger.

From the above discussion concerning the FD and MC conditions, it is clear that the maximum transmitted force for the MC condition was adequate to design a protection structure because it provided a safer estimate for impacts by rockfall. Also, building a wall using geocells spaced with gaps is difficult. Thus, the MC condition is more realistic and more amenable to actual designs.

3.7 Conclusion

This paper presented a numerical approach utilizing the FEM code LS-DYNA to model the sand cushion of a protection structure subjected to rockfall impact. The

numerical model and its parameters were carefully considered through a parametric study and validation steps. The behavior of a sand cell depending on the drop height of a weight was then evaluated using the validated model. The final results obtained by this study can be summarized as follows.

The characteristics of the sand used as a cushioning layer were investigated. The shear modulus G , bulk modulus K , angle of internal friction ϕ , and relationship of pressure versus volumetric strain of the sand were very important, as indicated by the results of the sand tank simulations.

The FEM simulation (LS-DYNA) using the “MAT_SOIL_AND_FOAM” model could reproduce the impact in the sand tank and on the sand cells with sufficient accuracy for practical use.

The impact behavior on the sand cell under the FD (free deformation) and MC (material confinement) conditions indicated that the lateral boundary conditions had a significant effect on the results.

The transmitted force for the MC condition was adequate to design a protection structure for a rockfall. The MC condition provided a safer estimate than the FD condition did.

The advantages of this research have been described above. The effectiveness of this simulation method was confirmed for drop heights of less than 10 m using a weight with a mass of 260 kg. However, further investigation is necessary to study impacts over a larger energy range.

This research contributes a better understanding of the influence of sand properties on impact behavior. The success of this research presents new possibilities concerning dynamic analysis by FEM of structures with a sand cushioning layer. The results of this study promote further investigations of impact issues using full-scale rockfall protection walls, galleries, and embankments with sand cells as the cushioning layer.

References

- Calvetti, F., Di Prisco, C., Experimental and numerical study of rock-fall impacts on granular soils, *Rivista Italiana Di Geotecnica*, pp. 95–109, 2009.
- Bertrand, D., Nicot, F., Gotteland, P., Lambert, S., Modeling a geo-composite cell using discrete analysis, *Computers and Geotechnics*, Vol. 32, pp. 564–577, 2006.

- Bourrier, F., Lambert, S., Heymann, A., Gotteland, P., Nicot, F., How multi-scale approaches can benefit cellular structure design, *Canadian Geotechnical Journal*, Vol. 48, pp. 1803–1816, 2011.
- Bhatti A.Q. Kishi, N., Impact response analysis of prototype RC girders with sand cushion using equivalent fracture energy concept, *International Journal of Damage Mechanics*, Vol. 20, Issue 7, pp. 1094–1111, 2011.
- Breugnot, A., Gotteland, Ph., Villard, P., Numerical modelling of impacts on granular materials with a combined discrete–continuum approach, *Numerical Methods in Geotechnical Engineering – Benz & Nordal*, pp. 477–482, 2010.
- Kieg R., D., A simple constitutive description for cellular concrete, Sandia report SC-DR-72-0883, 1972.
- Konno, H., Kishi, N., Nishi, H., Ishikawa, H., The effects of cushion materials on impact resistant behaviour of full-scale arch type RC structures, *Proceedings of PROTECT2009*, Hayama, Japan, Aug. 19–21, CD-ROM, 2009.
- Lambert, S., Gotteland, P., Nicot, F., Experimental study of impact response of geocells as component of rockfall protection embankment, *Natural Hazards and Earth Systems Science*, Vol. 9, pp. 459–467, 2009.
- Lambert, S., Nicot, F., Gotteland, P., Uniaxial compressive behavior of scrapped-tire and sand-filled wire netted geocell with a geotextile envelope, *Geotextiles and Geomembranes*, Vol. 29, Issue 5, pp. 483–490, 2011.
- Lambert, S., Heymann, A., Gotteland, P., Real-scale experimental assessment of cellular rockfall protection structures, *Interdisciplinary Rockfall Workshop 2011*, Innsbruck, 2011.
- LST (Livermore Software Technology), *LS-DYNA Keyword User’s Manual*, Vol. I, Version 971, 2011.
- Masuya, H., Nakata Y., Development of numerical model combining distinct element and finite element methods and application to rock shed analysis, *Proceedings of the Japan Society of Civil Engineering*, No 710/I, pp. 113–128, 2002.
- Masuya H., Aburaya Y., Futo S., Sato A., Nakamura S., Experimental study of the weight collision on a sand cushion and its impact action, *8th International Conference on Shock and Impact Loads on Structures*, Adelaide, Australia, 2009.

- Matsuo, O., Tsutsumi, T., Sasaki, T., Current states of practices and technical issues of rockfall disasters and their mitigation measures in Japan, Proceedings of the Joint Japan Swiss Scientific Seminar on Impact Load by Rock Falls and Design of Protection Structures, edited by Masuya, H. and Labiouse V., pp. 7–12, 1999.
- Matsuo, O., Ikeda, K., Muraishi, H., Countermeasures for rockfalls: 2. Outline of Countermeasures for rockfalls, Tsuti to Kiso, Journal of the Japanese Geotechnical Society, Vol. 50, No. 1, pp. 41–44, (in Japanese), 2002.
- Nicot, F., Gotteland, P., Bertrand, D., Lambert, S., Multi-scale approach to geocomposite cellular structures subjected to impact, International Journal for Numerical and Analytical Methods in Geomechanics, Vol. 31, pp. 1477–1515, 2007.
- Wang J.G., Sun W., Anand S., Numerical investigation on active isolation of ground shock by soft porous layers, Journal of Sound and Vibration, Vol. 321, pp. 492–509, 2009.
- Wang Z.L., Li Y.C., Wang J.G., Numerical analysis of attenuation effect of EPS geofoam on stress-waves in civil defense engineering, Geotextiles and Geomembranes, Vol. 24, pp. 265–273, 2006.
- Vogel, T., Labiouse, V., Masuya, H., Rockfall protection as an integral task, International Association for Bridge and Structural Engineering (IABSE), Vol. 2, No. 9, pp. 304–312, 2009.
- Wesseloo, J., Visser, A.T., Rust, E., The stress–strain behaviour of multiple cell geocell pack, Geotextiles and Geomembranes, Vol. 27, pp. 31–38, 2009.
- Yoshida, H., Masuya, H., Ihara, T., Experimental study of impulsive design load for rock sheds, IABSE Proceedings, pp. 88–127, 1998.

Chapter 4 Impact experiment on sand tank over steel H-beams

over steel H-beams

4.1 Introduction



Figure 4.1 Steel rockshed

In general, rockfall protection structures are classified into nets, fences, shelves, walls, embankments, and rocksheds, etc. (JRA, 2000), (Vogel et al., 2000). Rockshed is one of the safe and prevalent protection structures adapted to large energy of the target rockfall. In Japan, many steel galleries have been constructed, mostly to against snow avalanches and land-slides. However, some of these galleries are solid and accompanied with the cushion layer on roof to mitigate even rockfall (Figure 4.1), so called steel rockshed. This cushion layer is used to buffer the impact force due to the rockfall. Sand has been mostly used as a typical cushion material in Japan. Sand and a bag in which sand is filled are also used as a protection shelf or protection embankment for the same purpose. However, risk has occurred sometimes at the protection structures with large

energy beyond initial estimation, even firm pre-stressed concrete rocksheds (Schellenberg et al., 2009), (Delhomme et al., 2005).

Research of this shock absorbing material has been done for years (Masuya et al., 2009). However, the evaluation method of impact behavior, the energy absorbing efficiency and the transmitted energy to the structure through the cushion have not been clarified satisfactory enough. Empirically, the sand cushion has a good shock absorbing efficiency. Therefore, the use of sand cushion material for protection structures, such as a rockshed, is considered rationally.

When a protection structure is designed basing on the idea of a performance-based design, it is necessary to clarify the ultimate state of the protection structure, in which sand cushion is installed. It is also required to advance appropriate employment of cushion material for reparation and/or reinforcement purposes towards the existing structure. In this research, the series of impact experiments on H section steel beam with the sand cushion were conducted with the aim of obtaining the fundamental data about the impact action, facilitating designing a protection structure safely and rationally. This paper reports the knowledge acquired by investigating on the impact force, the absorbing effect of sand cushions, and dynamic interaction between the structure and cushion. Two empirical equations expressing the relationship between oscillation characteristics of the structure and dynamic factor and energy transfer rate were also established and presented in the paper.

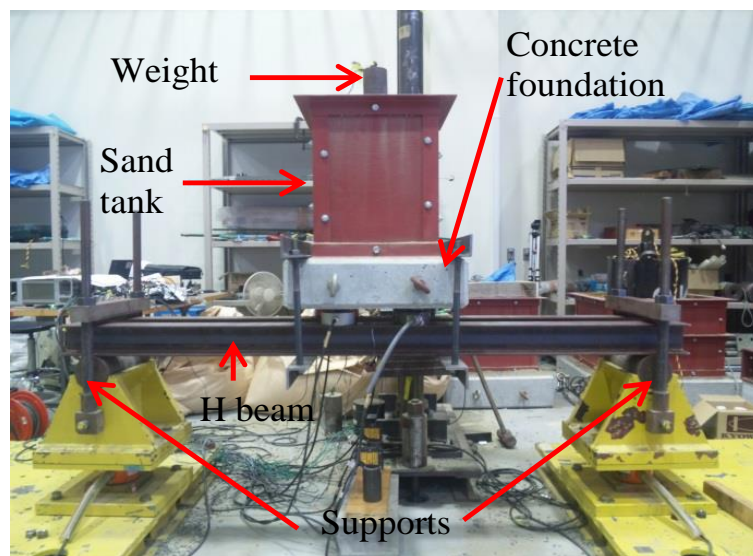


Figure 4.2 An impact experiment using 1.8 m span length

4.2 Outline of experiment

4.2.1 Method of experiment

Figure 4.2 shows the free-fall type devices for impact experiment set up at the Structure Engineering laboratory of Kanazawa University. The sand tank filled up with sand cushion material was fixed to two H-beams with the angle steel beams and bolts in the center of the H-beams, which were simply supported and located in parallel. The inner size of the sand tank was 0.35 m wide, 0.35 m deep and 0.50 m high.

Table 4.1 Properties of used cushions

Type	D_{10} (mm)	D_{30} (mm)	D_{60} (mm)	Effective particle size D_{50} (mm)	Uniformity coefficient C_u	Coefficient of curvature C_c
Sand	0.2	0.34	0.61	0.49	3.10	0.95
Gravel	4.0	5.5	6.5	6.1	1.63	1.16

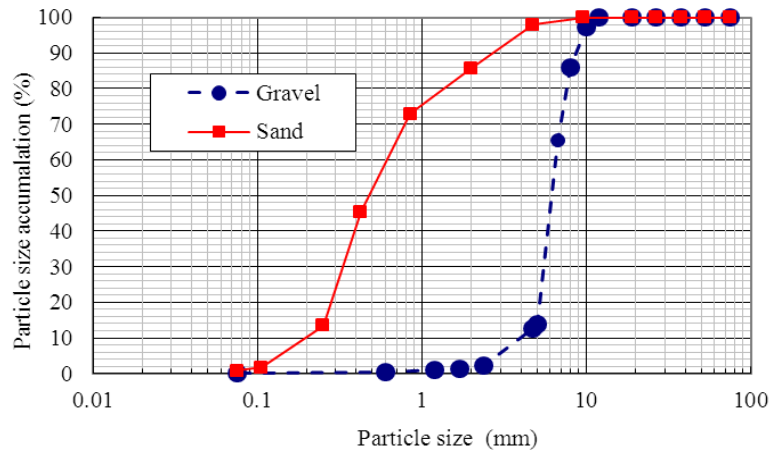


Figure 4.3 Particle size accumulation curve

The H-beams were H-100 × 100 × 6 × 8 (mm). The span lengths of beam were 1.3 m, 1.8 m, 2.8 m, and 3.8 m. The weight was a steel cylinder with diameter of 0.08 m, height of 0.185 m, and mass of 7.233 kg and the tip form was spherical. Regarding to laboratory conditions, for instance, containing tank and steel beam dimensions are small, loose sand and stone-crushed gravel with small particle sizes were used as two kinds of shock absorbing material. The characteristics of sand and

gravel and their grain size ranges were shown in Table 4.1 and Figure 4.3. These cushioning materials were laid (into the tank) layer by layer of 0.05 m with slight degree of compaction until the final thickness of 0.5 m.

Table 4.2 List of impact experiments

Cushion	Span length of beam (m)	Falling heights of weight (m)
Sand	1.3	0.50,0.75,1.00,1.25,1.50,1.75,2.00
	1.8	
	2.8	
	3.8	
Gravel	1.3	0.50,0.75,1.00,1.25,1.50,1.75,2.00
	1.8	
	2.8	
	3.8	

Table 4.2 indicates the list of all experiments carried out. The falling heights of the weight were seven kinds respectively 0.5 m, 0.75 m, 1.0 m, 1.25 m, 1.5 m, 1.75 m, and 2.0 m. For each case, the experiment was repeated three times.

4.2.2 Measurement Items and Measurement Method

Measurement devices include an accelerometer (Kyowa Electronic Instruments Co., Ltd., AS-100HA), load cell (Kyowa Electronic Instruments Co., Ltd., LUK-1TBS), laser displacement meter (Keyence Corporation, LB300), and strain gauge (Tokyo Sokki Kenkyujo Co.,Ltd., FLA-10-11-3-LT) as shown in Figure 4.4.

Concretely, the accelerometer was installed at the center of the weight to measure its acceleration. The laser displacement meter was used to measure deflection of the steel beams. The transmitted force of sand tank to H beams was summed from four measured loads by the load cells placed between the tank bottom and the beams. The strain gauges mentioned above were stuck to measure axial direction strain at the top and bottom flange of the central section of H beams.

Figure 4.5 describes the measurement system of this experiment. The output obtained from each measuring instrument was measured at intervals of the sampling of 100 μ s (sampling frequency: 10 kHz) and recorded by PC.

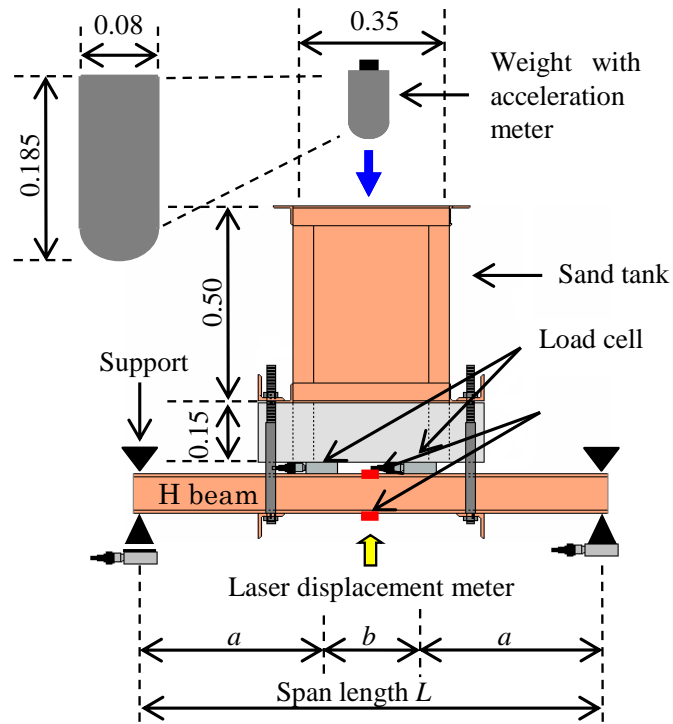


Figure 4.4 Measure devices and dimensions

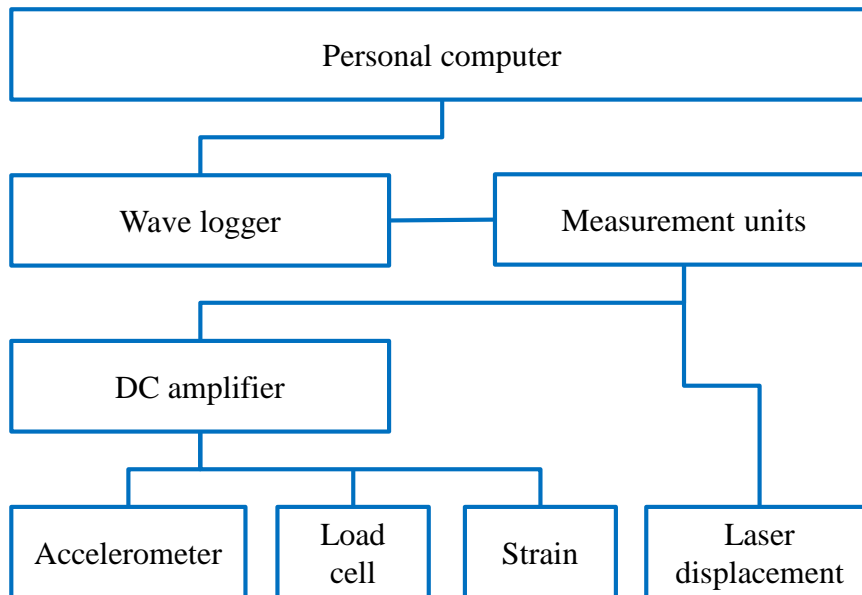


Figure 4.5 Measurement system

4.3 Results of experiment

4.3.1 *Dynamic behavior of impact experiment*

Figure 4.6 shows the time history of measured data in the case of using 1.8 m in span length, 2.0 m in falling height, and sand cushion. The acceleration of the falling weight reached the minus peak at approximately 0.01 s after having collision into the sand cushion and became zero at 0.02 s because of deceleration. The transmitted force under the sand tank appeared at 0.005 s, reached its peak at 0.016 s and became zero at 0.025 s. The damped oscillation of the transmitted force was shown afterward. Strain and displacement appeared at 0.01 s, also reached their peaks at approximately 0.016 s and became zero at 0.025 s. The similar damped oscillations were presented afterward in both time histories.

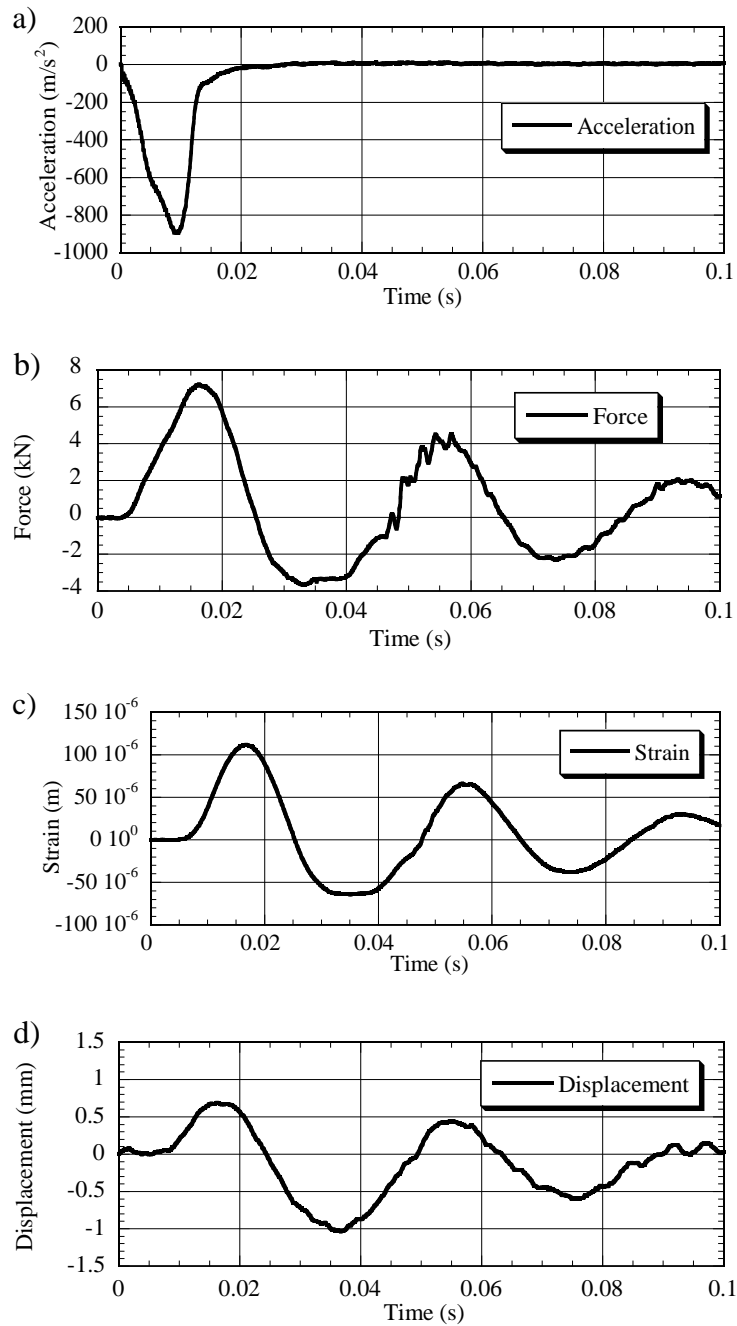


Figure 4.6 Time histories of measured data (Sand, 1.8 m in span length, 2.0 m in falling height): a) acceleration; b) transmitted force; c) strain; d) deflection

Generally, the dynamic behavior of structure under hard impact load is complicated. The hard impact herein means that the magnitude of impulse force is large and duration of impact is very short. Meanwhile, it is also known that the response of structure under relatively soft impact load is mostly quasi-static. Those beams used in this study had large mass at the center of span. The impact load, furthermore, occurred

due to the collision of the weight with the cushion is relatively smooth because of the shock absorbing effect of the cushion material. In that case, it can be assumed that the response of the beam was quasi-static. Figure 4.7 shows the deflection curve and the bending moment diagram of the simple beam under two static concentrated loads. Equivalent static forces can be determined according to the deflection and the strain resulted from bending moment under this assumption. Hence, P_s and P_d are two equivalent forces that were determined by the strain and the deflection respectively as follow.

$$P_s = \frac{2EI(\varepsilon_u + \varepsilon_l)}{ah} \quad 4.1$$

$$P_d = \frac{48EId}{a(8a^2 + 12ab + 3b^2)} \quad 4.2$$

In these equations, ε_u and ε_l are the measured strains at upper and lower flanges of H-beam, d is measured deflection of the beam, E and I are Young's modulus and moment of inertia of area, h is the height of H-section, and a and b are geometrical dimensions of the beams as shown in Figure 4.4 and 4.7.

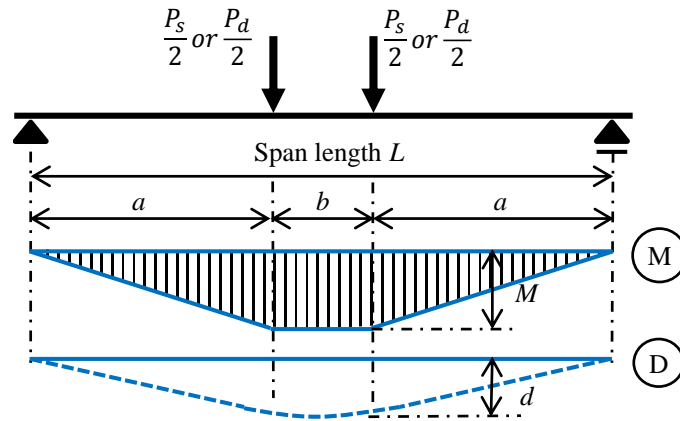


Figure 4.7 Bending moment diagram (M) and displacement curve (D) of the simple beam resulted from equivalent static forces P_d and P_s ; a and b are distances from support to load cell and between two load cells respectively

Figure 4.8 illustrates time histories of the impact force, transmitted force, and equivalent forces determined by strain and deflection for four cases, which are combinations of two types of span length (1.8 m and 3.8 m) and two types of cushion material (sand and gravel). The falling height H was 2.0 m in any case. Impact force P_a was calculated by multiplying the measured acceleration by the weight mass and expressed

in positive value. In the case of using sand cushion and span length $L = 1.8$ m, the impact force P_a was smaller than the other forces. The maximum of force was upward in the order of the transmitted force P_t , the strain equivalent force P_s and the deflection equivalent force P_d . By contrast, the impact force P_a was larger than other forces for the case of sand cushion and the longest span length $L = 3.8$ m. The shape of the first wave of the transmitted force P_t was similar to the impact force P_a . However, after the first wave, the shape of P_t , P_s , and P_d were similar. This characteristic was not observed for the span length $L = 1.8$ m. Furthermore, comparing the results of impact on sand with two span lengths indicated that the short span length obtained smaller impact force, larger transmitted and equivalent forces, and shorter oscillation periods than those with long span length did. For the gravel, the similar tendencies were observed.

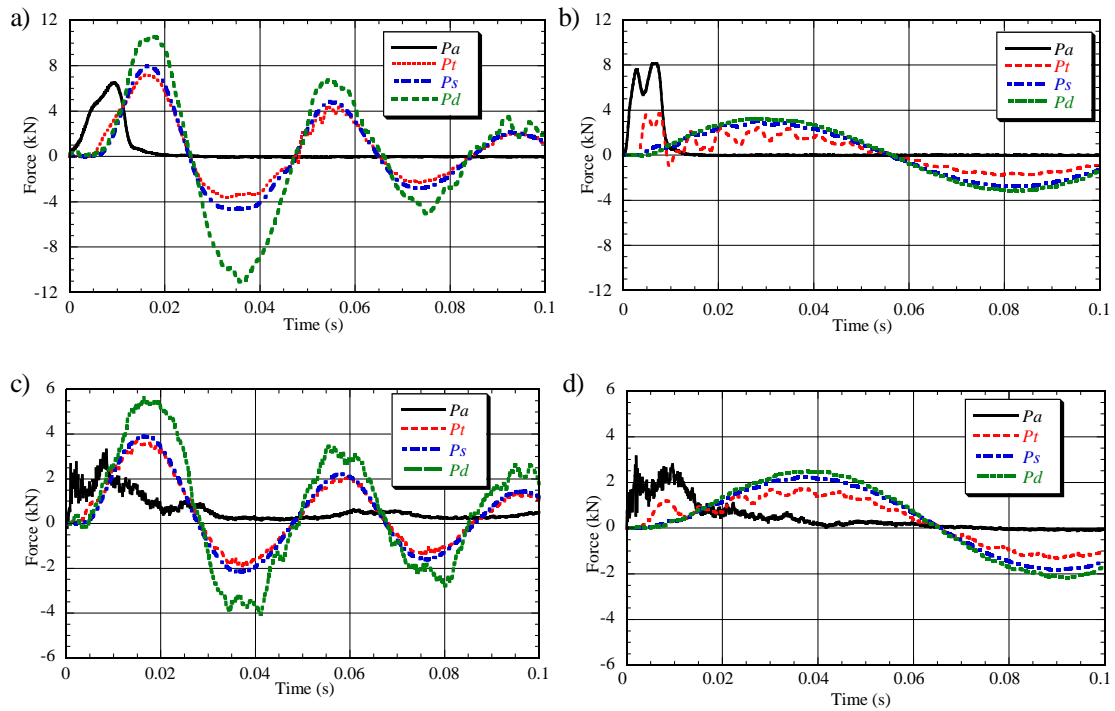


Figure 4.8 Impact force, transmitted force and equivalent forces by strain and deflection: a) Sand ($L = 1.8$ m, $H = 2.0$ m); b) Sand ($L = 3.8$ m, $H = 2.0$ m); c) Gravel ($L = 1.8$ m, $H = 2.0$ m); d) Gravel ($L = 3.8$ m, $H = 2.0$ m)

Maximum values of forces obtained by impact on gravel, however, were smaller than those values obtained by impact on sand. It becomes clear that the shock absorbing ability of the gravel was more efficient than that of the sand. The length of beam span itself also played an important role in the impact characteristics. In addition, due to

different from values of P_d to P_s and P_t , it is hereafter focused on the strain equivalent force only.

The final penetration depths obtained by double integrating with respect to time varied correspondingly to type of cushioning material and falling height. For example, the penetration depth varied from 0.012 m to 0.031 m in the case of sand cushion, and from 0.052 m to 0.115 m in the case of gravel cushion in accordance with the change of falling height from 0.5 m to 2 m. Contribution of beam deflection on penetration of the weight was slight degree. With increase of falling height, i.e., higher level of impact energy, the increase of penetration depth is reasonable. Concerning the influence of types of cushioning material to the penetration depth by which gravel resulted much higher depth than sand could be attributed to the compaction density of material, which is higher for sand because of its wide range of particle size (contrasting to almost uniform particle size of gravel).

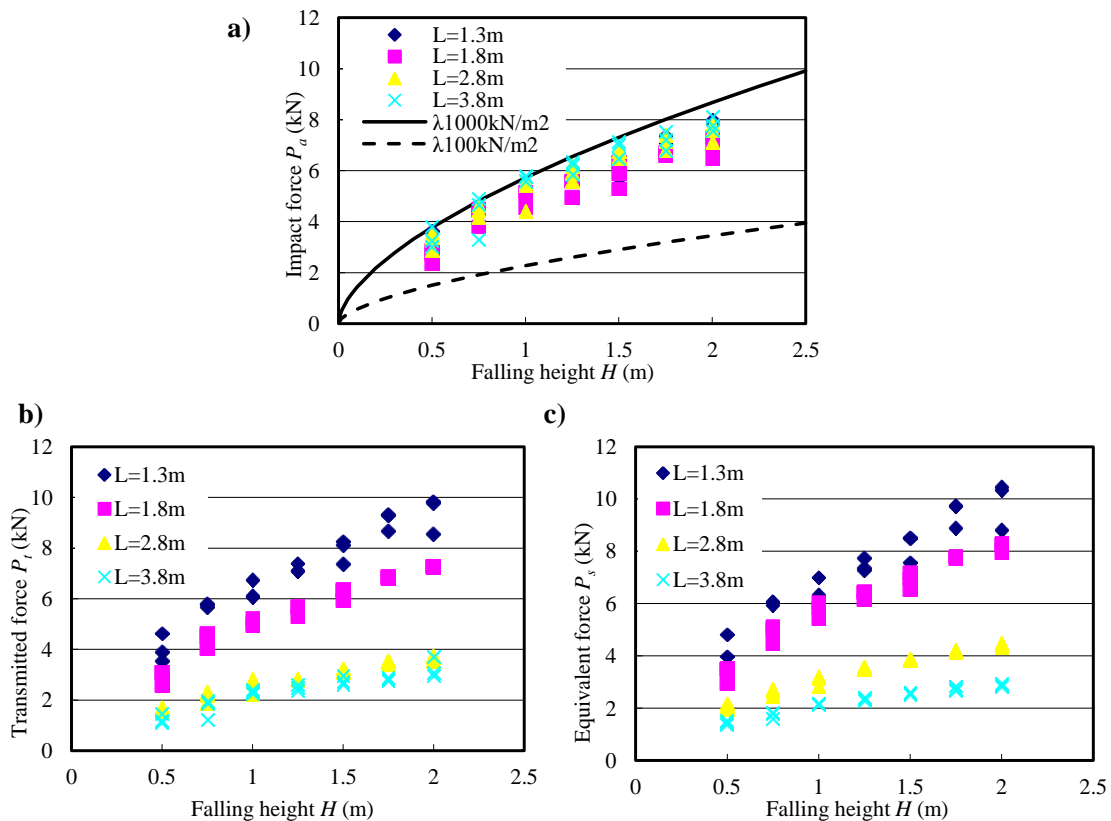


Figure 4.9 Relationship between falling height and various maximum forces for sand: a) Falling height and impact force P_a ; b) Falling height and transmitted force P_t ; c) Falling height and equivalent force P_s

4.3.2 Maximum impact force

Figure 4.9 shows the relationship between the falling height and various maximum impact forces for sand. In Figure 4.9 a), line graphs estimated by the design formula for the impact load due to rockfall are shown. The formula was drawn from the elastic contact theory and widely used in Japan. This design formula is expressed as the following equation 4.3.

$$P = 2.108(mg)^{2/3} \lambda^{2/5} H^{3/5} \quad 4.3$$

In this equation, m is the mass of a falling rock (ton), H is the height of a rockfall (m), λ is the Lamé coefficient of cushioning material (kN/m²) and g is the gravity acceleration (m/s²).

There is no significant difference in the impact force P_a with the change of span length L . A long time lag of the reactions of the beam, namely strain and displacement, could be a reason. For instance, from experimental results as shown in Figure 4.8 a), the impact force reached its peak at about 0.01 s, at that time, strain and deflection equivalent forces took first five of their maximum values. The upper limit of the impact force was expressed as result of the equation 4.3 with $\lambda=1000$ kN/m². Concerning the transmitted force P_t and the equivalent force P_s , it is understood that the longer span length, the smaller force. The strain equivalent force P_s was slightly larger than the transmitted force P_t .

Furthermore, Figure 4.10 shows the relationship between the falling height and various maximum impact forces for gravel. The maximum values of impact force P_a with gravel cushion varied also insignificantly with the difference span lengths L as observed in the case of sand. These values that distributed around the lower limitation of the impact force were expressed by equation (3) with $\lambda = 100$ kN/m². Except P_s was smaller than P_t , other features about P_s and P_t were also similar to those for sand cushion.

4.3.3 Impulse by impact force

Figure 4.11 presents impulse by impact for two kinds of cushion material with different falling heights and initial momentum. The impulse value resulted from integrating impact force with respect to time. In general, these impulse values varied in curves of quadratic function, the same as the relationship of the initial momentum and the falling height. Particularly, the impulse values by the impacts from the experiments

using sand cushion were much higher than that using gravel cushion and initial momentum. Additionally, the impulses by impact on sand and gravel cushion tended to be independent on the beam span length.

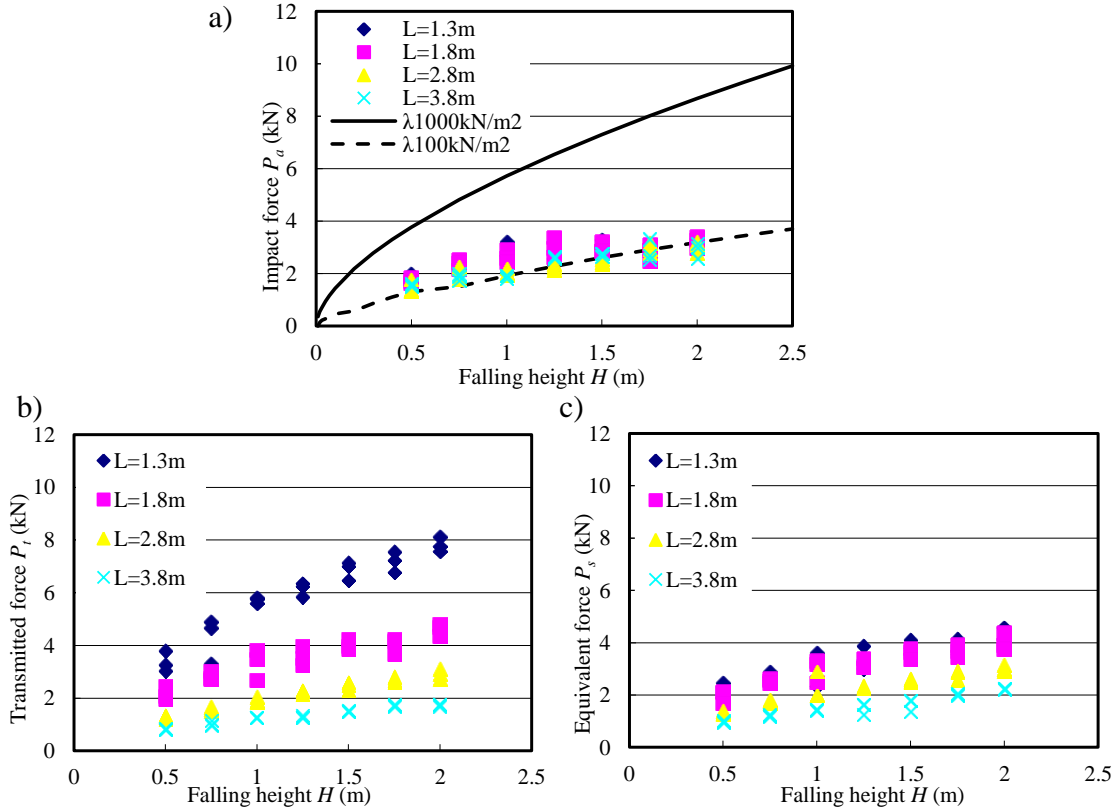


Figure 4.10 Relationship between falling height and various maximum forces for gravel: a) impact force P_a ; b) transmitted force P_i ; c) equivalent force P_s

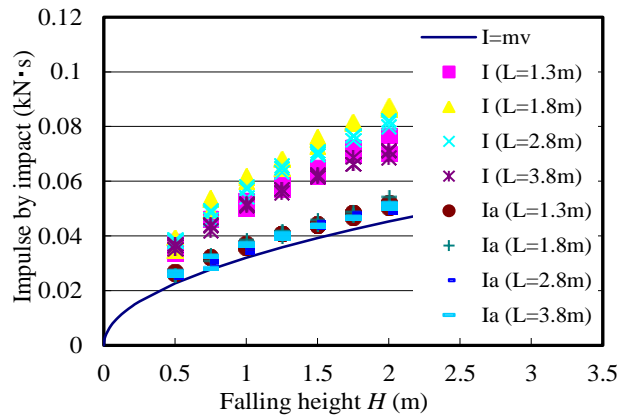


Figure 4.11 Relationship between falling height and impulse by impact force

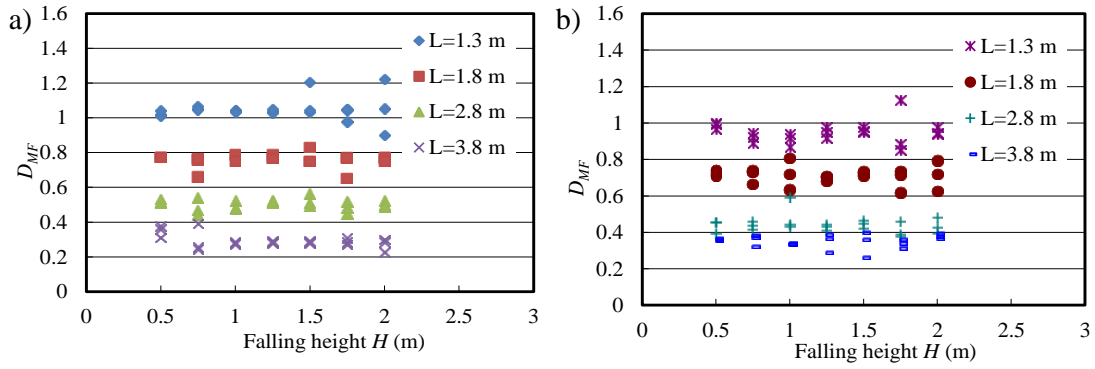


Figure 4.12 Falling height and dynamic multiplication factor (D_{MF}): a) sand cushion; b) gravel cushion

4.3.4 Dynamic multiplication and energy transfer

It is generally required to rationally and safely estimate the impact load for the practical design of protection structure. Some experimental results and discussions are shown in this section concerning the dynamic multiplication and energy transfer from the falling weight to the beam.

Figure 4.12 presents the results concerning the dynamic multiplication factor related to different falling heights for sand and gravel respectively. The dynamic multiplication factor is generally expressed as the following equation.

$$D_{MF} = \frac{R_{dyn}}{R_{st}} \quad 3.4$$

In this equation, R_{st} is the response of the structure when the maximum dynamic force acts statically and R_{dyn} is the dynamic response of the structure. In this case, strain is represented for the response of structure. It is clear that there was no particular relationship between the falling height H and the dynamic multiplication factor D_{MF} and this relation was mostly constant. In other words, D_{MF} was independent from energy magnitude. However, the larger the span length L of the beam, the smaller the dynamic multiplication factor D_{MF} . This is because the longer span beam had the longer first natural period T for mostly constant duration of impact force T_a . Furthermore, D_{MF} of the experiment with gravel cushion was smaller than that with sand cushion.

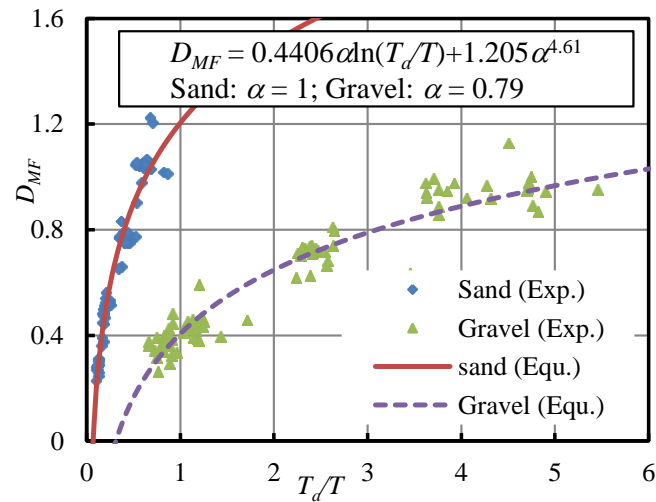


Figure 4.13 Relationship between T_a/T and dynamic multiplication factor D_{MF} (T_a : duration of impact force, T : the first natural period of beam) and its corresponding practical equation

Figure 4.13 shows the relationship between T_a/T and dynamic multiplication factor D_{MF} obtained by the experiments and practical equation. Whereas T_a/T is the ratio of duration of impact force and natural period of structure. It is clearly recognized that there is a logarithmic relationship between T_a/T and the dynamic multiplication factor D_{MF} . Therefore, the equation of the relation between D_{MF} and T_a/T obtained from nonlinear regression analysis was also established as follows:

$$D_{MF} = 0.4406\alpha \ln\left(\frac{T_a}{T}\right) + 1.205\alpha^{4.61} \quad 4.5$$

In this equation, α is material effect factor, and respectively to be 1 and 0.79 according to sand and gravel cushions. The correlation index, R^2 , of this equation is 0.93. As result of this equation, the line chart of sand cushion was steeper than that of gravel cushion. In other words, as above finding about characteristic of impact, the impact on structure using sand cushion was harder than that on structure using gravel cushion.

Figure 4.14 shows the relationship between β and energy transfer rate (ETR) with two kinds of absorbing material. ETR is the proportion (percentage) of transferred energy from the potential energy of the weight to the beam. It is evident that ETR declined as β became larger. ETR is greatly useful in designing structural components subjected to impact, such as roof, support beams, and columns of rockshed. Moreover, ETR can disclose the effectiveness of shock absorbing cushion. For instance, the case of gravel cushion had smaller ETR , i.e., higher energy absorption capacity. In this figure,

the equation of the relation between T_d/T and ETR is also presented with 0.83 of the correlation index.

$$ETR = -0.9266\beta \ln\left(\frac{T_d}{T}\right) + 0.8879\beta^{-0.71} \quad 4.6$$

In this equation, β is material effect factor and determined to be 1 and 0.69 corresponding to sand and gravel respectively. The line graphs shown in Figure 4.14 are results of this equation.

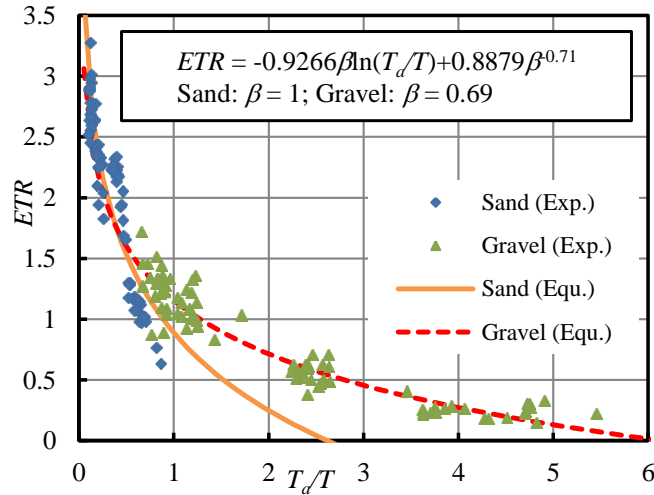


Figure 4.14 Relationship between T_d/T and of energy transfer rate (ETR) and its corresponding practical equation

The results of D_{MF} and ETR obtained from the equations as shown in Figure 4.13 and 4.14 indicate that with the same T_d/T the larger grain size of cushioning material used, the smaller dynamic multiplication factor D_{MF} and the larger energy transfer rate ETR as well. Furthermore, Figure 4.14 illustrates that if T_d/T was smaller than 0.5, ETR was similar with any types of cushioning material, i.e., independent from cushioning material, but rather depended on T_d/T . It is expected that further experimental results would give more general applicability range of equation 4.5 and 4.6.

4.4 CONCLUSION

In this chapter, series of impact experiments on H-section steel beam with sand cushion were conducted in order to obtain the fundamental data about the impact action. Obtained results in this research are summarized as follows.

1. The dynamic behaviors of steel H-beam with cushion under impact were concretely shown including characteristic of the impact force. The concept and actual data concerning the equivalent forces were introduced and shown.
2. With the increase of falling height H , the impact force P_a obtained by the acceleration of the weight colliding on sand cushion was constantly larger than that in the case of gravel cushion.
3. The transmitted force at the bottom of cushion P_t and two kinds of equivalent force P_s and P_d were evidently affected by the span length L , falling height H and cushion material, the larger L and H the higher maximum force. Thus, the force in gravel cushion was smaller than that in sand cushion.
4. Impulse by impact I had quadratic relationship with the falling height of the weight H for both sand and gravel cushion.
5. The dynamic multiplication factor D_{MF} had particular relationship with the natural period of the beam T and no relation with the falling height H .
6. The rate of energy transferring to the beam from falling weight, ETR , was concretely shown. It has been pointed out that the relationship between ETR and the natural period of the beam T should be considered.
7. Two equations evaluating dynamic multiplication factor D_{MF} and energy transfer rate ETR were established and presented. This achievement offers an application for the similar impact protective structure with sand cushion.

References

- JRA - Japan road association, Handbook of preventatives against rockfalls, 2000 (in Japanese).
- Vogel T., Labiouse V. and Masuya H., Rockfall Protection as an Integral Task, Structural Engineering International, Vol. 9, No.3, pp.304-3124, 2000.
- Schellenberg, K., On the Design of Rockfall Protection Galleries, Doctoral theses, Swiss Federal Institute of Technology Zürich, No. 17924, 2009.
- Delhomme F., Mommessin M., Mougin J.-P., and Perrotin P., Behavior of a structurally dissipating rock-shed: experimental analysis and study of punching effects, Int. J. Solids Struct., Vol. 42, No.14, pp. 4203–4219, 2005.

Masuya H., Aburaya Y., Futo S., Sato A. and Nakamura S., Experimental study of the weight collision on a sand cushion and its impact action, Proceedings of 8th International Conference on Shock & Impact Loads on Structures, pp. 429-434, 2009.

Chapter 5 Numerical simulation of impact on rockfall protection fence

5.1 Introduction

Rockfall disasters sometimes occur in mountainous areas together with landslides or debris. Recently, many rockfall protective structural countermeasures including galleries, embankments, nets, and fences have been developed, tested, and applied against the ravages of rockfall hazards. Relative small scale landslide and debris mass covering on the mountainous side of the gallery and embankment seems to have a certain influence on the structure in service. However, it is generally thought that the covered mass on fence or net should be removed to avoid unexpected effects when a rockfall may occur successively. This idea could be true for the fence and net using energy absorbing devices because the death load caused by the covered mass weight remaining for a long time may affect the mechanical behavior of the devices. When there is no enough space between maintain slope and road at the site, the fence as one of structural countermeasures is constructed without energy absorbing devices as presented in Figure 5.1, the behavior, allowable state and limit state of the fence should be carefully and thoroughly investigated for the accurate evaluation.

Protective fence has been widely used (Volkwein et al., 2011) worldwide. Therefore, it has drawn special concerns in many studies related). Many types of fence have been investigated both experimentally and analytically such as ring netting fences (Gentilini et al, 2012), cable wire fences (Tran et al., 2012), pocket-type nets (Dhakal et al., 2011), and cable netting fences (Cazzani et al., 2002 and Nishita et al., 2011). These fences involve either energy absorbing elements or additional upslope ropes.

Studying on sand behaviors as cushioning layers in rockfall protection structures has been conducted widely with experiments (Masuya et al., 2009 and Kishi et al, 1993) and simulations (Ho et al., 2013). The use of sand-pack to induce the death load acting as landslides was first mentioned in Nishita et al. (2011) with a series of experiments,

and some remarkable notices were found in the study. Long time and high cost are required to verify the performance for various compositions of structure and boundary conditions, which should be considered. This issue prevents technical development and actual construction of protective structures. Numerical approach used in this study, which is expected one of the effective method to solve the limitations of the experiments and gain significant insights into mechanical characteristics of structure.



Figure 5.1 Rockfall protection fence

As mentioned above, Nishita first presented his experimental studies on effects of sand-pack on impact phenomenon of the net and fence. At first, a cable netting fixed to a firm steel frame was subjected to a drop weight, the net was or was not covered by sand-packs. Impact force, impulse by impact, and reaction forces mobilized from the connections at the corners of the netting were obtained and those data were used to evaluate the effect of sand-pack (Nishita et al., 2011). Subsequently, full-scale models of fences were designed for a series of impact experiments to deal with varied impact energy magnitudes and mass of the covered sand-pack as well as failure of structure (Nishita, 2012). The fences used in this study had not any energy absorbing device. Therefore, steel post with high performance were utilized as the main supporting structure referring to the real structure as shown in Figure 5.1. The obtained results from this study provided an overall view of a rockfall collision on fence following a land-

slide. However, the experimental studies seem hardly to reveal insights into structure responses.

To obtain the achievement, the fence models which were simulated by LS-DYNA explicit finite element method (FEM) code underwent a careful validation. This numerical tool has been successfully used to reproduce the impact behaviors of sand and sand cell subjected to dynamic load of the drop weight by Ho et al., (2013). The validated models were used to investigate the mechanical behaviors of the fence corresponding to the change of the impact energy magnitude. The results indicated that sand-pack or landslide mass remarkably influences the mechanical characteristics of the fence bringing both advantages and disadvantages points. For the positive effects, the sand pack could be considered to be used for some practical applications.

5.2 Outline of preceding experiments

The experiments were conducted at the site located in Niigata, Japan. The aims of the achieved experiments were to test the performance of the new multi-purpose protection fence against rockfalls, landslides, and debris and to obtain insights into impact behavior of fence as well as to provide useful data for numerical approach.

This type of fence is generally installed vertically to catch boulders and debris from mountainous side as shown in Figure 5.1. A large and suitable site area and many specific experimental tools are required to reproduce perfectly the dynamic behavior of a fence with horizontal impact. For the sake of simplicity and safety, series of experiments were conducted using the fence installed horizontally. The fence was subjected to a vertical impact by a free falling weight.

In this study, two types of impact experiments on rockfall protection fence, namely the fence excluding sand-pack cushion (FES) and the fence including sand-pack cushion (FIS) were conducted. Each type of fence was conducted with two different drop heights of 10 m and 7 m, corresponding to the energy magnitudes of 100 kJ and 70 kJ respectively.

5.2.1 Setup of the fence excluding sand-pack (FES)

Figure 5.2 and Figure 5.4 show the drawings of the fence used for the experiment and the installation view. This fence with three 5 m-long-spans consisted of three

interceptive cable and hexagonal steel nets, four posts, a border cable system and a rigid frame. The cable and hexagonal steel nets were 5 m long and 4 m wide, installed within the interspace of the posts. The cable net was woven by impaling one 12 mm-diameter cable wire (FC6×24, denoted Cable A) through another (denoted Cable B) to create a mesh with a square grid of 0.5 m in diagonal as shown in Figure 1 c). Steel wire ropes FC6x24 were specified by JIS 7301 corresponding to ISO 2408 (Steel wire ropes for general purposes–Characteristics). This weave type enabled the Cable B (parallel with diagonal of the net) to slide on the Cable A at the mesh joints. The cable net was one of main interceptive parts of fence system. The surface of cable net was covered by hexagonal steel net with 2.7 mm–diameter wire to disperse partly impact energy and arrest debris.

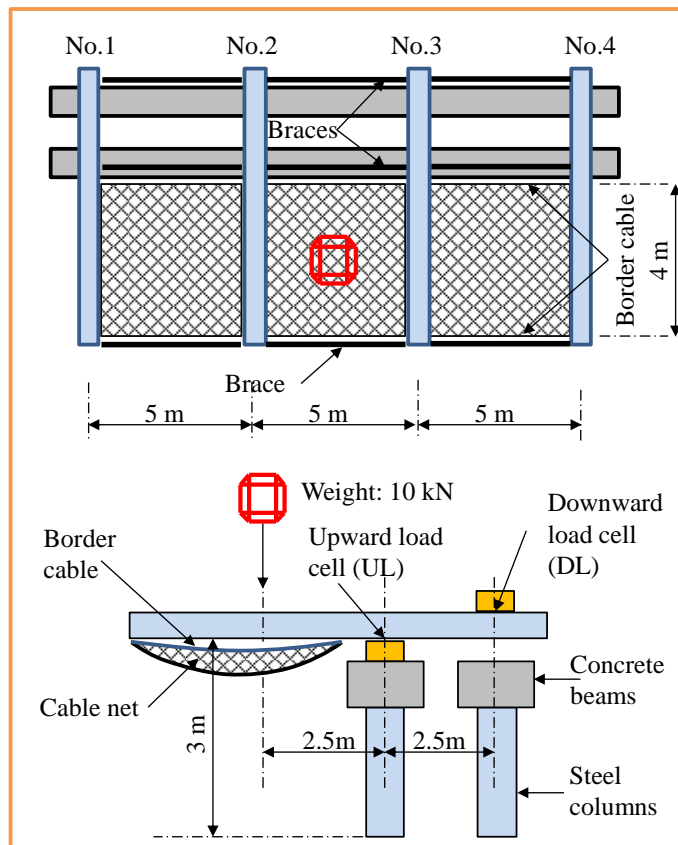


Figure 5.2 Drawing of the fence excluding sand–packs (FES)

The post was the unique structure to support cable net in this type of fence. Therefore, it was designed as a high strength post which made from a 318.5 mm–diameter steel tube (thickness: 6 mm) and nineteen 60.5 mm–diameter steel tubes (thickness: 3.2 mm) inside as shown in Figure 5.3. The grade of both steel tubes is STK400, which is

one of grades of carbon steel tubes for general structure specified by JIS (JIS G 3444, 2010). Space between outer tube and inner tubes was filled with mortar of which compressive strength was 76 MPa. These posts were numbered from No. 1 to No. 4, left to right. Each post was rigidly clamped at two positions on the top of concrete beams as shown in Figure 5.4.

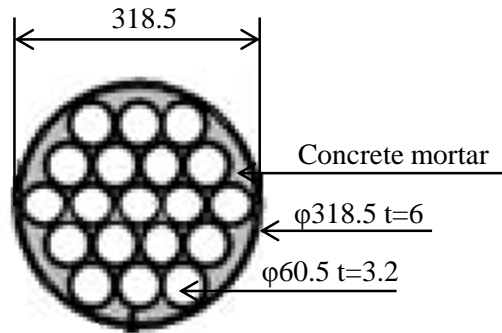


Figure 5.3 Cross-section of steel post.

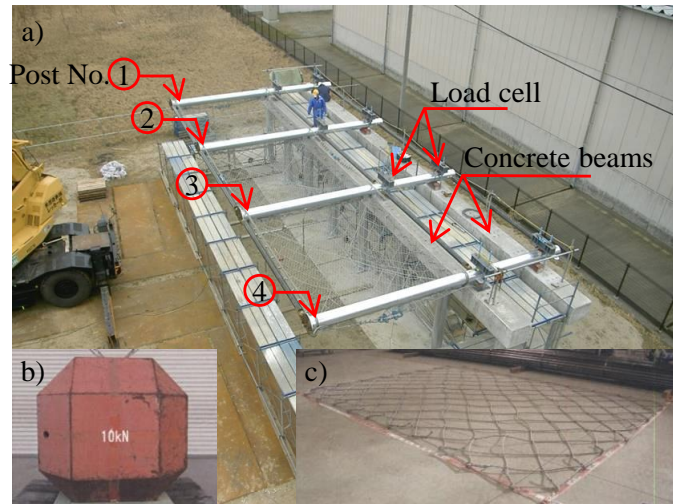


Figure 5.4 Full-scale fence installation: a) view of experiment; b) weight; and c) cable net

Dynamic loads were transferred from the interceptive nets to the posts through a cable system installed along the sides of the nets, (hereinafter, it is called border cable). These cables consisted of two longitudinal ropes at the top and bottom of the fence and four cross ropes (parallel to the posts). The longitudinal rope was a double cable with a diameter of 2x22 mm (FC6x24) fixed at ends namely post No. 1 and No. 4. This rope was threaded through the rings attached to the middle posts (No. 2 and No. 3). This connection type had an advantage of supporting contribution from the side posts. The diameter of the cross cable rope was 22 mm (FC6x24). This rope was fastened to head

and bottom of the post. The border cables were connected to the nets by U shaped bolt connectors.

The weight had a mass of 1 ton, made from a steel shell filled concrete with a polygonal shape as shown in Figure 5.4b according to the European technical approval guidelines (ETAG 27, 2008). The maximum height of the weight block was 0.84 m. To enhance the stability of the structure, some longitudinal bracing members were used at the top and bottom of the fence and bottom of posts.

To avoid any effects of contact between the kits of the fence and ground, the whole configuration was installed on two parallel concrete beams with a gap of 2.5 m. These beams were placed at the top of two rows of steel column to secure the space of 3 m between the fence and the ground.

This fence did not possess any special energy absorbing devices and additional supporting cables. Therefore, the posts were the unique supporting structures of the fence. Impact energy was mostly dissipated based on deformation of the net, border cables, and posts as well as the friction sliding at connecting points.

At the clamped supports of the post on concrete beams, load cells were installed to measure the reaction forces. The load cells, named UL, were placed under the posts to measure upward the reaction forces, while the load cells were placed on the upper side of the posts, named DL, to measure downward reaction forces, as shown in Figure 5.2. Four displacement meters were installed at the top of the posts to measure their vertical deflection. One advantage of vertical impact test is that the weight almost drops down without rotation. Therefore, an accelerometer was laid at the center of the weight to measure the vertical acceleration during impact. One crane with an electrical controlled device to release a weight was used to lift up the weight. Several cameras located in different positions were used to capture the images of the whole experiment phenomenon. One of these cameras was high speed camera with the speed of 200 frames per second, placed on the front of the fence at a suitable level and distance to record the event clearly.

5.2.2 Set-up of the fence including sand-pack (FIS)

In the experiment of the fence including sand-pack (FIS), diagonal cable ropes with a diameter of 22 mm (FC6x24) were added to each span of the FES as described above and 14 sand-packs were arranged on the fence as shown in Figure 5.5. The added

diagonal cables were to avoid large net sag and concentration of sand-packs at the central position of the net. For this experiment, sand-pack filled with sand was utilized to reproduce the landslide or debris covered on the mountainous side of the fence. The sand-pack had about $1.1 \times 1.1 \times 1.1$ m in dimensions and 15 kN in mass, including sand fill and geotextile bag. Six sand-packs, equally 90 kN, were placed on the middle span; and four packs, equally 60 kN, were used for each side span.

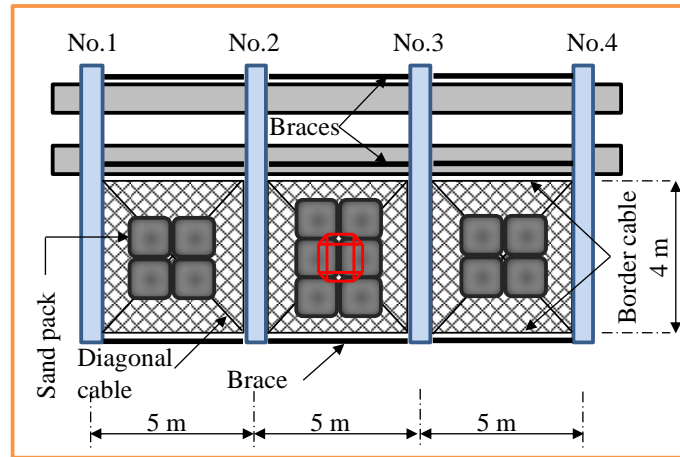


Figure 5.5 Drawing of the fence including sand-packs (FIS)

Table 5.1 Material characteristic of steel tubes

Type	Outside diameter (mm)	Thickness (mm)	Yield strength (MPa)	Tensile strength (MPa)
Outer tube	318.5	6	287	429
Inner tube	60.5	3.2	373	465

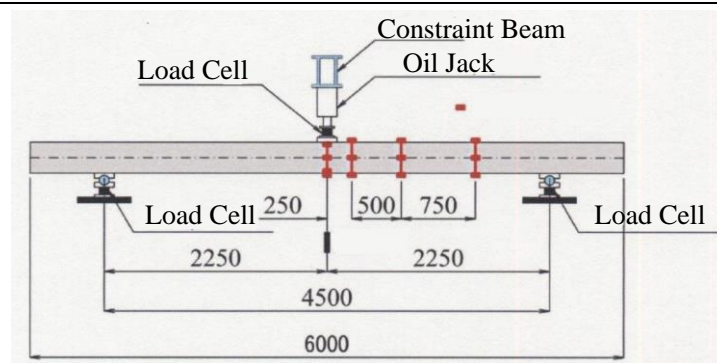


Figure 5.6 Design drawing of bending test for post (unit: millimeter)

5.2.3 Experiment implementation

Some component tests such as bending strength test for post, tensional strength tests for cables, and tensional tests for geotextile bags were conducted before the actual full-scale test. The tested post with the characteristic as described above had 6-m-long,

subjected to a static bending load by an oil jack at center point. The details of this test are presented in Figure 5.6 and its result is shown in Figure 5.7, expressing the relationship between bending moment and curvature. Two 0.5-m-long cable ropes with different diameters used for the experiment as listed in the Table 5.1 were taken for the tensional tests. The results of these tests are presented in Figure 5.8. The mechanical characteristics of geotextile bags were also obtained through a tensional test on a sample with 4 cm wide. The results are shown in the Figure 5.9.

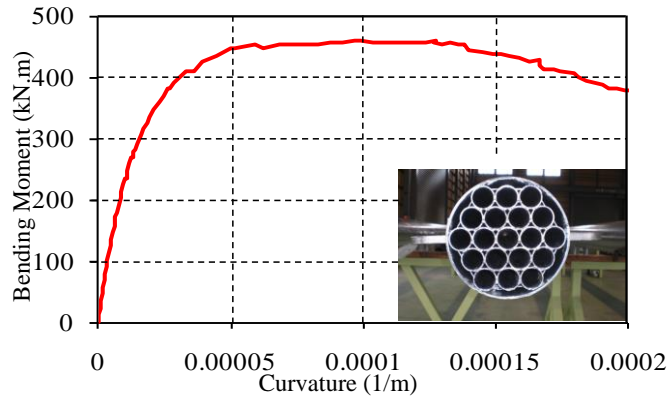


Figure 5.7 Bending test result of post and its cross section

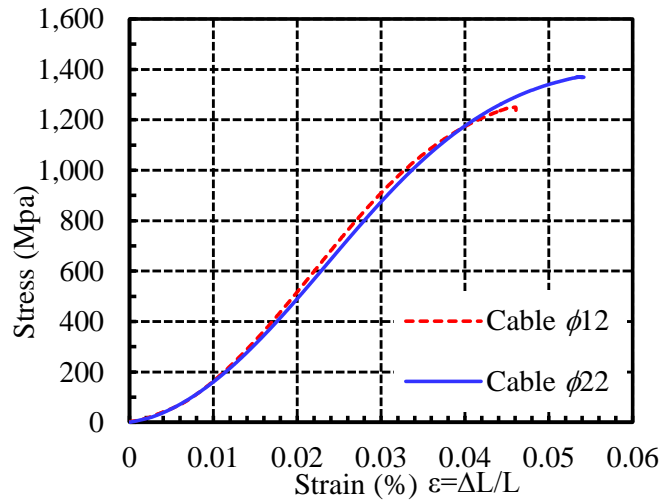


Figure 5.8 Tensional test results on cables

The drop height was 10 m for the FES experiment and 7 m for the FIS experiment. For the sake of simplicity, hereinafter they are called FES_10 and FIS_7 respectively. Impact positions were the center point of the middle span. The drop heights were determined from the lowest point on the weight to the contact point on fence. The impact response was evaluated mainly based on the impact force, reaction force and

displacement of the top of the post. The impact force denoted by F_{im} was calculated by multiplying the measured deceleration of the weight by its mass,. The reaction forces denoted by F_{re_UL} and F_{re_DL} , were measured directly by the load cells. Reaction bending moments at UL supports were calculated by multiplying the reaction force F_{re_DL} by the distance between two supports. Displacement of each post was measured directly by the displacement meter while penetration of the weight on fence, denoted p , was integrated from deceleration.

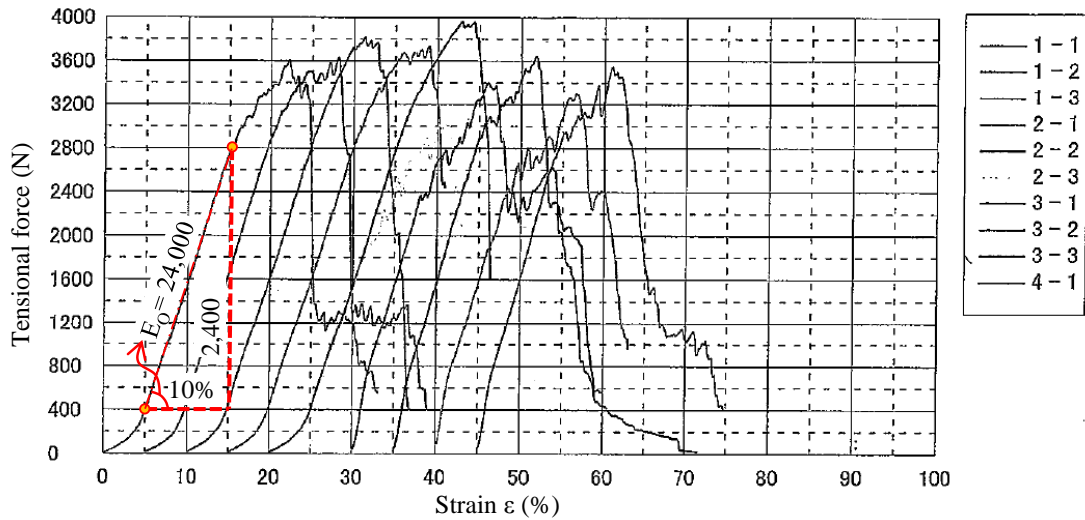


Figure 5.9 Tensional test results on geotextile

5.3 Numerical model approach

5.3.1 Setup of fence configurations and weight in numerical analysis

The numerical models in this study were idealized to simulate full-scale protection fences. Therefore, all components of the fences (e.g., posts, cable nets, border cables, bracing members, diagonal cables and sand-packs and weight) were simulated as the same geometrical dimensions as experimental models of FES_10 and FIS_7. Hexagonal nets as described in the experiment were neglected due to their low dynamic role. Instead of setting up the fence on the firm frame structure (made from reinforced concrete and steel), numerical fence was fixed at support points, hence this frame structure of experiment was also neglected. In order to shorten the computation time, rather than dropping the weight from the initial height of 7 m and 10 m, rock-boulder

was placed close to the fence with an initial velocity. In this case, the initial drop heights were converted to the initial velocities v_0 and the remains of drop height.

5.3.2 Finite element model

The cable net fence is composed of flexible wires and rigid steel posts by many contact types. It has been generally thought difficult to simulate the behavior with sufficient accuracy because of its complexity of structure. This difficulty could be increased more when the fence was accompanied by granular materials such as sand or sand-pack. However, the finite element method of LS-DYNA code has become to be considered one of practical and proper approaches to simulate the fence with sand-pack. Because this commercial code offers various linear and non-linear material models, element and contact types for implicit and explicit dynamic analysis and it gives various possibilities for application Actually, T. S. Ho et al. (2011) has successfully validated material models used for sand and geotextile.

Table 5.2 Geometrical dimension of kits of fence

Components	Type	Diameter D (mm)	Thickness t (mm)	Area A_{eff} (m^2)
Net cable	FC6×24	12	-	6.91×10^{-5}
Border cable	FC6×24	2×22	-	3.36×10^{-4}
Diagonal cable	FC6×24	22	-	1.68×10^{-4}
Hexagonal netting	-	2.7	-	-
Bracing member	STK400	139.8	4.5	1.91×10^{-3}
Geotextile	-	-	0.5	-

Figure 5.10 presents numerical model of FES_10 and FIS_7 while Table 5.3 lists the main parameter for numerical simulation. The posts were equivalently modeled by Belytschko-Schwer beam elements (LST, 2011), while cable net and border cable were simulated by discrete beam elements. Geometrical parameters are shown in Table 5.2. Four-node solid tetrahedron elements and eight-node solid hexahedron elements were used to simulate the weight and sand, and four-node shell elements were used for geotextile bags. Each bracing member was simply adopted by a truss beam element with its cross section area $A_{tr} = 0.0102 \text{ m}^2$. The FES_7 model was comprised of 4,097 nodes, 4,070 beam elements and 81 solid elements. On the other hand, the FIS_10 model was

comprised of 28,410 nodes, 4,190 beam elements, 3,080 shell elements and 17,581 solid elements.

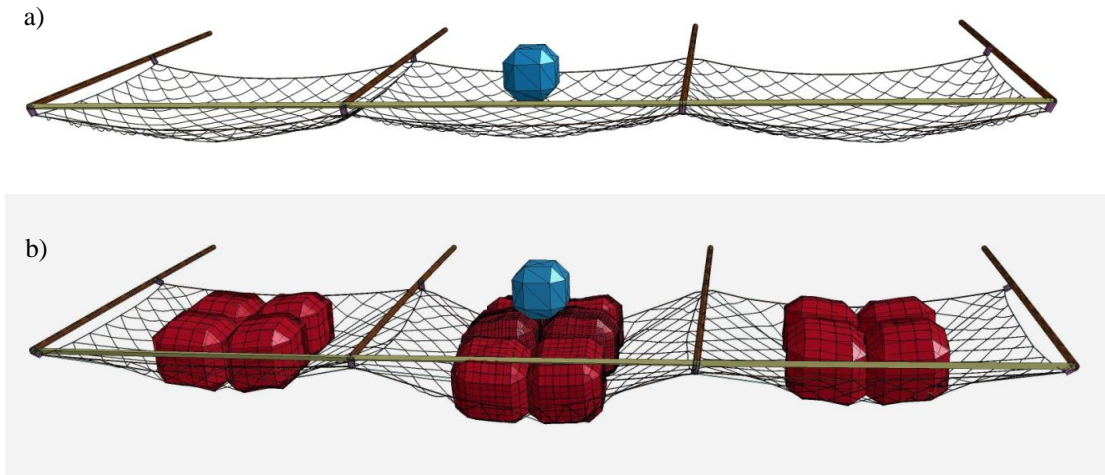


Figure 5.10 Finite element models: a) fence excluding sand-packs (FES_10); b) fence including sand-packs (FIS_7)

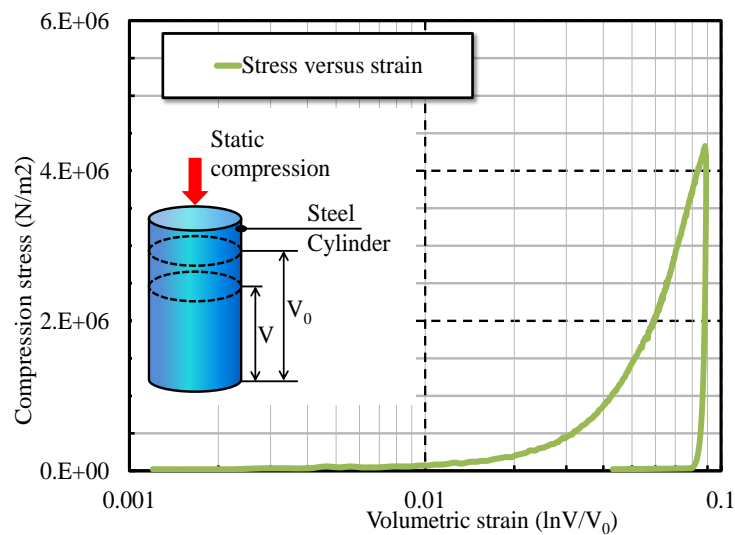


Figure 5.11 Stress versus strain relationship of sand and the test schematic

5.3.3 Constitutive law of material and contact types

The suitable material models used for each component of the fence were considered based on their characteristics and existing data obtained from material tests and relevant research results. Therefore, nonlinear elastic model of so called Mat_166 based on the relationship of bending moment as a function of curvature were used for the post as shown in Figure 5.7. The nonlinear elastic model of called Mat_71 was employed for net cables and border cables. The constitutive law of cable was defined as stress versus

strain obtained from tensional tests as shown in Figure 5.8. The “Soil and Crushable Foam with Failure” model of called Mat_14 applying the Drucker–Prager yield criterion was used for sand fills. The precision and the verification of validity of the analysis using this model were shown by T. S. Ho, et al. (2011) Figure 5.11 presents the pressure versus volumetric strain relationship for the used sand and schematic drawing of test. The other used properties of sand were the density ($\rho = 1333 \text{ kg/m}^3$), shear modulus ($G = 1.54 \times 10^7 \text{ kN/m}^2$), bulk modulus ($K = 3.03 \times 10^8 \text{ kN/m}^2$), internal friction angle ($\varphi = 32.5$ degree) and cohesion ($C = 1 \text{ kN/m}^2$). The weight, braces, and bags were composed of linear elastic materials with their material parameters as shown in Table 5.3. For the weight and braces, representative modulus of concrete and steel were used. The modulus of bag $E = 12 \times 10^5 \text{ N/m}$ was approximately determined by equation (1) considering the result of tensile test shown in Figure 7. The geotextile was treated as a perfect elastic material in this study.

$$E = \frac{E_o}{wt} = \frac{24,000}{0.04 \times 0.0005} = 12 \times 10^5 \text{ N/m} \quad 5.1$$

Where: E_o is determined as shown in the Figure 5.9; $w = 0.04 \text{ m}$ is the width of testing sample; and $t = 0.0005 \text{ m}$ is the thickness of geotextile.

Table 5.3 Main material parameters used for numerical analysis

Components	Density ρ (kg/m^3)	Young modulus E (N/m^2)	Poisson ratio μ
Post	7,850	Δ	-
Net cable	7,850	Δ	-
Border cable	7,850	Δ	-
Sand	1,333	Δ	0.47
Weight	2,600	3.0×10^7	0.3
Girder	7,850	2.1×10^{11}	0.3
Bag	1,200	6.0×10^7	0.3

Δ : refers to experimental data as shown in the figures

The protection fence consisted of various components, which interact to each other to transfer impact wave and dissipate energy. It is no doubt that precise reproduction of the contact behaviors between components might be a significant. The interactions used in the models are divided into 4 following groups: (1) Fixed joint contact (assigned for fastened-joint at cable wire ends and clamped support at post foots); (2)

Node_to_surface contact (between weight and nodal points of the cable); (3) Guided_cable contact (at mesh joints and connections between the net cable and border cable); and (4) Surface_to_surface contact (assigned for reaction between sand and bag and between weight and sand-pack). The penalty method was used to simply and efficiently reproduce friction for the contacts as mentioned above, except for the fixed joint contact. The coefficients of friction were considered for each type of contact according to the used material and contacting surface properties through sensitive analyses. The details of this procedure are not presented here for the sake of simplicity.

5.3.4 Numerical analysis

The initial static sags of net and border cables subjected to their self-weight were evaluated by trial calculation dealing with offset length for cable elements until numerical sag equals to experimental sag. The cable fence is a flexible structure, which could vibrate due to even a small transient load. Therefore, the certain duration was spent to calculate the initial state of structure with the increase of gravity until structure became stable state and to achieve expected initial sag. In addition, the different mass damping factors were considered for separate components and they varied in time corresponding to running stage of structure e.g., gravitational loading, before, during, and after launching. The sensitivity analyses for damping are also not presented here for brevity.

5.4 Numerical model validation

The numerical models according to the description as presented above were validated through the comparison between numerical results and the results obtained from the experiment. The fence models of FES_10 and FIS_7 were respectively subjected to impact of the weight from the drop heights of 10 m and 7 m. The results involve the whole deformation of fence (Figure 5.12 and 5.13), the time history of displacement of the weight (Figures 5.14 and 5.15), the time histories of impact force and impulse by the impact force (Figures 5.16 and 5.17). Typical response values for FES_10 and FIS_7 are also summarized in Table 5.4. The agreement between numerical and experimental results is valued as follows.

5.4.1 Displacement of the fence and weight

Figures 5.12 and 5.13 compare experimental and numerical whole deformation of the fence of FES_10 and FIS_7 through actual video images and simulated animation images captured during collision. It can be observed that the response of whole deformation of fence obtained from numerical simulation is almost similar to the response of experiment in both two cases.

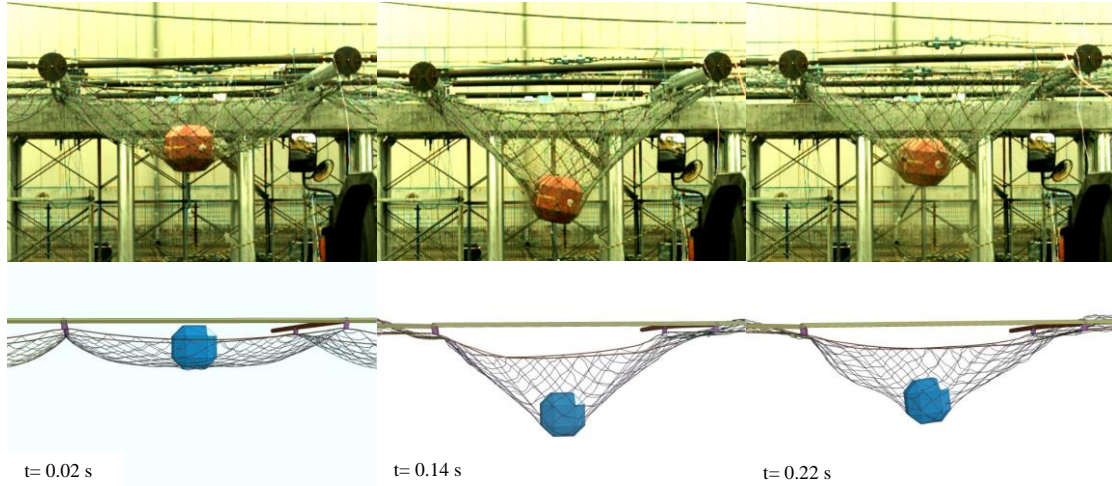


Figure 5.12 Displacement of FES_10 model from experiment and simulation corresponding to three different timepoints during collision

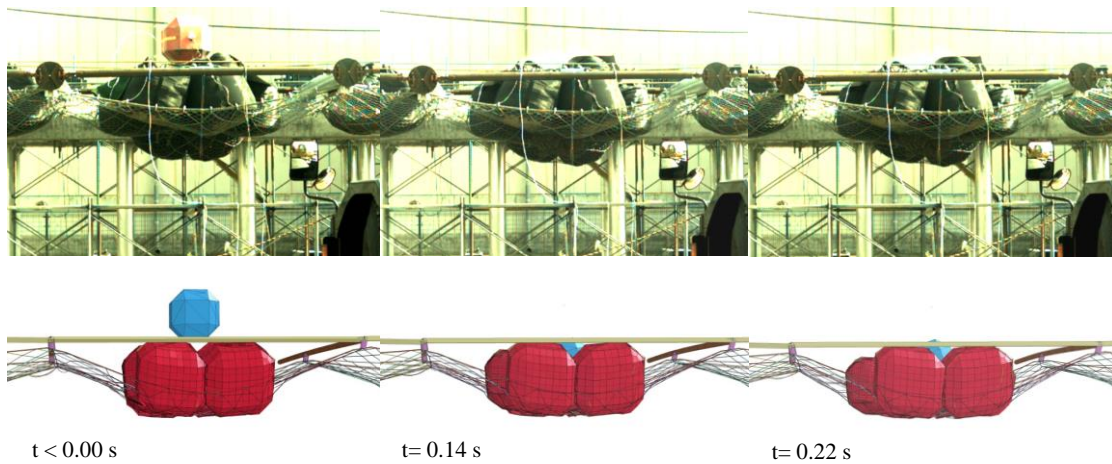


Figure 5.13 Displacement of FIS_7 model from experiment and simulation corresponding to three different timepoints during collision

Figures 5.14 and 5.15 illustrate the time histories of displacement of the weight obtained from both experiment and simulation respectively for FES_10 and FIS_7. It is clear that the results of numerical analysis and experiment are minor differences.

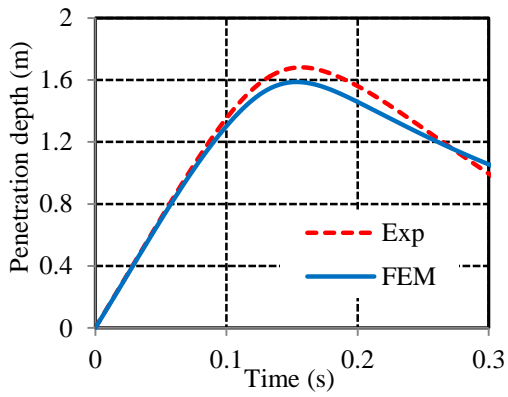


Figure 5.14 Experimental and numerical weight displacement from FES_10 model

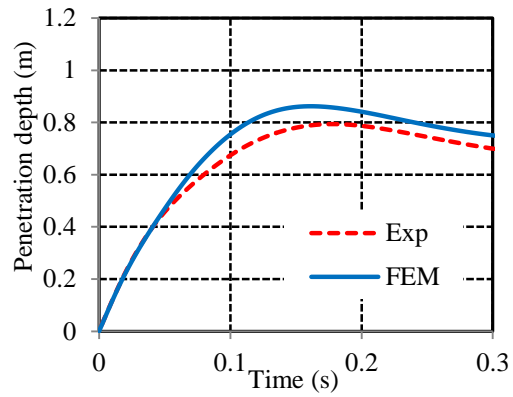


Figure 5.15 Experimental and numerical weight displacement from FIS_7 model

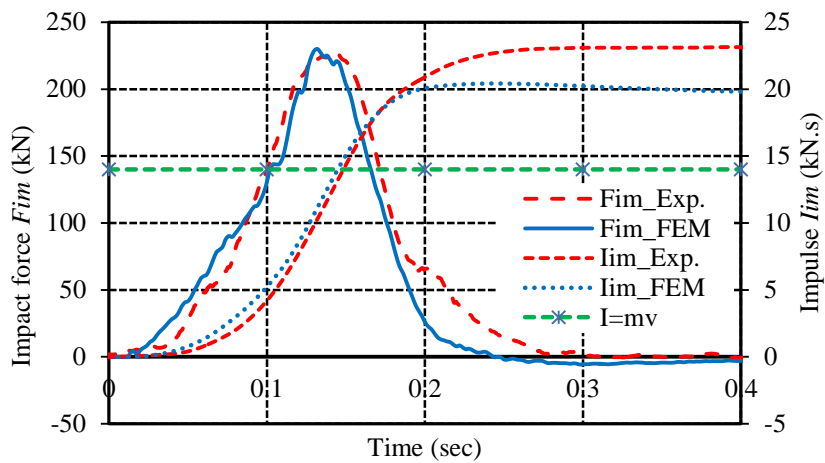


Figure 5.16 Impact force and impulse by impact time–histories from the experimental and numerical result of FES_10 model

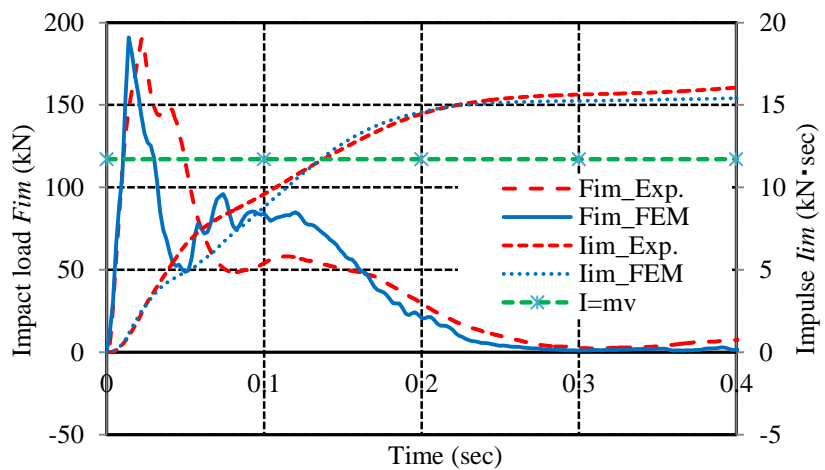


Figure 5.17 Impact force and impulse by impact time–histories from the experimental and numerical result of FIS_7 model

5.4.2 Impact force and impulse by impact

The impact force and impulse by impact are regarded as very important characters to evaluate the accuracy of the numerical simulation. The time histories of those from the experiment and simulation are illustrated in Figures 5.16 and 5.17, comparing with the initial momentum. In these figures, the left vertical axis expresses the impact force values, while the right vertical axis shows the impulse values. The results of FES_10 model in Figure 5.16 show a good agreement between the experimental and numerical curves of the impact force. However, there was a minor gap between two impulse curves obtained from the experiment and simulation from 0.2 s onwards. The final impulse values from simulation and experiment are about 6 and 9 kN.s higher than the initial momentum, respectively, causing the larger rebound as seen in Figure 5.14. Such results of FIS_7 model implies a good agreement between experimental and numerical impact and impulse time history curves as presented in Figure 5.17. The above impact forces also are expressed in the relationship with the weight displacement shown in the Figure 5.18 and 5.19. Minor differences between experimental and numerical results can be seen.

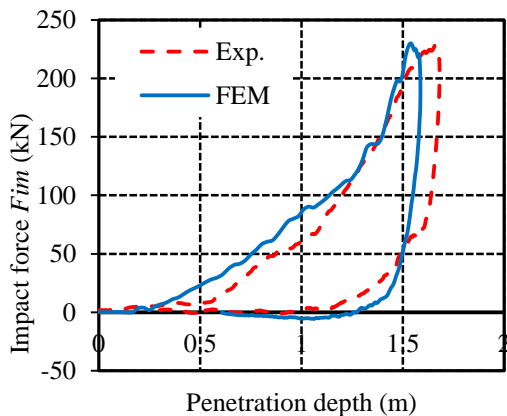


Figure 5.18 Relationship of impact force and weight displacement of FES_10 model

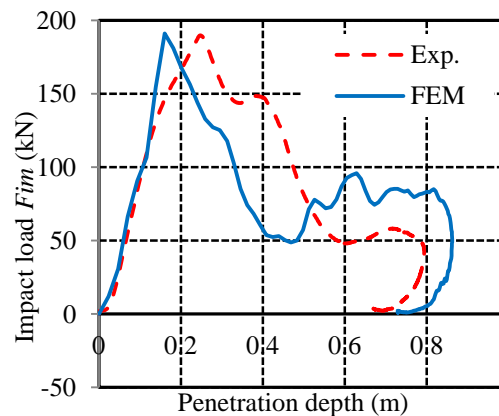


Figure 5.19 Relationship of impact force and weight displacement of FIS_7 model

5.4.3 Deflection of the top of the post

Figure 5.20 and 5.21 give a comparison between the experimental measured and numerical calculation values of displacements of the top of two middle posts (No. 2 and

N. 3) from two fence models. It can be seen the results of FES_10 model have small differences in the maximum values and good matches in the periods. In contrast, for FIS_7 model, the experimental deflections are quite smaller than those of simulations, typically from 0.15s to 0.5 s. After the peaks, the deflections obtained from the experiments decreased linearly to zero. The durations of the deflection are the same.

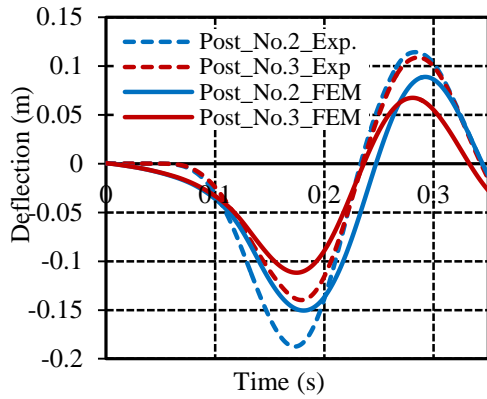


Figure 5.20 Deflection of the top of the post No. 2 and No. 3 of FES_10 model

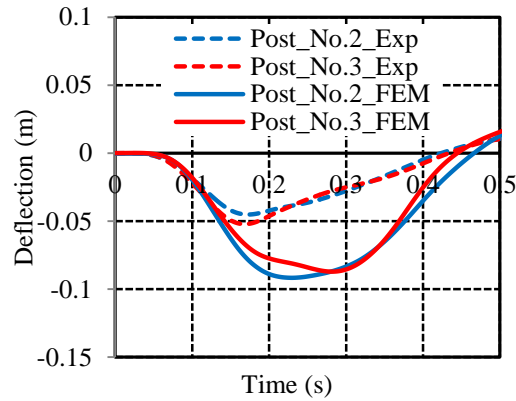


Figure 5.21 Deflection of the top of the post No. 2 and No. 3 of FIS_7 model

5.4.4 Reaction forces

The reaction forces mobilized at the clamped supports on two middle posts are shown in Figures 5.22 and 5.23 with the respect to time. The experimental reaction forces were measured by upward load-cell and downward load-cell corresponding to the positions of fixed nodes on the feed of the post of numerical model. The tendency of results of FES_10 model from the experiment and simulation is almost the same, especially durations of reaction forces as shown in Figure 5.22. The maximum values of reaction force from the experiment are somehow larger than those values from the simulation. Figure 5.23 shows a comparison of reaction forces of experimental and numerical FIS_7 models. The numerical results are lightly higher than experimental results during the unloading process.

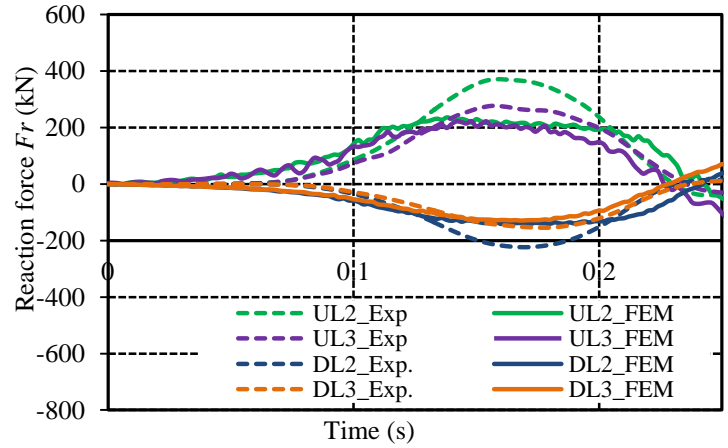


Figure 5.22 Reaction force histories of FES_10 model

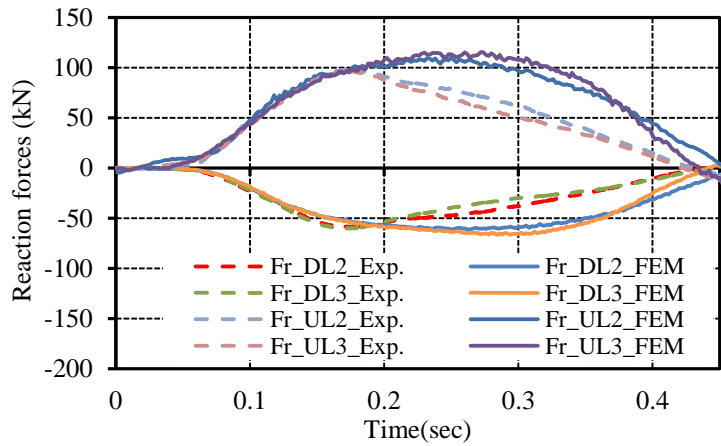


Figure 5.23 Reaction force histories of FIS_7 model

5.4.5 Other parameters

Typical response values for FES_10 and FIS_7 obtained from the experiments and simulation are also summarized in Table 4. The maximum values of displacements, impact force, impulse by impact, and other response values and their ratios of experimental and numerical values for two cases FES_10 and FIS_7 are shown. In this table, the maximal impact force, impulse, displacement of the weight, and time duration are abbreviated to $F_{im(max)}$, $I_{im(max)}$, D_{max} , and T_{im} , respectively. It can be confirmed that these results of simulations show mostly a good match with the results of experiments. Particularly, Table 5.4 also presents the absorbing energy ratios (abbreviated to R_e), determined based on the total energy magnitudes and absorbed energy value, which was evaluated from initial velocity and rebounding velocity (at the instant, the weight was

disconnected from the net). The absorbing energy ratios R_e obtained from the simulation are similar to those obtained from the experiment, especially for FIS_7 model.

Table 5.4 also enumerates the maximal values of reaction forces and moment at every support point of two middle posts. The reaction forces obtained by upward load cells and downward load cells on feet of posts No. 2 and No. 3, referred to Figures 5.2 and 5.3, were abbreviated to Fr_{UL2} , Fr_{UL3} , Fr_{DL2} , Fr_{DL3} and the reaction moments at upward load cells determined by downward reaction forces and their levers were abbreviated to M_2 , M_3 . The minor scatters between experimental and numerical reaction forces and moments are observed at post No. 3. Those forces and moments at post No. 2 show greater scatters. The assumption of boundary condition of the feet of the posts in simulation is thought a reason of these differences. Although clamped support points at feet of the posts were treated as completely fixed joints in analysis, in reality, the compression loads at the support points of the experimental fence were fastened moderately.

Table 5.4 A comparison between numerical and experimental models based on concrete parameters

Model name		FES_10			FIS_7			
Parameter	Unit	FEM	Exp.	Exp./FEM	FEM	Exp.	Exp./FEM	
$F_{im(max)}$	kN	230.04	228.34	0.99	191.06	189.92	0.99	
$I_{im(max)}$	kN.s	20.43	23.21	1.14	15.40	16.01	1.04	
P_{max}	m	1.59	1.68	1.06	0.86	0.79	0.92	
R_e	%	89.35	82.40	0.92	87.68	88.15	1.01	
Reaction force	$F_{R_{UL2}}$	kN	236.20	371.42	1.57	110.21	97.99	0.89
	$F_{R_{UL3}}$	kN	222.99	277.49	1.24	116.35	96.74	0.83
	$F_{R_{DL2}}$	kN	141.06	223.41	1.58	61.11	58.60	0.96
	$F_{R_{DL3}}$	kN	129.15	154.58	1.20	66.74	60.38	0.90
Reaction Moment	M_2	kN.m	141.06	223.41	1.58	61.11	58.60	0.96
	M_3	kN.m	129.15	154.58	1.20	66.74	60.38	0.90
	T_f	s	0.24	0.27	1.13	0.28	0.30	1.07

5.4.6 Conclusion for validation step

Generally, the experimental and numerical results of the displacement response, impact force, impulse by impact, absorbing energy ratio, reaction force, and moment for two models show a good and consistent agreement. This result confirms that the ability of the FEM model has enough ability to reproduce the behavior of full-scale fence with

and without sand-pack subjected to impact of drop weight and also provides useful possibility as a tool to investigate further effects of sand-pack on impact phenomenon.

5.5 Investigation into the effects of sand-packs according to the increase of drop height

Instead of assessing the role of sand-pack on the fence models through the models validated above, for the sakes of providing a wide view, these numerical models were used to investigate a wide range of energy from 20 kJ to 140 kJ. The questions of how land slide affects rockfall protection fence and what advantages and disadvantages of using sand-pack for the fence are were answered in the content of this section. Seven drop heights, varying from 2 to 14 m were conducted for two numerical models of FES and FIS by changing the initial velocity v_0 .

5.5.1 General impact phenomenon

The maximum values of the impact force from two models of FES and FIS as shown in Figure 5.24 increases almost linearly corresponding to the increasing of drop height. Thus, the results of FES model are very slightly larger than those results of FIS model. However, both are almost same. On the other hand, as illustrated in Figure 5.25, there are some differences concerning the impulses by these impact forces. It is observed that the impulse value from FIS model is clearly smaller than that value from the FES model for the same drop height. This indicates that FIS with sand-pack has larger impulse buffer ability than FES.

Figures 5.26 and 5.27 present the relationship between the drop height and the maximum values of the reaction force at upward and downward load cells on the posts No. 2 and 3 obtained from two models. Generally, the reaction forces obtained from the FIS model are about 15-30% larger than those from the FES model. However, it is noticeable that the reaction forces as mentioned above involve dynamic and static reaction forces, which are not mentioned on the Section 5.4. Clearly, the static reaction forces obtained from the FIS model are much higher than those forces from the FES model due to the weight of sand-packs. For FIS model, the static reaction forces are 178 kN and 100 kN at upward and downward load cells respectively, comparing with 23 kN and 13 kN for the FES model.

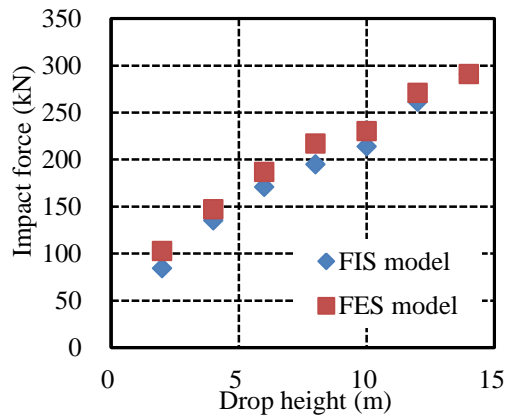


Figure 5.24 The relationship between drop height and maximum impact force of FES and FIS models

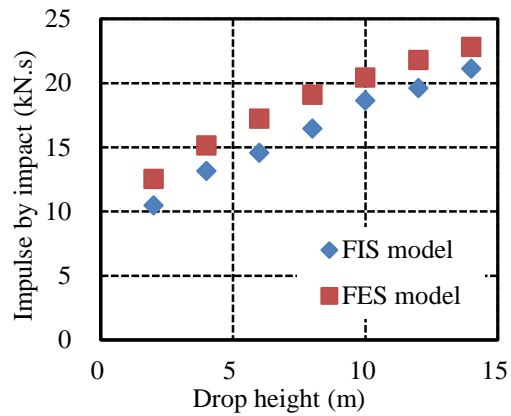


Figure 5.25 The relationship between drop height and impulse by impact of FES and FIS models

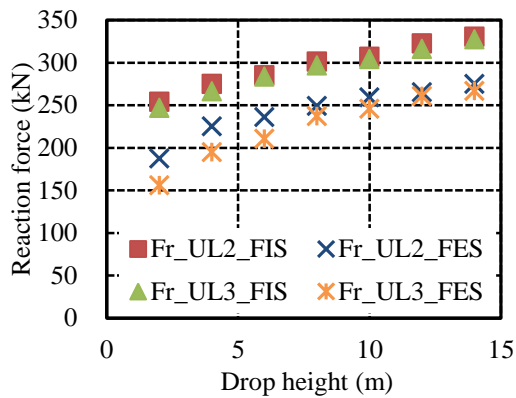


Figure 5.26 The relationship between drop height and maximum reaction force of FES and FIS models at upward load cells

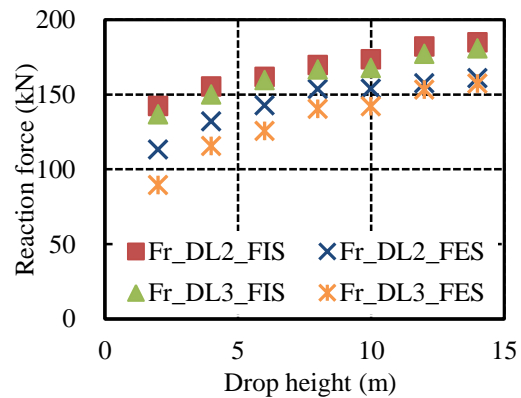


Figure 5.27 The relationship between drop height and maximum reaction force of FES and FIS models at downward load cells

5.5.2 Energy dissipation and transmission

Figure 5.28 shows the ratio of the maximum transferred energy in fence and sand-packs to initial kinetic energy of falling weight. The absorbing energy ability of fence and sand-packs may be more or less due to the characteristics of the used material or construct of these components. It can be seen that the proportions of impact energy transferred within sand-packs from the FIS model are much greater than those proportions of the fence of both FIS and FES models. Moreover, the transferred energy proportions of the fence of FES model double these proportions of the fences of FIS

model. Figure 5.29 gives an example of the variations of total energy within the mentioned components. It can be seen clearly that the transferred energy values within sand-pack component is much higher than those values within other components. Particularly, for sand-pack component, the total energy value reached the maximum value and remained stably by mean of plastic deformation and displacement of sand-pack, while the total energy of fence components decreased to zero after getting the peaks due to elastic deformation of the fences.

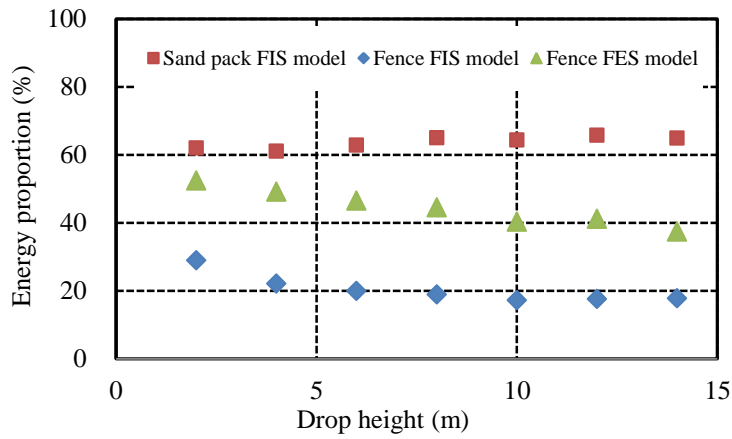


Figure 5.28 Proportion of the maximum total energy transferring through sand-packs of FIS model, fence of FIS model and fence of FES models with respect to drop height

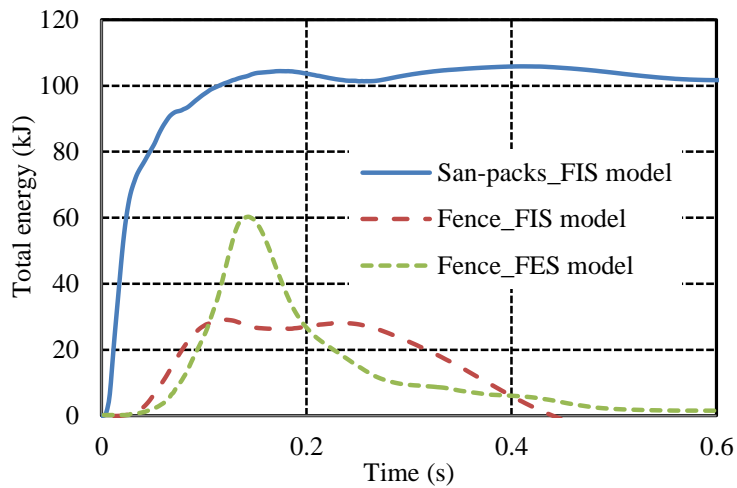


Figure 5.29 Variation of energy transferring through sand-packs of FIS_14 model, fence of FIS_14 model and fence of FES models with 14 m of drop height

5.5.3 Cable stress distribution

The fence used in this study has no breaking devices, the wire cable could be broken when the force of the wire cable exceeds its tensile strength. The cables, which

were directly struck by the weight, are most affected. Therefore, Figures 5.30 and 5.31 present the maximum tensile stresses of the cables obtained by numerical analysis in the FES and FIS models respectively, mobilized at the net cables (involving the Cable_A and Cable_B), border cables, and diagonal cables. With reference to Figure 5.30, the maximum tensile stress of Cable_B is three times greater than that in the border cable. The differences of the maximum tensile stresses between two Cable_A and B indicate the asymmetry of the nets of the fence. The maximum tensile stress in the Cable_B is greater than that in the Cable_A. Regarding cable stresses obtained from the FIS model, Figure 5.31 shows that the tensile stresses in the net cable and border cable are almost the same, and they are smaller than the stress in the diagonal cable.

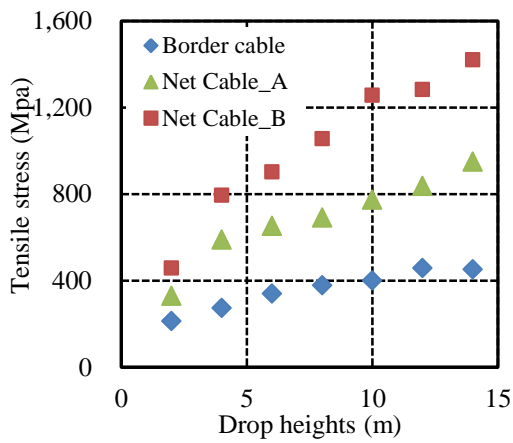


Figure 5.30 The relationship between maximum tensile stress of cable and drop height from FES model

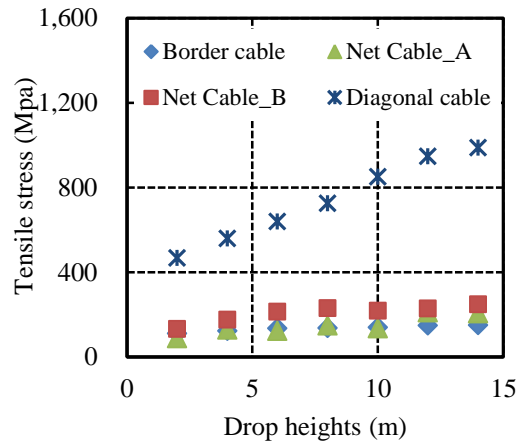


Figure 5.31 The relationship between maximum tensile stress of cable and drop height from FIS model

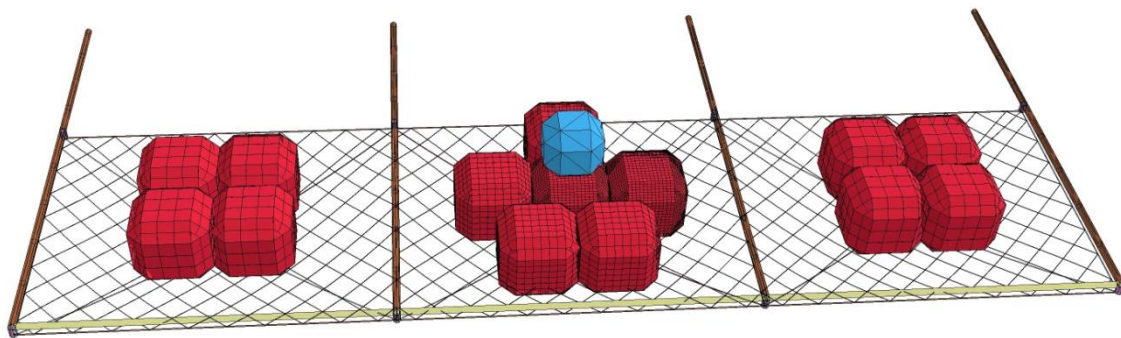


Figure 5.32 FEM model of impact at center of sand-pack (FIS_7_C)

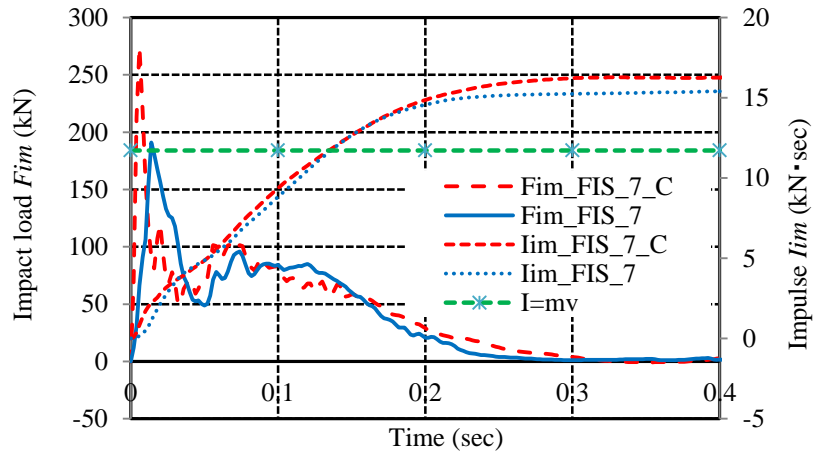


Figure 5.33 Histories of impact force and impulse of FIS_7 and FIS_7_C models

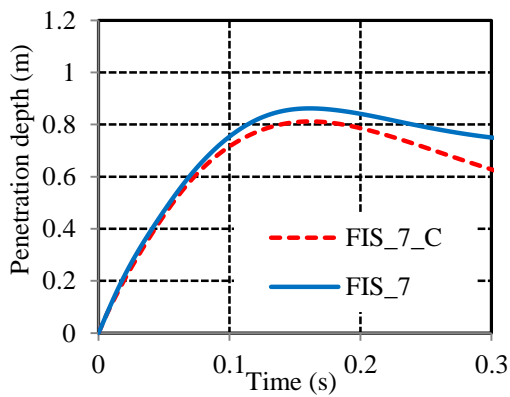


Figure 5.34 Histories of penetration depth of the weight of FIS_7 and FIS_7_C models

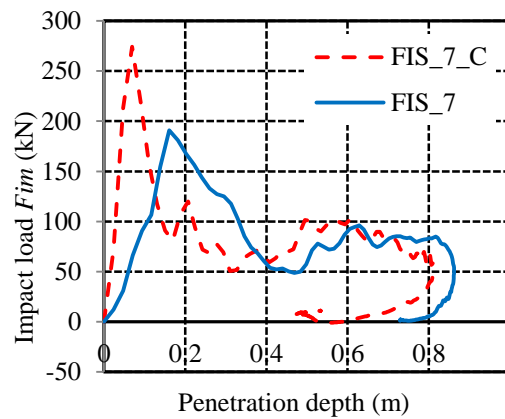


Figure 5.35 The relationship between impact force and penetration depth of the weight of FIS_7 and FIS_7_C models

5.6 Application

5.6.1 Effects of collision point on sand-pack

In the numerical model of FIS_7 used for validation step, the sand-packs on the mid span were arranged so that the weight collided at the sides of two neighbor sand-packs. In order to investigate the effects of position impact on the sand-pack, the sand-packs on the mid span of FIS_7 model were, therefore, rearranged to create the new model as shown in Figure 5.32, so called FIS_7_C. In this model, the weight was dropt at the center of one sand-pack from the height of 7 m. Results of this model were mobilized to compare with the results of FIS_7 model, as shown in the Figures 5.33 –

5.36. Obviously, the histories of impulse by impact, displacement of the weight, and reaction force obtained from FIS_7 and FIS_7_C model are almost similar, however, small scatters can be seen in the results of impulse and displacement. Typically, the maximum value of impact force of FIS_7_C model is about 80 kN higher than that value of FIS_7 model, although the histories curves of these forces have the same tendencies. The differences in displacement and impact force are also presented in the relationship of impact force and displacement of the weight as shown in Figure 5.35.

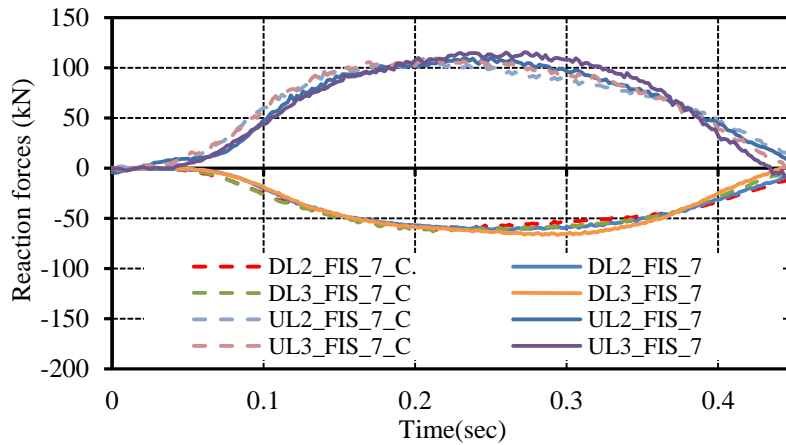


Figure 5.36 Histories of reaction force of FIS_7 and FIS_7_C models

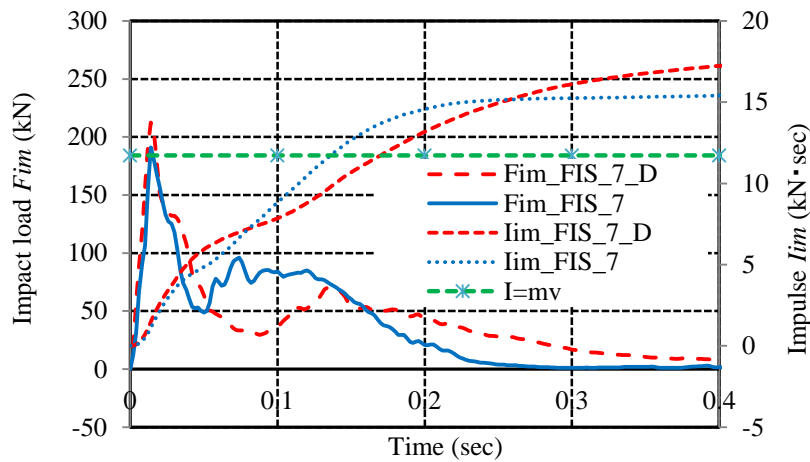


Figure 5.37 Histories of impact force and impulse by impact of FIS_7_D and FIS_7 models

5.6.2 Effect of diagonal cables

The differences in construct between FIS model and FES model are not only sand-packs, but also diagonal cables added under the cable nets to avoid concentrated mass of sand-packs. To investigate the role of the diagonal cables as well as the effects themselves on impact phenomenon, FIS_7_D model was created by removing the diagonal

cables in the FIS_7 model. The results of impact force, impulse by impact, penetration, reaction force, and tensile stress of net cable of FIS_7_D model are taken into a comparison with those results of FIS_7 model as shown in Figures 5.37–5.41. Figure 5.37 shows small difference of the maximum value of impact force and impact duration between two models, resulting to small scatter between final impulse of FIS_7_D and FIS_7 models. The final penetration depth of FIS_7_D model is larger than that obtained from FIS_7 model as shown in Figure 5.38. These differences can be also seen in the relationship of impact force and penetration depth of the weight as shown in Figure 5.39. Diagonal cables seem to be not affected much to reaction force, then the reaction force histories obtained from two models are almost the same. Typically, diagonal cables strongly affected to tensile stresses of net cable, for instance, the maximum cable stresses in Cable_A and B of FIS_7_D model without diagonal cables are twice larger than those stresses of FIS_7 model with supports of diagonal cables as presented in Figure 5.40.

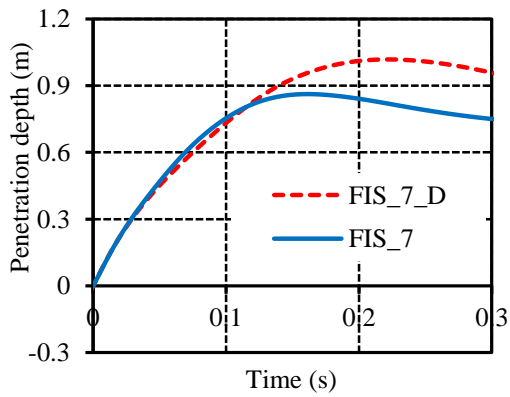


Figure 5.38 Histories of penetration depth of the weight of FIS_7_D and FIS_7 models

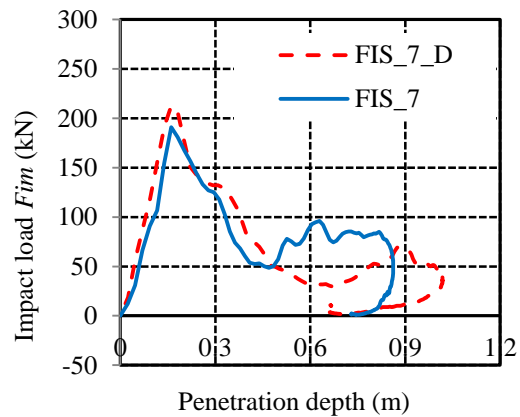


Figure 5.39 The relationship between impact force and penetration depth of the weight of FIS_7_D and FIS_7 models

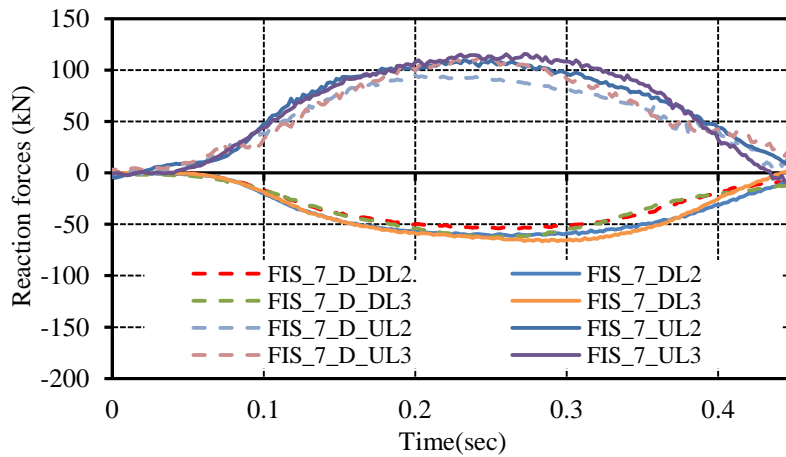


Figure 5.40 Histories of reaction force of FIS_7_D and FIS_7 models

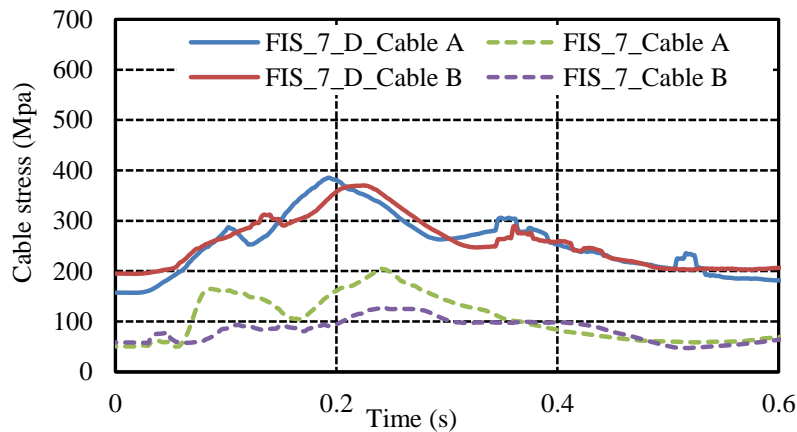


Figure 5.41 Histories of tensile stresses in net cable of FIS_7_D and FIS_7 models

5.6.3 Effect of impact direction

Guido Gottardi (2010) noticed that vertical drop test system absorbs up to 15% more energy due to the actual position of the deepest state of the block comparing with those from horizontal test. Based on this ideal, this study proposed to investigate and make a comparison between impact phenomenon results obtained from simulations with two directions of impact. For the vertical impact, FES_10 model was used. The gravity acceleration, therefore, applied for weight and fence is co-axial with movement direction of weight. The horizontal collision, denoted as FES_10_H, which was modified from FES_10 model by changing the direction of gravitation and weight movement. For this case, the acceleration due to gravity caused initial displacement mostly on cable net, cable system and the free fall weight, which were perpendicular to collision direction.

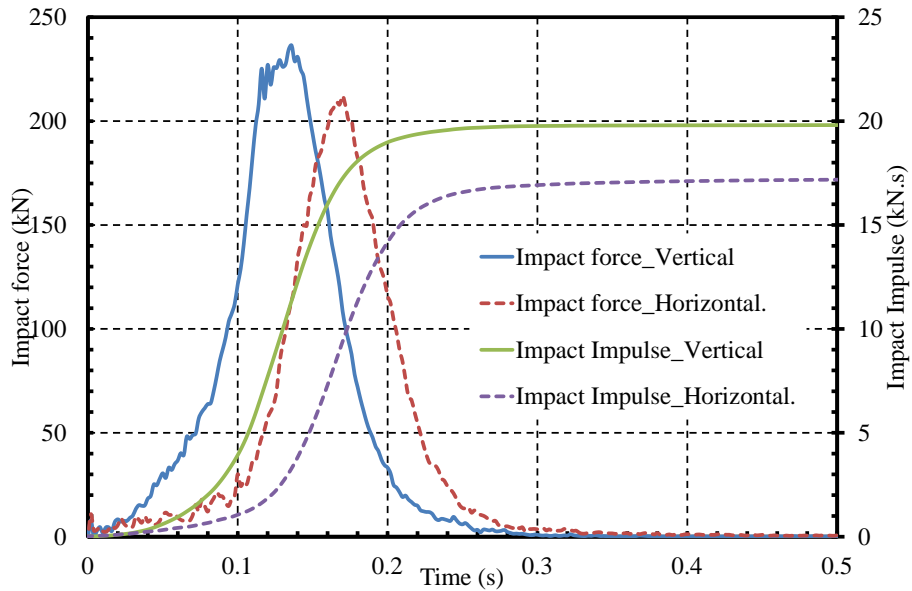


Figure 5.42 Impact and impulse by impact force histories obtained from FES_10 and FES_10_H

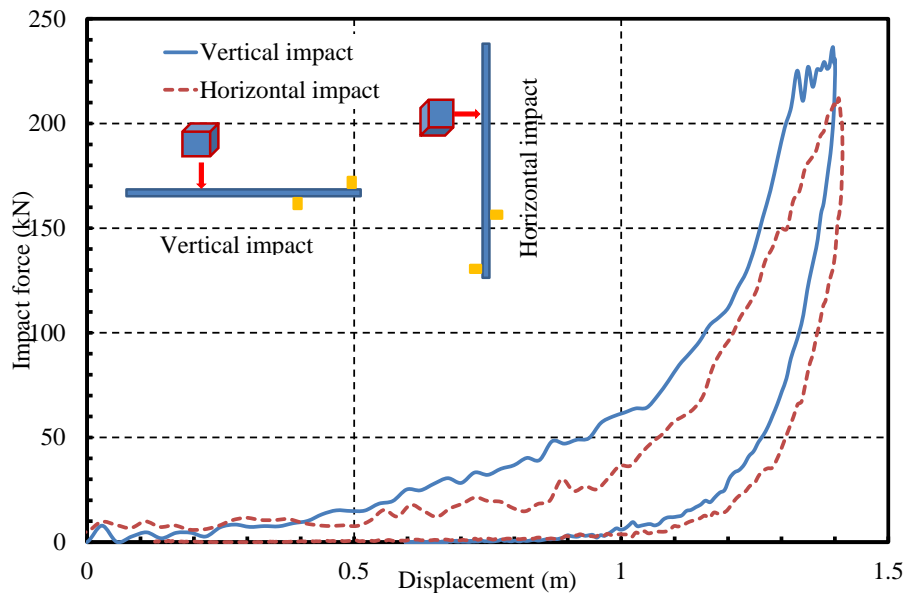


Figure 5.43 The relationship of impact force and displacement from FES_10 and FES_10_H

The calculation results as shown in Figure 5.42 indicate impact force from horizontal impact has a time lag of about 0.04s comparing to that from vertical impact. In addition, the maximum values of impact force and final impact impulse from horizontal collision are 10% and 15% lower than those values from vertical collision, respectively. Figure 5.43 illustrates the relationship of displacement and impact force. The maximum value of impact force from vertical collision is larger, whereas the final displacement values from both cases are almost similar. In the reality as presented in Figure 5.1, the

total displacement from horizontal impact includes initial vertical displacement, which was transferred from vertical direction to horizontal direction at the beginning of impact process. This feature caused the time lag of the impact force histories between two cases as shown in Figure 5.41.

5.7 Discussion and conclusion

After validating the numerical models, these models were taken into account for a further investigation. The results of numerical models were analyzed carefully. Therefore, many features of impact response of the fence with and without sand-packs should be discussed more deeply. The asymmetric of the fence and cable net can be seen in the results of reaction forces, post deflections, and cable stresses, as illustrated in Figures 5.20, 5.22, 5.26, 5.27, 5.30 and 5.41 and as well as Table 5.5. The weave used for cable net as described in outline of experiment could be a possible reason for this asymmetry. The asymmetry of net and post ably results greater stress in one component of the structure than in the others, stresses in Cable_A are much larger than stresses in Cable_B in FES model, for instance. This characteristic may limit the capacity of the fence.

The significant effects of sand-packs on rockfall protection fence can be seen clearly, mostly because of the high ability of energy absorption of sand to induce larger plastic deformation and displacement and the role of sand-packs to redistribute impact force on the surface of net.

The asymmetry of deflection and reaction force histories of FIS_7 model obtained from the experiment as shown in Figures 5.21 and 5.23 properly caused by the failure of the posts at clamped supports after several repeating impact observed during the test. Therefore, although there are the remained differences between the above-mentioned results of experiment and simulation, FIS model in this study is potential to further practical application.

In this study, many numerical models of rockfall protection fence with and without sand-packs simulated by FEM have been done successfully. The validated models have been, then, applied for deeper investigation to reach insight into structural response. According to the numerical result analysis and discussion, the content of the study are concluded as follows.

1. Generally, sand-packs covered on the fence have strong effects on impact characteristics of rockfall protection fence, such as impact force, impulse by impact, displacement, reaction force and cable stress.
2. The arrangement of sand-packs as well as diagonal cables under the net play an important role in dynamic response of the fence.
3. The results of vertical and horizontal impact models are precisely different, however, for safety side consideration, vertical impact test is acceptable choice for experiment.
4. Among the above effects of sand-packs, high ability to absorb impact energy and redistribute impact force could be utilized for cushioning layer of the fence.
5. The promising results of numerical model using FEM code of LS-DYNA provide a possibility of application of FEM approach for flexible cable fence combining with granular material of sand-packs.
6. Failure of structure or the effects of size and shape of the weight, which were neglected in this study are the remained limitations.
7. Further investigation into the response of the fence combining with sand-packs as well as proposal of new fence type using sand-packs cushioning layer are going to conduct in the near future.

References

- Cazzani, A., Mongiovi, L., Frenez, T., Dynamic finite element analysis of interceptive devices for falling rocks, *Int. J. Rock Mechanics and Mining Sciences*, 39, pp.303-321, 2002.
- Cristina Gentilini et al (2012). Three-dimensional numerical modeling of falling rock protection barriers. *Computers and Geotechnics*, 44, 58-72.
- Gottardi, G., & Govoni, L. (2009). Full-scale Modelling of Falling Rock Protection Barriers. *Rock Mechanics and Rock Engineering*, 43(3), 261-274. doi:10.1007/s00603-009-0046-0
- EOTA: ETAG 027 – guideline for the European technical approval of falling rock protection kits, Tech. rep., European Organization for Technical Approvals, Brussels, 2008.

- Hallquist, J. O. (2006). Theory manual.
- Kishi, N., Nakano, O., Matsuoka, K., and Nishi, H., Field test on absorbing capacity of a sand cushion, *Journal of Structure Engineering*, 39A, 1587-1597, 1993 (in Japanese).
- Lambert, S., Gotteland, P., Nicot, F. (2009): Experimental study of impact response of geocells as component of rockfall protection embankment, *Natural Hazards and Earth Systems Science*, Vol. 9, pp.459-467.
- LST (Livermore Software Technology) (2011): LS-DYNA Keyword User's Manual, Vol. I, Version 971.
- Masuya, H., Aburaya Y., Futo S., Sato A., Nakamura S. (2009): Experimental study of the weight collision on a sand cushion and its impact action, 8th International conference on shock and impact loads on structures, Adelaide, Australia.
- Nishita, Y., Inoue, S., Masuya, H., Experimental Study on the Performance of Impact Absorption of Sand Cushion on Wire Net, *Proceedings of the 9th International Conference on Shock & Impact Loads on Structures*, pp.527-532, Nov. 2011.
- Nishita, Y., 落石や土砂による衝撃を受ける柔防護構造物の動的挙動と性能評価に関する研究, doctoral thesis, 2012 (in Japanese).
- Dhakal, S., Bhandary, N. P., Yatabe, R., Kinoshita, N., Experimental, numerical and analytical modeling of a newly developed rockfall protective cable-net structure, *Nat. Hazards Earth Syst. Sci.*, 11, 3197-3213, 2011.
- Phuc Van Tran, Koji Maegawa, Saiji Fukada (2012) Experiments and dynamic finite element analysis of a wire-rope rockfall protective fence, *Rock mechanics and rock engineering*, doi: 10.1007/s00603-012-0340-0
- Tam Sy Ho, Hiroshi Masuya, Yoichi Nishita and Stéphane Lambert, Numerical simulation on impact of sand filled pack, *Proceedings of 19th International Conference on Shock and Impact Loads on Structures*, Fukuoka, pp. 365-372, Nov., 2011.

Chapter 6 Conclusion

Today, sand has been used effectively and popularly in many countries for many types of structures against rockfall hazards. To design a protective structure with the ideal of performance-based design, it is necessary to evaluate the limitation capacity of structure as well as get insight into structural response. Experimental approach in cooperation with numerical simulation has been assumed the most economic and promising method. Basing on these points of view, this research generally focuses on the performance of sand cushioning layer in rockfall protection structures. Sand is either filled in the tank to reproduce a direct use of sand on the rockfall galleries or to be contained in the container (case or bag) to make a sand-cell on the surface of walls or fences. The first sub-research, as shown in Chapter 3, uses FE method to create the numerical model of sand as well as to apply this model for further investigation. With the aims of testing the reactions of sand cushioning layer on steel rockfall galleries, the second sub-research of Chapter 4 concerns series of impact experiment on sand tank over steel H-beams. Chapter 5 in this study shows the content of the third sub-research, dealing with simulation of the dynamic reaction of flexible rockfall fence with and without covered sand-packs by using FE approach. The validated models of the fences, then, are gone through many applicable investigations. The results achieved in the present study are summarized as follows.

1. Risks of rock fall as well as other natural hazards have uncertainty of probability of occurrence and its scale. The grasp of updated obvious risk at the site is necessary. It is considered that research on improving the capacity of rockfall protection structure basing on the better knowledge of structural insight behavior is importance and necessary to secure required safety for expected risk.
2. This research is successful to model the impacts on sand tank and sand-cell acting as a component of rockfall walls or galleries by using FEM code of LS-DYNA. The results of parametric study using this numerical model indicate that geometrical parameters of sand such as the shear modulus G , bulk modulus K ,

angle of internal friction φ , and relationship of pressure versus volumetric strain are very important for numerical model of sand. Boundary conditions surrounding sand-cell strongly affect impact characteristics, e.g. impact force, transmitted force, weight displacement, and impulse by impact.

3. The experimental study on sand tank over steel H-beams indicates that the energy absorbing effective of gravel cushion is higher than that of sand cushion. On the other hand, the transmitted force (P_t) at the bottom of sand tank and two equivalent forces (P_s, P_d) are evidently affected by the length of beam span L . The relationships between the dynamic multiplication factor (D_{MF}) and energy transfer rate (ETR) and ratio of T_d/T are clearly approximated by exponential functions.
4. The results of numerical study on fence with and without sand-packs clearly show the effects of sand-packs on structural impact response, e.g. displacements, impact forces, impulses by impact, reaction forces, cable stresses, and deflections of the posts.
5. The sand-packs may not reduce much the impact forces, but evidently redistribute impact force on cable net and reduce tensile stresses of net cables. In other words, the role of sand-packs in this study is also the same as cushioning layer of rockfall walls and galleries rather than braking devices of the normal flexible fence.
6. Arrangement of sand-packs and diagonal cables under the net are also affected to structure response, especially impact forces, impulses by impact and displacements of the weight and fence.
7. The recent researches on rockfall protection structures have obtained remarkable achievements so far, however, there have been some remained limitations, needed to advance e.g. low impact energy range, small grain size range, short and small size of steel beams as well as single size and shape of the weight. Among these limitations, dynamic behavior of discrete material of sand cushion dealing with above-mentioned characteristics should be revealed more.

For the future work, the author will step by step solve the above-mentioned limitation by mean of other parametric and geometric studies and advancing numerical

material model so that enable to reproduce the failure of structures. Basing on achieved numerical models and experimental practical equations, some applications or prototype fences will be proposed and analyzed.